# Iterative receivers with channel estimation for MIMO and multi-user OFDM systems

Hammarberg, Peter

2012

# Iterative receivers with channel estimation for MIMO and multi-user OFDM systems

Peter Hammarberg

Lund University

Ph.D. Thesis, February 2012

Department of Electrical and Information Technology
Lund University
Box 118, SE-221 00 LUND
SWEDEN

This thesis is set in Computer Modern 10pt
with the LaTeX Documentation System

Series of licentiate and doctoral theses
ISSN 1654-790X ; No. 37
ISBN 978-91-7473-264-1


Printed in Sweden by *Tryckeriet i E-huset*, Lund.
January 2012.

*Till Mia och Sigrid*

# Populärvetenskaplig sammanfattning

Idag tar de flesta för givet att man när och var som helst kan komma åt sin e-post, ladda upp bilder till Facebook eller söka kunskap på Wikipedia från sin mobiltelefon eller dator. Den trådlösa teknologi som gjort detta möjligt har utvecklats oerhört det senaste årtiondet, men behöver utvecklas ännu mer för att möta det ökande behovet av trådlös kommunikation.

I denna avhandling har vi undersökt hur man på ett effektivare sätt kan utnyttja de begränsade resurser som finns tillgängliga i form av radiospektrum. Mer specifikt så har vi tittat på s.k. iterativa metoder för att i en mottagarenhet, t.ex. en basstation, på ett effektivt sätt separera information skickad samtidigt från flera användare eller flera antenner. Flerantennssystem, eller MIMO-system (från engelskans multiple-input-multiple-output), är en relativt ny teknik som kan ge en avsevärd ökning i överföringskapacitet. För att fullt ut ta del av denna kapacitetsökning behöver man utveckla mottagaralgoritmer som på ett effektivt och tillförlitligt sätt kan separera signalerna från de olika sändarantennerna. De algoritmer som vi har utvecklat och undersökt i denna avhandling kan användas för att i framtiden skapa trådlösa nätverk med större datakapacitet.

De iterativa mottagaralgoritmer som vi utvecklat består av tre komponenter, som alla samarbetar på ett iterativt sätt för att detektera informationen som skickats från de olika användarna eller antennerna. De tre delarna är kanalestimator, fleranvändardetektor och avkodare. Fleranvändardetektorn separerar signalerna från de olika användarna och avkodaren avkodar de olika skickade meddelandena. För att man ska kunna separera användarna behöver man känna till hur kanalen mellan sändare och mottagare ser ut, d.v.s. hur den har påverkat de olika signalerna.

Den trådlösa kanalen består av alla objekt som befinner sig runt och emellan sändare och mottagare. Dessa objekt kommer att ge upphov till ekon av de

sända signalerna som sedan adderas ihop hos mottagaren. Kanalestimatorn har till uppgift att räkna ut hur dessa ekon ser ut och sedan meddela detta till fleranvändardetektorn. För att kunna beräkna ekonas utseende skickar man vanligtvis kända referenssignaler, tillsammans med de på förhand okända informationsbärande signalerna. För att få hög tillförlitlighet kan man behöva skicka många referenssignaler, speciellt om man har många användare. Dessa signaler tar då upp plats för de informationsbärande signalerna, vilket leder till en förlust i överföringskapacitet. I denna avhandling har vi tittat närmare på en teknik där vi även använder de skickade informationssignalerna, tillsammans med referenssignalerna, för att beräkna kanalen. Detta innebär att vi kan minska den förlust i datakapacitet som uppstår när referenssignaler skickas. Eftersom informationssignalerna är okända från början måste man beräkna ungefärliga värden på dessa. Detta görs med hjälp av fleranvändardetektorn och avkodaren. De tre komponenterna i mottagaren skickar sedan iterativt signaler fram och tillbaka mellan varandra ett flertal gånger, för att till slut få fram pålitliga värden på den skickade informationen.

I de publikationer som utgör stommen i denna avhandling har vi undersökt olika typer av kanalestimator och fleranvändardetektor. Vi har sett att relativt enkla sådana kan leverera bra prestanda. Det är också tydligt i våra resultat att man genom att använda de informationsbärande signalerna i kanalestimatorn kan få högpresterande system med en begränsad mängd referenssignaler. Framtida trådlösa system kan med denna typ av mottagaralgoritmer göras än mer effektiva, vilket alltså behövs för att möta det ökande behovet av trådlös kommunikation.

# Abstract

The traffic in wireless networks has been showing an exponential growth over the last decade. In order to meet the demand, and support a continuation of this growth, the scarce radio resources need to be efficiently used. The use of multiple antenna (MIMO) systems and iterative (turbo) receivers have significantly improved the realizable system performance. Still, many challenges exist in the development of efficient wireless receivers. In this thesis, which is written in the form of a collection of papers, we have investigated and developed iterative receivers with channel estimation for multi-user systems.

Paper I investigates different iterative receiver algorithms for an uplink multi-user MIMO orthogonal frequency division multiplex (OFDM) system. For the given receiver structure, different combinations of multi-user detectors (MUD) and decision-directed channel estimators are compared. The comparison focuses on the complexity-performance tradeoff for the receiver configurations. The results show that low complexity algorithms, despite requiring more receiver iterations, tend to have the lowest overall complexity for a given bit error rate (BER).

Paper II presents how the convergence behavior of an iterative receiver with channel estimation for an uplink multi-user MIMO-OFDM system can be modeled through multi-dimensional extrinsic information transfer (EXIT) charts. Although single-input single-output EXIT charts have been well studied, the multiple input-output case has generally been overlooked in the literature. Such charts are suitable for studying multi-user systems. The presented EXIT chart predictions show good correspondence with the true convergence behavior of the receiver.

Paper III discusses the use of channel measurement data in system evaluations. We discuss and exemplify a number of issues related to the use of such data, and also provide potential solutions. The issues include problems with measurement noise and measurement antenna directivity.

Paper IV investigates the performance gains that can be harvested through base station cooperation in an uplink multi-user MIMO-OFDM system. An

iterative receiver with channel estimation is evaluated using unique mobile dual-link MIMO channel measurement data. The results point at the large performance gains which can be harvested through cooperative processing in a real environment.

Paper V presents and evaluates a number of channel estimation algorithms for an OFDM interleave division multiple access (IDMA) system. We look at different pilot based algorithms as well as decision-directed algorithms being part of the iterative process of the receiver. As for paper I, the comparison focuses on the complexity-performance tradeoff, and the results show that low-complexity algorithms can be competitive alternatives when looking at the overall receiver complexity.

# Preface

The journey towards this thesis started with the underlying question: How can we design efficient channel estimation algorithms for future MIMO-OFDM systems? A short bit into the journey, it stood clear that just looking at the estimator was not enough in the quest for high performing systems. The estimator is an important part of the wireless receiver, but treating it as a stand-alone unit is not sufficient for future systems aiming at high spectral efficiencies achieved through spatial multiplexing. Instead, by allowing it to cooperate with other parts of the wireless receiver the performance, as well as the spectral efficiency, can be improved. Therefore, the question that this thesis is trying to shed some light on is: How can we design efficient iterative receivers incorporating channel estimation?

Answering this question is not straightforward. Designing a wireless receiver is a complicated task, which involves much more than what can be covered by a single thesis. We are therefore restricting the investigations to three functions of the receiver; channel estimation, multi-user/multi-antenna detection and data decoding. More specifically, we have looked at iterative receiver algorithms, where the channel estimator is exploiting decisions on the transmitted data symbols along with pilot symbols. Our work has involved receiver design with a focus on the complexity versus performance tradeoff. This has also included the development and assessment of strategies for performance evaluation.

This thesis thus concludes my work as a Ph.D. student, and consists of two parts. The first part provides an overview of the research field in which I have been working, as well as a brief summary of the included papers and my contributions to these. The second part contains five scientific papers which constitute the main part of my scientific work. The included papers are the following:

[1] P. Hammarberg, F. Rusek and O. Edfors, "Iterative Receivers with Channel Estimation for Multi-User MIMO-OFDM: Complexity and Perfor-

mance," to appear in *EURASIP Journal on Wireless Communications and Networking*.

[2] P. Hammarberg, F. Rusek, P. Salvo Rossi, and O. Edfors, "EXIT Chart Evaluation of a Receiver Structure for Multi-User Multi-Antenna OFDM Systems," in *Proc. IEEE Global Communications Conference (GLOBECOM)*, Dec. 2009.

[3] P. Hammarberg, F. Tufvesson and O. Edfors, "Using Measured Channels in Performance Evaluations of Multi-User OFDM Systems," manuscript, Jan. 2012.

[4] P. Hammarberg, P. Salvo Rossi, F. Tufvesson, O. Edfors, V.-M. Kolmonen, P. Almers, R.R. Muller, A.F. Molisch, "On the Performance of Iterative Receivers for Interfering MIMO-OFDM Systems in Measured Channels," in *Proc. Asilomar Conference on Signals, Systems, and Computers*, Oct. 2008.

[5] P. Hammarberg, F. Rusek and O. Edfors, "Channel Estimation Algorithms for OFDM-IDMA: Complexity and Performance," to appear in *IEEE Transactions on Wireless Communications*.

The following papers, which are not included in the thesis, have also been published during, or in conjunction with, my Ph.D. studies at Lund University:

[6] P. Hammarberg and O. Edfors, "A Comparison of DFT and SVD Based Channel Estimation in MIMO OFDM Systems," in *Proc. IEEE International Symposium on Personal, Indoor and Mobile Radio Communications (PIMRC)*, Sept. 2006.

[7] P. Salvo Rossi, P. Hammarberg, F. Tufvesson, O. Edfors, P. Almers, V.-M. Kolmonen, J. Koivunen, K. Haneda, R.R. Muller, "Performance of an Iterative Multi-User Receiver for MIMO-OFDM Systems in a Real Indoor Scenario," in *Proc. IEEE Global Communications Conference (GLOBECOM)*, Dec. 2008.

[8] P. Hammarberg, W. Shuang, X. Chen, J. Wang, O. Edfors, "Coded IDMA System Performance with Parallel Interleavers," in *Proc. Wireless Advanced (WiAD)*, Jun. 2010.

[9] Y. Zhang,O. Edfors, P. Hammarberg, T. Hult, X. Chen, S. Zhou, L. Xiao, J. Wang, "A General Coupling-based Model Framework for Wideband MIMO Channels," to appear in *IEEE Transactions on Antennas and Propagation*.

# Acknowledgements

First of all I would like to thank my supervisor Prof. Ove Edfors who gave me the opportunity to pursue my Ph.D. studies. With his deep knowledge in the area of communication, enthusiasm and eye for details, he has guided me along the winding path towards this thesis. I am also grateful for the support given by Dr. Fredrik Rusek, who has co-supervised me for the last two years. His sharp mind and enthusiasm for science has been a big inspiration. I would also like to thank Prof. Viktor Öwall, who was my co-supervisor during the first few years. I also thank Dr. Fredrik Tufvesson, for his guidance through the jungle of channel measurements and models. I would also like to thank some research colleagues abroad. Prof. Pierluigi Salvo Rossi at the Second University of Naples, who was a big help during the first few years, and my friends and colleagues at Tsinghua University, foremost Dr. Yan Zhang and Prof. Xiang Chen. I also thank my Finnish friends at Aalto University, for the collaboration within the WILATI project.

Apart from those being directly involved in the scientific work, I would also like to thank my friends, along with current and former colleagues, at the Dept. of Electrical and Information Technology. Dr. Peter Almers for being my mentor and always bringing energy and enthusiasm, Dr. Johan Kåredal for always being helpful and supportive, Lic. Telmo Santos for letting us try his smelly Portuguese sausages, Dr. Anders Johansson for the kayak tours around Malmö, and Johan Lövgren for being my coding guru. I also thank the signal processing gang; Dr. Frida Sandberg, Dr. Ulrike Richter, Dr. Martin Stridh and the others, for entertaining discussions during lunch and coffee breaks. I am also grateful to my friends and colleagues in the Radio Systems corridor; Nafiseh Seyed Mazloum, Meifang Zhu, Rohit Chandra, Taimoor Abbas, Adnan Prlja, Dzevdan Kapetanovic, Tommy Hult, Xiang Gao, Carl Gustafson, Muhammad Atif Yaqoob and Palmi Thor Thorbergsson. I also thank all my other friends at the department. Many thanks also goes to the technical and administrative staff at the department, for their dedicated work and excellent service.

Finally, I would like to thank my family. My mother Monika, and my two

brothers, Tobias and David. A special thanks goes to my grandfather Bertil, who was a big inspiration. I also thank my daughter Sigrid for helping me to put things in perspective. And most importantly, I thank my wife Maria for her unconditional love, patience and support during this long journey.

Peter Hammarberg

# List of Acronyms and Abbreviations

**3D** Three dimensional

**AWGN** Additive White Gaussian Noise

**BER** Bit Error Rate

**BPSK** Binary Phase Shift Keying

**BS** Base Station

**CDF** Cumulative Distribution Function

**CDMA** Code Division Multiple Access

**CE** Channel Estimator

**COST** European COoperation in Science and Technology

**CSI** Channel State Information

**CP** Cyclic Prefix

**DFT** Discrete Fourier Transform

**DPS** Discrete Prolate Spheroidal

**EM** Expectation Maximization

**ESE** Elementary Signal Estimator

**EXIT** EXtrinsic Information Transfer

**FEC** Forward Error correcting Code

**FDMA** Frequency Division Multiple Access

**FFT** Fast Fourier Transform

**ICI** Inter-Carrier Interference

**IDMA** Interleave Division Multiple Access

**IEEE** Institute of Electrical and Electronics Engineers

**IFFT** Inverse Fast Fourier Transform

**IID** Independent and Identically Distributed

**ISI** Inter-Symbol Interference

**ITU** International Telecommunications Union

**LLR** Log-Likelihood Ratio

**LS** Least Square

**MAP** Maximum A-posteriori Probability

**MIMO** Multiple-Input Multiple-Output

**ML** Maximum Likelihood

**MPC** Multi-Path Component

**MRC** Maximum Ratio Combining

**MRT** Maximum Ratio Transmission

**MMSE** Minimum Mean Squared Error

**MSE** Mean Squared Error

**MU** Multiple User / Mobile User

**MUD** Multiple User Detection/Detector

**OFDM** Orthogonal Frequency Division Multiplexing

**OFDMA** Orthogonal Frequency Division Multiple Access

**PCSI** Perfect Channel State Information

**PDP** Power Delay Profile

**PIC** Parallel Interference Cancellation

**SAGE** Space Alternating Generalized Expectation Maximization

**SDMA** Space Division Multiple Access

**SER** Symbol Error Rate

**SISO** Soft-Input Soft-Output

**SIC** Successive Interference Cancellation

**SIR** Signal-to-Interference Ratio

**SNR** Signal-to-Noise Ratio

**SVD** Singular Value Decomposition

**TDMA** Time Division Multiple Access

**QPSK** Quadrature Phase Shift Keying

**WGN** White Gaussian Noise

**ZF** Zero Forcing

# Contents

# Part I

# Overview of the Research Field

# Chapter 1

# Introduction

## 1.1 Background

The history of wireless communication started in the late 19th century, with the work of Marconi, Lodge, Popov, Tesla, Hertz and others [1]. With the groundbreaking technology of radio transmissions, it was possible to transmit signals without cables, e.g., between ships or other moving objects. Furthermore, messages could be broadcasted to many people at the same time, in the form of radio and later TV transmissions. During the 20th century, wireless communication has gone through a remarkable development, which has gone hand in hand with the progress in electronic circuit design. Today, there is a large number of wireless communication systems, both public, military and commercial, sharing the available radio resources.

Over the last few decades, there has been an exponential increase in the amount of information being transmitted over the air. Looking at the first commercial mobile wireless networks, they were only providing analog voice services requiring relatively small portions of the radio spectrum. The breakthrough of personal computers, and more importantly the Internet revolution, has dramatically changed the way people use wireless services. Today, consumers are expecting high-speed Internet access in their mobile devices, wherever they are, which comes at an increased use of radio spectrum. The wireless industry foresees that the mobile data traffic will increase by 35 times between year 2009-2014 [2]. In order to support this rapid growth, larger chunks of radio spectrum need to be made available, and at the same time more efficiently used. The challenge of making more efficient use of the radio spectrum has been taken on by researchers at companies and research institutions around the world, and large improvements have been obtained over the last few decades.

A significant breakthrough came in late 1980's when the adaptive use of multiple-input multiple-output antenna (MIMO) systems was proposed. By using multiple antennas at both transmitter and receiver side, it was shown that parallel channels can be created, all using the same radio spectrum [3, 4]. In theory, the channel capacity increases linearly in the minimum of the number of receive and transmit antennas.

Another important breakthrough occurred around the same time, which was the invention of turbo codes and iterative decoding [5]. With these new codes, performance close to the the Shannon limit can be obtained. The decoding of these codes could be performed iteratively, with several decoding units exchanging information between iterations. The obtained performance was shown to be close to optimal decoding, but with a realizable complexity as compared to optimal algorithms. Since the discovery of turbo codes, the "turbo principle" has been used to reduce complexity of other tasks in the wireless receiver, e.g., equalization, channel estimation and multi-user detection [6]. These methods have further improved the performance and efficiency of wireless receivers.

In the last decade there has been intensive research performed on iterative receivers of various kinds, both for single and multiple antenna systems. The research has provided improvements, and additional understanding, of this type of receivers in various system settings. Furthermore, iterative receivers are already being used in the latest wireless networks being deployed. Never the less, there are still things that have not been fully investigated, e.g., aspects related to low-complexity channel estimation and iterative receiver processing.

In this thesis we are providing additional insight into the performance and behavior of iterative receivers employing channel estimation based on both pilots and detected data symbols. We have investigated the convergence behavior of this type of receivers, and also look at how complexity and performance are related. Furthermore, we have investigated the use of wireless channel measurements when used for performance evaluation of receiver algorithms.

## 1.2 Outline

In the rest of Part I, we will provide additional background to the area of wireless communication, and to the research field of iterative receivers. The purpose is to give a general introduction to the type of systems that have been investigated in the research papers included in the thesis. For a reader who is familiar with the area of modern wireless communication systems, Part I will mainly serve as a refresher.

In Chapter 2 we present the basics of orthogonal frequency division mul-

tiplexing (OFDM), MIMO and multi-user communication. The purpose is to provide an introduction to OFDM and MIMO communication, which have become popular choices for high speed wireless communication systems, and which have been the main technologies for the investigations in the included papers. Furthermore, we go through different ways in which multiple users can share the available radio channel. In this thesis, we have investigated systems exploiting both the code domain and the spatial domain for this purpose.

In Chapter 3, we discuss the multi-user receiver, with a focus on multi-user detection and channel estimation. We discuss ways of achieving these two tasks both with, and without, prior information of the transmitted data symbols. Since we in the included papers in Part II are investigating various iterative receivers for multi-user systems, the purpose of the chapter is to provide a background to this area. Therefore, we also introduce an iterative receiver structure which, in various configurations, has been under investigation in the thesis.

In Chapter 4 we discuss the evaluation of iterative receivers. We briefly discuss the choice of channel models, the use of channel measurements, and means of investigating the convergence behavior of the receiver.

Finally, in Chapter 5, we provide a summary of the included papers, and also point out the specific contributions of the author.

# Chapter 2

# OFDM, MIMO and multi-user systems

During the last century, a number of different approaches have been proposed for efficiently utilizing the available radio spectrum. In order to support multiple simultaneous users in a system, methods for exploiting the frequency, time, code and more recently the spatial domain have been presented. In this chapter we present a subset of these ideas, related to wideband transmissions. The purpose is to provide an introduction to the transmission systems which have been under investigation in the thesis, as well as a general overview of the area. In all of the included papers we are looking at multi-user OFDM communication. In papers I-IV we investigate multiple antenna systems, while Paper V addresses an interleave division multiple access (IDMA) system.

We start this chapter by presenting OFDM, which has become a popular wideband transmission technology in later years. We then review the area of multiple-antenna systems, which can provide large performance gains as compared to traditional single antenna systems, before the basics of multi-user communication is introduced.

## 2.1 Orthogonal Frequency Division Multiplexing (OFDM)

For high data rate systems, the transmission of wideband signals is necessary, which creates challenges for the receiver due to channel induced inter-symbol interference (ISI). For wideband transmissions, the received signal is a super-

position of a number of cyclically shifted and attenuated replicas of the transmitted signal. Delayed replicas of earlier symbols will therefore interfere with the current symbol, creating ISI. As the transmission bandwidth increases, the number of interfering symbols can grow large. This adds significantly to the complexity of equalizer, which needs to handle the ISI. A popular technology to handle ISI channels, and to reduce the equalizer complexity, is OFDM.

The main idea behind OFDM is to divide a frequency selective channel into a set of narrowband subchannels. Over these subchannels, or subcarriers, orthogonal narrowband signals are transmitted in parallel. Since each of these signals experiences flat fading, a simple scalar channel equalization can be performed. Furthermore, since the subcarriers are orthogonal there is essentially no cross talk between signals (for a well designed system), which simplifies the detection process.

In Figure 2.1 a discrete time baseband model of an OFDM system is shown. Starting with the transmitter at the left of the figure, $M$ complex symbols $x[m]$

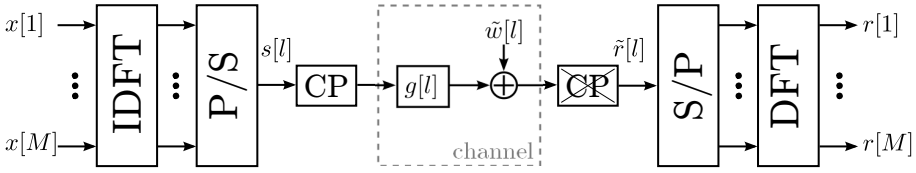


**Figure 2.1:** A baseband OFDM system model.

are fed to the $M$-point inverse discrete Fourier transform (IDFT) block. The IDFT performs the OFDM modulation, where each column of the underlying IDFT matrix corresponds to one of the subcarriers of the OFDM symbol. After a parallel to serial conversion, the time domain signal yields

$$s[l] = \frac{1}{\sqrt{M}} \sum_{m=0}^{M-1} x[m] e^{j2\pi \frac{lm}{M}} , \tag{2.1}$$

for $l = 0, \ldots, M-1$. As can be seen, this is nothing but a sum of complex exponentials, i.e., sine and cosine functions.

The structure of an OFDM symbol is exemplified in Figure 2.2, where a continuous OFDM signal is shown in time and frequency. The time domain signal also contains the CP. Note that all the signal components are orthogonal over an interval $T$.

After the addition of a cyclic prefix (CP), the signal is transmitted over a time dispersive channel with impulse response $g[l]$, which is assumed to be

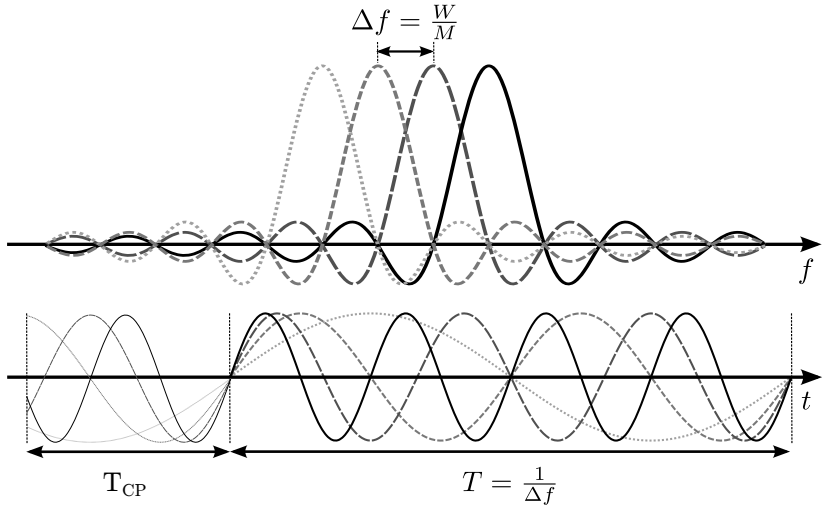


**Figure 2.2:** Frequency and time representation of a OFDM signal.

no longer than the CP. Then, white Gaussian noise (WGN) is added. At the receiver, assuming accurate synchronization and after the removal of the CP, the received time domain signal $\tilde{r}[l]$ contains a superposition of delayed replicas of the transmitted OFDM symbol.

In a time dispersive channel, the CP is needed in order to preserve the orthogonality between the subcarriers. The requirement for orthogonality is that all delayed replicas of a transmitted OFDM symbol overlap in an observation interval of length $M$ (or $T$ in continuous time). This is achieved through an addition of a CP. Orthogonality is required for a discrete Fourier transform (DFT) to perfectly separate the different signal components of the OFDM symbol at the receiver. Without the CP, replacing it with an empty guard interval, the delayed signals would partly fall outside the observation interval, and orthogonality between subcarriers would be lost. It should be noted that this orthogonality problem can be solved through post-processing at the receiver [7].

An alternative mathematical view of the guard interval is that it turns the linear convolution of the signal and the channel impulse response into a cyclic convolution. The received signal can then be written as

$$\boldsymbol{r} = DFT(IDFT(\boldsymbol{x}) \circledast \boldsymbol{g} + \tilde{\boldsymbol{w}}) = \boldsymbol{x} \odot \boldsymbol{h} + \boldsymbol{w}\,, \tag{2.2}$$

where $\boldsymbol{r}$, $\boldsymbol{x}$, $\boldsymbol{g}$, $\tilde{\boldsymbol{w}}$ and $\boldsymbol{w}$ are vectors collecting the $M$ samples of the received and transmitted symbols, channel impulse response, noise, and transformed noise,

respectively. Furthermore, $\boldsymbol{h} = DFT(\boldsymbol{g})$ is the channel frequency response, and $\circledast$ and $\odot$ represent circular convolution and element wise multiplication, respectively.

## 2.2 Multiple antenna systems

Even though multiple antennas have been used almost since the invention of radio to achieve directive antennas and to harvest diversity [8,9], a fundamental breakthrough came in the late 1980's [3] with the discovery of spatial multiplexing. Several important contributions on the properties of MIMO systems were made during the 1990's [4, 10], and the area is still heavily researched.

As mentioned above, multiple antennas can be used for beamforming, diversity or spatial multiplexing. By applying suitable transmission schemes, e.g., space-time codes, these different techniques can be exploited in different ways. A transmission scheme can be designed to harvest one, or a combination of, three different gains; array gain, diversity gain and multiplexing gain. It should be noted that the three gains cannot simultaneously be fully exploited. The choice of transmission scheme therefore involve a tradeoff between the three, where focus is often placed on the latter two who potentially have larger gains [11]. Below, we briefly go through the different gains one at a time. For a more detailed discussion on MIMO and space-time codes we refer, e.g., to [8] or [12].

For the presentation of the gains of multiple antenna systems we consider a narrowband baseband model. Note that in the case of a wideband system, OFDM can be used to obtain a set of parallel narrowband sub MIMO systems. For a system with $K$ transmit and $N$ receive antennas, the received signal can be expressed as

$$\boldsymbol{r} = \boldsymbol{H}\boldsymbol{x} + \boldsymbol{w}\,, \tag{2.3}$$

where $\boldsymbol{r} \in \mathbb{C}^{N\times 1}$ is the received signal, $\boldsymbol{H} \in \mathbb{C}^{N\times K}$ the MIMO channel matrix, $\boldsymbol{x} \in \mathbb{C}^{K\times 1}$ the transmitted symbols, and $\boldsymbol{w} \in \mathbb{C}^{N\times 1}$ is the receiver noise ($\sim \mathcal{CN}(\boldsymbol{0}, \sigma_w^2\boldsymbol{I})$ distributed). If nothing else is stated, we will assume that $\boldsymbol{H}$ has independent zero mean complex Gaussian distributed entries.

### 2.2.1 Array gain

With multiple antenna elements at the receiver, more of the transmitted energy can be collected, thus creating an antenna array gain. By coherently collecting the signal received at the different antennas, the average SNR as compared to a single receive antenna system is increased. Assuming $K = 1$ transmit antenna, the optimal operation is maximum ratio combining (MRC) where the signal

at the different antennas are combined coherently and weighted according to strength, i.e.,

$$z = \boldsymbol{H}^H \boldsymbol{r} = \|\boldsymbol{H}\|^2 x + \boldsymbol{H}^H \boldsymbol{w} \,. \tag{2.4}$$

With this type of receive beamforming, an SNR gain equal to the number of antennas can be achieved, as compared to a single antenna systems.

If we instead have multiple antennas at the transmitter only, along with channel state information (CSI), maximum ratio transmission (MRT) can be performed where transmit beamforming focus the energy towards the receiver. The maximum achieved array gain is in this case equal to the number of transmit antennas. With multiple antennas at both ends, MRC and MRT can be combined to achieve dominant eigenmode transmission In this case, an SNR gain equal to the strongest eigenmode of the channel is achieved.

### 2.2.2 Diversity gain

In a multi-path channel, the delayed replicas of the transmitted signal will either add constructively or destructively, depending on their relative phase. If the phase changes, e.g., due to motion, the received power level will fluctuate, which is generally referred to as fading. When an antenna is in a fading dip the instantaneous signal-to-noise ratio (SNR) will be low, resulting in unreliable communication. If multiple antennas are used, spatial diversity techniques can be used to reduce the destructive fading of the channel. The probability that multiple independent antenna channels simultaneously are in a fading dip is the product of their individual fading probabilities. Through the use of diversity schemes, the average symbol-error-rate (SER) is therefore reduced for a given average SNR. At high SNR, we have that [8]

$$SER \propto SNR^{-\mu} \,, \tag{2.5}$$

where $\mu$ is referred to as the diversity order. In the single antenna case the diversity order is unity.

With multiple antennas at the receiver, a number of diversity combining techniques can be used to increase the diversity order, e.g., MRC or antenna selection, where the antenna with the best signal is selected. A diversity order equal to the number of receive antennas can be achieved. Transmit diversity can, e.g., be achieved through the use of space-time codes, with the most famous being the Alamouti code which can achieve full diversity with two transmit antennas [13]. It should be noted that the maximum achievable diversity order is limited by the product of the number of transmit and receive antennas, i.e., $\mu \leq K \cdot N$.

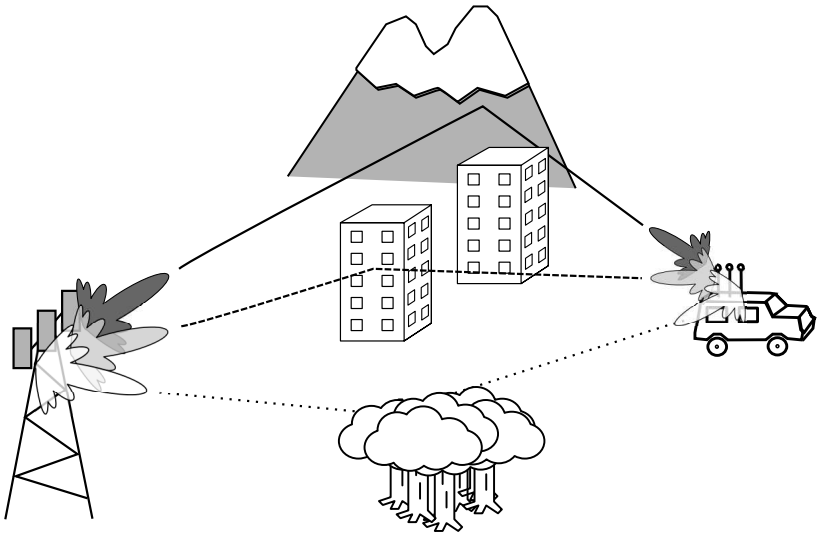

**Figure 2.3:** An example of a MIMO link, where the transmitting base station creates three different spatial beams towards the intended user.

### 2.2.3 Multiplexing gain

The multiplexing gain is the most recent discovery of multiple antenna usage, and is exploited in spatial multiplexing. The gain refers to the increased degrees of freedom made available for communication through the use of multiple antennas. For a system composed of $K$ transmit, and $N$ receive antennas, a maximum multiplexing gain of $\min(K, N)$ can be achieved [14]. Even though a tradeoff between multiplexing gain and diversity gain can be obtained through appropriate transmission schemes, we will for the rest of this section focus on pure spatial multiplexing.

The idea behind spatial multiplexing is to exploit the spatial properties of the wireless channel to transmit multiple data streams simultaneously over the same bandwidth, which is illustrated in Figure 2.3. Since the transmit antennas are located at different spatial positions, they will be given different spatial signatures by the channel. Under the assumption of a rich scattering channel, and with antennas being sufficiently separated in space, each of the transmitted signals from each antenna will experience a unique spatial signature. A receiver equipped with multiple antennas can then separate the different signals through their spatial signatures. In this way several signals can be spatially multiplexed, which can significantly increase the transmission capacity.

The potential gains of spatial multiplexing can be exemplified by performing a singular value decomposition (SVD) of the channel matrix. Let $\boldsymbol{H} = \boldsymbol{U}\boldsymbol{\Sigma}\boldsymbol{V}^H$, where $\boldsymbol{U}$ and $\boldsymbol{V}$ are unitary matrices, $\boldsymbol{\Sigma}$ a diagonal matrix collecting the singular values of $\boldsymbol{H}$, and $(\cdot)^H$ denotes the Hermitian transpose operation. The number of non-zero singular values of $\boldsymbol{H}$ equals $\min(M, N)$, given that $\boldsymbol{H}$ is full rank. By multiplying the transmitted vector with $\boldsymbol{V}$, and the received vector with $\boldsymbol{U}^H$, the resulting input-output model becomes

$$\tilde{\boldsymbol{r}} = \boldsymbol{U}^H\boldsymbol{r} = \boldsymbol{U}^H\left((\boldsymbol{U}\boldsymbol{\Sigma}\boldsymbol{V}^H)\boldsymbol{V}\boldsymbol{x} + \boldsymbol{w}\right) = \boldsymbol{\Sigma}\boldsymbol{x} + \tilde{\boldsymbol{w}}. \tag{2.6}$$

As seen, through the transmit and receive filtering, the channel becomes transformed into a number of parallel, orthogonal, subchannels which can be used for communication.

From an information theoretic point of view, the capacity of a MIMO channel can be increased by a factor of $\min(K, N)$, as compared to a single antenna case. For the case of no channel state information at the receiver, the capacity is given by [10]

$$C = \log_2 \det\left(\boldsymbol{I} + \frac{\rho}{N}\boldsymbol{\Sigma}\boldsymbol{\Sigma}^H\right) = \sum_{i=1}^{r} \log_2\left(1 + \frac{\rho}{N}\Sigma_r^2\right)\ bits/s/Hz, \tag{2.7}$$

where $r$ is the rank of the channel, $\Sigma_r$ the r:th entry of $\boldsymbol{\Sigma}$, and $\rho$ is the average SNR per receiver branch. If the channel is full rank we reach a capacity increase of $r = \min(K, N)$ at high SNR. Due to this potential gain in capacity, MIMO has become a key technology for future high speed wireless systems.

## 2.3 Multi-user systems

In most wireless communication systems, multiple users are to be served with data. To avoid that inter-user interference deteriorates the system performance, suitable communication strategies need to be applied. The purpose of these is to allow the different user signals to be separated at the receiver. The receiver can either be a base station, who's task is to detect the signals of all users, or individual users who are only interested in their own data.

The separation of the different signals can be performed in any of the available dimensions, i.e., time, frequency, code or space. Below we will go through the basics for the different transmission strategies exploiting the mentioned dimensions.

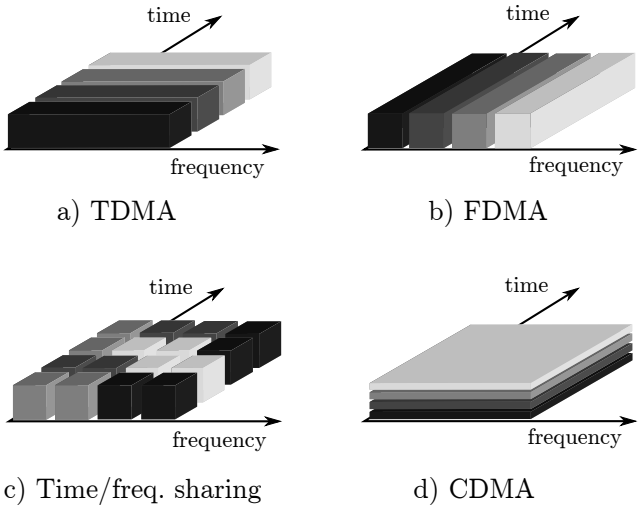


**Figure 2.4:** The separation of users can be performed in, e.g., a) time, b) frequency, c) a combination of time/frequency and d) code domains.

### 2.3.1 TDMA and FDMA

The conceptually simplest domains for user separation are time and frequency. In time-division multiple-access (TDMA), different users are scheduled to transmit at different time slots. That is, each user is given a short (recurring) time slot, and transmit their signal within this time frame having the full system resources available. The users are thus transmitting successively, orthogonal in time, as shown in Figure 2.4a. In a time dispersive channel, guard intervals may be needed between the users to avoid inter-user interference. Furthermore, appropriate synchronization is needed, especially if the difference in propagation delay is large between users.

As an alternative to TDMA, frequency division multiple access (FDMA) can be used. In FDMA the available frequency spectrum is divided into a number of parallel subchannels, as illustrated in Figure 2.4b. The users are then assigned to different spectral subchannels, and thus separated in frequency. In general, e.g., due to spectral broadening caused by transceiver imperfections, the channels need to be separated by guard bands which reduce the spectral efficiency. One way to overcome this, and to further add resistance to channel delay, is to separate the users through the use of OFDM.

As seen in Section 2.1, OFDM divides the available spectrum into a number of orthogonal subchannels. A subset of these subchannels can then be

assigned to a specific user, thus allowing multiple users receiving/transmitting within the same OFDM symbol. Such approaches, generally referred to as orthogonal-FDMA (OFDMA), also have the advantages that the extension to two dimensional resource sharing in time/frequency comes natural. In Figure 2.4c such sharing is exemplified, where different users are assigned certain regions in the resulting time-frequency grid. This strategy is, e.g., used in LTE [15]. Furthermore, a flexible scheduling also opens up the possibility to obtain a multi-user diversity gain by assigning users to grid points where their respective channels are good [15].

### 2.3.2 Spread spectrum systems

An alternative to sharing the available resources in the time or frequency domains is to exploit the code domain, by using spread spectrum techniques. In TDMA/FDMA each user is transmitting with as high data rate as possible within the given orthogonal subchannel. For spread spectrum type of systems, the users transmit simultaneously at low data rates within the same time frame and bandwidth, as illustrated in Figure 2.4d. This can be interpreted as if the users are consuming more spectrum than they "need" in order to support a given data rate. This is achieved by performing a bandwidth expansion of the original data signal before transmission. For a definition of, and a discussion on, spread spectrum communication see [16].

Since these type of systems tend to be wideband in nature, they will experience ISI. One way to handle the ISI channel, as discussed earlier, is to use OFDM. In that case the spreading is performed over the different subcarriers, and possibly over several OFDM symbols [17]. This is, e.g., performed in Paper V, where we investigate an OFDM-IDMA system.

Below, two different, yet similar, approaches to spread spectrum communication will be briefly discussed; code division multiple access (CDMA) and interleave division multiple access (IDMA).

#### CDMA

In CDMA the bandwidth expansion is most commonly achieved by assigning unique, ideally uncorrelated, wideband spreading sequences to the users. The users then multiply their data symbols with the spreading sequence before transmitting the resulting wideband signal. At the receiver, user separation can, e.g., be achieved by a correlating filter matched to the specific spreading sequence. Under the assumption of an pure additive WGN (AWGN) channel and perfectly uncorrelated spreading sequences, the outputs are noisy versions of the original data symbols.

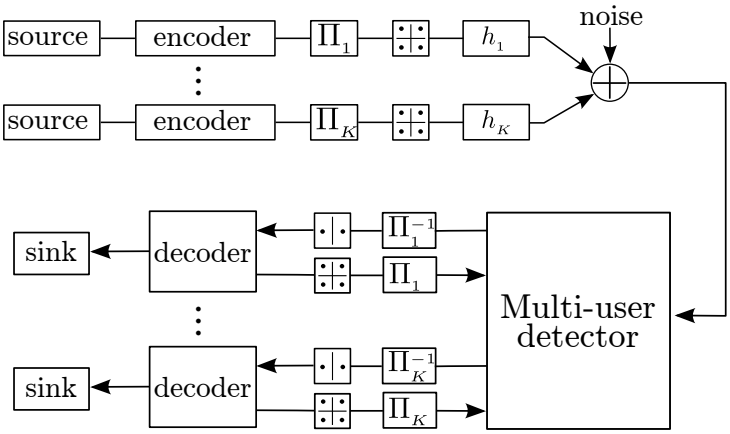


**Figure 2.5:** A baseband IDMA system model.

Many other receiver algorithms exist, ranging from the optimal joint maximum likelihood (ML) detector to suboptimal low-complexity approaches based on, e.g., successive interference cancellation and iterative decoding. Please refer [18] and [19] for detailed overviews. There also exists proposals for CDMA systems where the entire bandwidth expansion is devoted to coding [20,21]. For example, in [21] low-rate codes together with user specific scrambling codes are proposed. Despite being optimal[1], such CDMA systems will require more complex receiver structures.

### IDMA

An alternative spread spectrum technology, being born out of the increased understanding of turbo-like systems and iterative decoding in the early 2000's, is IDMA [23]. In IDMA user separation is obtained through user-specific interleavers, rather than spreading/scrambling as in CDMA. An illustration of a baseband uplink IDMA system is shown in Figure 2.5.

At the transmitter, spreading is achieved by a low rate code, often a suboptimal choice of a concatenation between an error correcting code and a repetition code. The code bits are then interleaved by a user specific interleaver $\Pi_k$, followed by symbol mapping, before transmitted over the wireless channel. In this way the entire bandwidth expansion can, potentially, be used for coding. With this structure of the transmitted signal, a relatively simple

[1]The capacity of the multiple access channel is maximized if the entire bandwidth expansion is devoted to coding [22].

iterative multi-user receiver structure can be constructed, showing close to single user performance [23]. The details of the receiver structure is outlined in Section 3.1.2. As mentioned earlier, in Paper V an OFDM-IDMA system is considered, where we compare low-complexity channel estimation approaches in terms of complexity and performance.

### 2.3.3 SDMA

The separation of multiple users can also be performed in the spatial domain, through space division multiple access (SDMA). One direct way to achieve this, which has been used since the early days of radio, is directive antennas. In its simplest form, a base station with narrow beam antennas can direct the antenna towards a specific user, obtaining a good signal-to-interference ratio (SIR) given that no co-located users exist (in the angular domain). In cellular systems, directional antennas are commonly used to divide a cell into different sectors in the angular domain, thus achieving user separation.

More recently with the increased research on array processing, and with improved digital signal processing capabilities, antenna arrays arose as potential tools for adaptive user separation in the spatial domain [24]. With so called smart antenna arrays, the effective antenna array pattern can be changed adaptively. This is achieved through appropriate pre- or post-processing, where complex-valued weights are used to steer the amplitude and phase at the different antenna elements. The array pattern can then be formed in order to, e.g., maximize SNR or to minimize interference for a specific user.

Since the breakthrough of MIMO communication, in particular spatial multiplexing, the area of multi-user MIMO (MU-MIMO) has received considerable attention (see, e.g., [25–27]). In such systems, the base station is equipped with multiple antennas, and the users with one or more antennas. If the users are assumed to be synchronized, the uplink may be seen as a conventional point-to-point MIMO system. Obviously the properties of the resulting equivalent MIMO channel are different as compared to a conventional MIMO system. For example, users distributed over a larger area potentially result in larger power variations and lower inter-antenna correlation. Additionally, the physical separation between users restrict the use of cooperative transmissions. Nevertheless, most of the receiver algorithms available for MIMO can generally be applied to the MU-MIMO uplink, which will be further discussed in Chapter 3. As mentioned previously, we consider MU-MIMO-OFDM communication in the included papers I-V where we, e.g., compare different receivers incorporating channel estimation in Paper I.

For the downlink channel, the design of efficient transmit schemes has generated a large amount of research. The proposed transmission schemes range

from the optimal dirty paper coding, to the simple zero-forcing precoding. For an overview, please consult, e.g., [28].

# Chapter 3

# Multi-user receivers for wireless systems

Finding the data symbols transmitted simultaneously, by a number of users, over a wireless channel is a challenging task. The receiver, e.g., a base station, commonly separates the task of finding the transmitted data bits into synchronization, channel estimation and detection/decoding. As previously mentioned, uplink multi-user systems based on both MIMO-OFDM and OFDM-IDMA have been investigated in the included papers. More precisely, we have investigated iterative receiver algorithms incorporating channel estimation, multi-user detection (MUD) and data decoding, where focus has been placed on the former two. This chapter therefore focuses on providing a brief overview of these two tasks, where we restrict the discussion to OFDM communication. For more details on synchronization and coding/decoding we refer to standard text books, such as [29] and [30].

We will start by describing MUD strategies for MU-MIMO systems, ranging from the optimal ML detector to low complexity suboptimal approaches. Then we proceed with a description of the IDMA specific MUD. We then take a closer look at pilot based and decision-directed channel estimation. At the end of the chapter we describe the type of iterative receiver structure used in the included papers.

## 3.1 Multi-User Detection (MUD)

For multi-user systems based on TDMA and FDMA, an advanced MUD is not needed as long as the orthogonal properties of the user channels are preserved.

On the other hand, for non-orthogonal systems, such as spread spectrum and MU-MIMO, a well designed MUD can significantly improve performance. In this section we first consider MUD schemes for MU-MIMO systems, before the specific IDMA MUD is presented. For MUD in CDMA we refer to, e.g., [18,19].

### 3.1.1 Uplink MU-MIMO detection

As mentioned before, most detection algorithms developed for MIMO are applicable to synchronous uplink MU-MIMO systems. In this section we start by briefly reviewing MIMO detection algorithms producing hard decisions on the transmitted symbols. Then, algorithms producing soft decisions, exploiting prior information about the received information bits. The latter class is suitable to use as part of an iterative receiver, exchanging information with the data decoders. We assume that the MIMO detection and data decoding tasks are separated, with a note that joint processing could be performed, at the cost of an increased receiver complexity. Since the presented detection approaches are applicable to both single and multi-user systems, we will interchangeably use the words *transmit antenna* and *user*. For the presentation of the different algorithms, we use the narrowband model given in (2.3).

#### Hard decisions

If we have no prior information available, the optimal detector is the ML detector which, for the model given in (2.3), selects the transmitted symbols which minimize the Euclidean distance metric

$$\hat{\boldsymbol{x}}_{ML} = \min_{\boldsymbol{x} \in \mathcal{X}^K} \|\boldsymbol{r} - \boldsymbol{H}\boldsymbol{x}\|^2 \,, \tag{3.1}$$

where $\mathcal{X}^K$ is the set of all possible transmitted sequences. In order to find $\hat{\boldsymbol{x}}_{ML}$, the receiver needs to compute $\|\boldsymbol{r} - \boldsymbol{H}\boldsymbol{x}\|^2$ for all possible sequences. This process can be visualized through a tree search [31], where each sequence corresponds to a path leading from the root up to a leaf node, as illustrated in Figure 3.1 for binary phase shift keying (BPSK), and two transmit and receive antennas. The tree can be obtained by first performing a QL-factorization of the channel matrix, $\boldsymbol{H} = \boldsymbol{Q}\boldsymbol{G}$, where $\boldsymbol{Q}$ is a unitary matrix, and $\boldsymbol{G}$ a lower triangular matrix. By multiplying the received signal with $\boldsymbol{Q}^H$, the equivalent received signal is given by

$$\tilde{\boldsymbol{r}} = \boldsymbol{G}\boldsymbol{x} + \tilde{\boldsymbol{w}} \,, \tag{3.2}$$

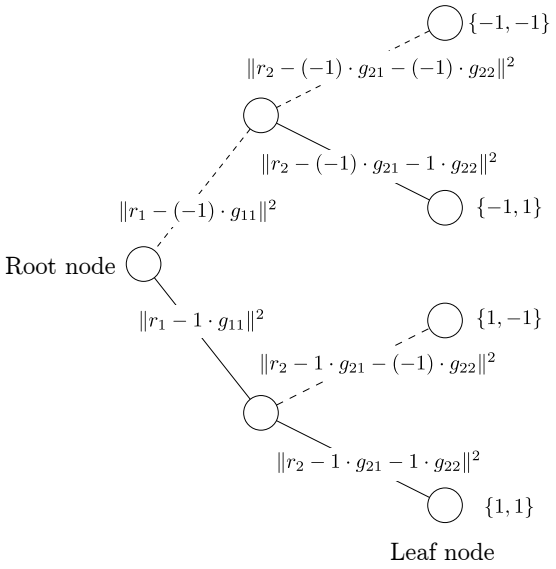


**Figure 3.1:** Code tree

where $\tilde{\boldsymbol{r}} = \boldsymbol{Q}^H \boldsymbol{r}$, and $\tilde{\boldsymbol{w}} = \boldsymbol{Q}^H \boldsymbol{w}$. Since $\boldsymbol{Q}$ is unitary, $\tilde{\boldsymbol{w}}$ and $\boldsymbol{w}$ have the same Gaussian distributions. For the example in Figure 3.1, (3.2) can be written

$$\begin{bmatrix} r_1 \\ r_2 \end{bmatrix} = \begin{bmatrix} g_{11} & 0 \\ g_{21} & g_{22} \end{bmatrix} \begin{bmatrix} x_1 \\ x_2 \end{bmatrix} + \begin{bmatrix} \tilde{n}_1 \\ \tilde{n}_2 \end{bmatrix}. \tag{3.3}$$

In Figure 3.1, we have included the branch metrics for the transitions between pair of nodes. The solution to (3.1) is then found by summing the branch metrics from the root to all of the different leaf nodes, before choosing the path with the smallest distance value.

The number of leaf nodes to visit equals $n = 2^{qK}$, where $q$ is the number of bits per constellation point, and $K$ the number of transmit antennas. If the number of users is high, and large constellations are used, finding the ML solution by visiting all leaf nodes becomes infeasible. One popular approach to avoid this is sphere decoding, where the code tree is searched under a constraint $R$ on the total distance [32]. In principle, sphere decoding works as follows. If the accumulated distance of a branch, before reaching a leaf node, is larger than than $R$, all sequences corresponding to that branch are discarded. If $R$ is chosen well, only a small number of leaf nodes are visited, leading to a largely decreased complexity as compared to an exhaustive search. Despite the reduction, the average complexity is still exponential [33].

As an alternative to the tree search based algorithms, sub-optimal linear receiver algorithms are attractive due to their low complexity. These include the minimum mean square error (MMSE) detector, and zero-forcing (ZF) detector [8]. Taking a look at the ZF detector, it minimizes the same Eucledian distance metric as the ML detector, but without being constrained to the valid symbol positions. That is, the ZF detector is derived as

$$\tilde{\boldsymbol{x}}_{ZF} = \min_{\boldsymbol{x}\in\Re^K} \|\boldsymbol{r} - \boldsymbol{H}\boldsymbol{x}\| = (\boldsymbol{H}^H\boldsymbol{H})^{-1}\boldsymbol{H}^H\boldsymbol{y}\,. \tag{3.4}$$

The final decision is then given by mapping $\tilde{\boldsymbol{x}}_{ZF}$ to the closest valid data vector. One of the drawbacks with this simple approach is the well known noise enhancement problem for ill conditioned channel matrices. The problem can, e.g., be somewhat alleviated through the use of the MMSE detector [8].

**Soft decisions**

If the MU-MIMO detector is to be used as part of an iterative receiver, it is essential that it can exploit and produce soft values on the transmitted information bits. In general, the soft information is exchanged between the different components of an iterative receiver in the form of log-likelihood-ratio (LLR) values on the transmitted bits. More precisely, extrinsic LLRs are exchanged as discussed below.

With prior information available, the optimal detector is given by the symbol wise maximum *a posteriori* probability (MAP) detector. Considering soft outputs, the detector produces conditional *a posteriori* LLR values on the transmitted information bits $b_i$, for $i = 1 \ldots qK$, i.e.,

$$\Lambda(b_i|\boldsymbol{r}) = \ln\frac{p(b_i=1|\boldsymbol{r})}{p(b_i=0|\boldsymbol{r})} \tag{3.5}$$

$$= \ln\frac{p(\boldsymbol{r}|b_i=1)p(b_i=1)/p(\boldsymbol{r})}{p(\boldsymbol{r}|b_i=0)p(b_i=0)/p(\boldsymbol{r})} \tag{3.6}$$

$$= \underbrace{\ln\frac{p(\boldsymbol{r}|b_i=1)}{p(\boldsymbol{r}|b_i=0)}}_{\Lambda_{ext}(b_i)} + \underbrace{\ln\frac{p(b_i=1)}{p(b_i=0)}}_{\Lambda_a(b_i)}, \tag{3.7}$$

where $\Lambda_{ext}(b_i)$ and $\Lambda_a(b_i)$ are the extrinsic and *a priori* LLR values, respectively. The extrinsic values play an important role in iterative decoding, since they are exchanged between the decoding units. The values correspond to the independent information produced in each unit, and becomes *a priori* values for the next unit.

For the considered system model, the extrinsic LLR values can then be evaluated as

$$\Lambda_{ext}(b_i) = \ln\left(\frac{\sum_{\boldsymbol{x}:b_i=1}\exp\left(-\frac{\|\boldsymbol{r}-\boldsymbol{H}\,\boldsymbol{x}\|^2}{\sigma_w^2}\right)}{\sum_{\boldsymbol{x}:b_i=0}\exp\left(-\frac{\|\boldsymbol{r}-\boldsymbol{H}\,\boldsymbol{x}\|^2}{\sigma_w^2}\right)}\right). \tag{3.8}$$

As for the ML detector, the MAP detector has a prohibitive complexity in most situations, and more practical approaches are therefore needed.

An attractive set of low-complexity alternatives to the MAP detector is given by interference canceling detectors. Instead of solving the joint detection problem, a per transmit antenna solution is obtained. We restrict the presentation to parallel interference cancellation (PIC), where outputs on all transmitted symbols are produced in parallel. The alternative is successive interference cancellation, where one transmitted symbols is processed at a time.

From the perspective of the $j$:th user, (2.3) can be rewritten as

$$\boldsymbol{r} = \boldsymbol{h}_j x_j + \sum_{k\neq j}\boldsymbol{h}_k x_k + \boldsymbol{w}\,, \tag{3.9}$$

where $\boldsymbol{h}_k$ is the $k$:th column of $\boldsymbol{H}$. If we set $\boldsymbol{r}_j = \boldsymbol{h}_j x_j$ the soft interference canceled output for user $j$, at the $i$:th iteration, is given by

$$\hat{\boldsymbol{r}}_j^{(i)} = \boldsymbol{r} - \sum_{k\neq j}\boldsymbol{h}_k \tilde{x}_k^{(i-1)}\,, \tag{3.10}$$

where $\tilde{x}_k^{(i-1)}$ are the soft information symbols available from the previous iteration. The cancellation is performed in parallel for all users/antennas.

Once the interference canceled outputs are available, different combining filter techniques can be applied to obtain the symbol outputs. Appropriate filters range from the simple spatial matched filter, which maximizes the useful received power, to the interference aware MMSE filter. For the former, we have that

$$\hat{x}_j^{(i)} = \frac{\boldsymbol{h}_j^H}{\|\boldsymbol{h}_k\|^2}\,\hat{\boldsymbol{r}}_j^{(i)}\,, \tag{3.11}$$

with LLRs produced as (in case of BPSK)

$$\Lambda_j^{(i)} = \frac{2\,\|\boldsymbol{h}_k\|^2}{\sigma_j^2}\,\hat{x}_j^{(i)}\,, \tag{3.12}$$

where $\sigma_j^2$ is the variance of the residual interference plus noise term for user $j$, given by

$$\sigma_j^2 = \sigma_w^2 + \sum_{k \neq j} \left| \boldsymbol{h}_k^H \boldsymbol{h}_j \right|^2 \left( 1 - |\tilde{x}_k^{(i-1)}|^2 \right). \tag{3.13}$$

In Paper I, we evaluate the performance and complexity of the matched filter approach, along with other MUDs when used in an iterative receiver.

### 3.1.2 IDMA detection

As mentioned in Section 2.3.2, in IDMA the different users are assigned different unique interleavers. User separation can then be performed by a relatively simple iterative interference canceling MUD, exploiting *a priori* information made available by the channel decoders. An illustration of a baseband uplink IDMA system with $K$ users can be found in Figure 2.5.

At the IDMA receiver, multi-user detection is obtained through an iterative symbol-by-symbol based soft interference cancellation detector. The detector, commonly referred to as an elementary signal estimator (ESE) [23], derives extrinsic LLRs $\Lambda_{ESE}(b_k)$ on the transmitted (coded) bits, assisted by soft symbol estimates provided by a block of $K$ data decoders. The LLR outputs are then fed to the data decoders, and the receiver continues to iterate between the two LLR producing units.

The LLR outputs of the ESE are derived under the assumption that the noise plus interfering signals follow a Gaussian distribution. In Paper V we consider an OFDM-IDMA transmitting QPSK symbols over a frequency selective channel. In this section, for notational clarity we assume a real valued narrowband single receive/transmit antenna system. The received baseband signal at time instance $s$ is then given by

$$r[s] = \sum_{k=1}^{K} h_k x_k[s] + w[s], \tag{3.14}$$

where $r[s]$ is the received signal, $h_k$ the channel attenuation for the $k$:th user, $x_k[s]$ the symbol transmitted by the $k$:th user, and $w[s]$ is noise. In the perspective of the $j$:th user, the received signal may be written

$$r[s] = h_j x_j[s] + \sum_{k \neq j} h_k x_k[s] + n[s] = h_j x_j[s] + \xi_j[s], \tag{3.15}$$

where $\xi_j[s] \sim \mathcal{N}(m_{\xi_j[s]}, \sigma^2_{\xi_j[s]})$, is collecting both noise and interference. Estimates of the mean, $m_{\xi_j[s]}$, and variance, $\sigma^2_{\xi_j[s]}$, can be derived from *a priori*

information provided by the data decoders [23, 34]. For the given Gaussian model, the LLRs are given by (in case of BPSK)

$$\Lambda_{ESE}(x_j[s]) = 2h_j \frac{r[s] - m_{\xi_j[s]}}{\sigma^2_{\xi_j[s]}} \,. \tag{3.16}$$

The ESE is here presented for a real valued ISI free channel, but has been derived for ISI channels in [23], and complex multi-path channels with complex symbols in [35]. The extension to multi-carrier communication is found in, e.g [36], and to multiple antenna systems in [37]. As we have mentioned before, Paper V investigates decision-directed channel estimation for an OFDM-IDMA system, where we consider QPSK transmission over a complex channel.

## 3.2 Channel estimation

In most communication systems the wireless channel needs to be estimated at the receiver in order to allow for decoding of the transmitted message. An efficient channel estimator is thus an important part of the wireless receiver. As we have seen, the MUD techniques we have reviewed make use of CSI, i.e., knowledge of $\boldsymbol{H}$, when performing user separation. If the CSI is unreliable, so will the separation and detection be. The design of the estimator is therefore an important piece of the receiver puzzle.

Even though there exists so called blind channel estimation techniques which only exploit statistical properties of the transmitted signal [38–40], known pilot symbols are generally transmitted for practical reasons. These reasons include high complexity and slow convergence. Furthermore, pilot symbols are also exploited for time and frequency synchronization. In addition to using known pilot symbols, decisions on transmitted data symbols can be used to improve the quality of the channel estimate. This can also help to reduce the amount of pilot symbols which are needed, leading to an improved spectral efficiency. The cost of such decision-directed estimation is generally an increase in the estimator complexity. This is seen, e.g., in papers I and V, where we compare a number of decision-directed channel estimation algorithms in terms of complexity and performance.

In Sections 3.2.1 and 3.2.2, we go through the basics of pilot based channel estimation, and iterative decision-directed estimation, respectively, for single antenna systems. The discussion is then extended to multi-user and MIMO systems in Section 3.2.3. We will focus on channel estimation for OFDM systems.

### 3.2.1 Pilot based estimation

A model for the received baseband signal in a single antenna OFDM system was given in (2.2), which can be written equivalently as

$$\boldsymbol{r} = \boldsymbol{X}\boldsymbol{h} + \boldsymbol{w}\,, \tag{3.17}$$

where $\boldsymbol{X}$ is a diagonal matrix collecting the transmitted complex symbols on all $M$ subcarriers, $\boldsymbol{h}$ the complex valued frequency response, and $\boldsymbol{w}$ a vector containing complex WGN. For simplicity, we assume that all entries of $\boldsymbol{X}$ are known to the receiver, i.e., it contains only known pilot symbols. It should be noted that pilot symbols are often transmitted on dedicated subcarriers in specific OFDM symbols, and we briefly discuss pilot symbol placement later in this section.

A simple least square (LS) estimate of the frequency response can be obtained by multiplying the received vector with the inverse of the transmitted symbols. That is, the estimate is given by

$$\hat{\boldsymbol{h}}_{\mathrm{LS}} = \boldsymbol{X}^{-1}\boldsymbol{r}\,. \tag{3.18}$$

The LS estimator, as presented above, does not exploit the frequency correlation inherent in OFDM systems.

A more potent alternative is to produce an MMSE estimate of the frequency response. This is achieved by solving

$$\hat{\boldsymbol{h}}_{\mathrm{MMSE}} = \arg\min_{\hat{\boldsymbol{h}}(\boldsymbol{r})} \mathbb{E}\left\{ \left\| \boldsymbol{h} - \hat{\boldsymbol{h}}(\boldsymbol{r}) \right\|^2 \right\}, \tag{3.19}$$

where $\hat{\boldsymbol{h}}(\boldsymbol{r})$ indicates that the estimate is based on the received signal $\boldsymbol{r}$. Restricting to linear solutions of this problem, and assuming that $\boldsymbol{h}$ is zero mean, it can be shown that [41]

$$\hat{\boldsymbol{h}}_{\mathrm{MMSE}} = \mathbf{R}_{\boldsymbol{hr}}\mathbf{R}_{\boldsymbol{rr}}^{-1}\boldsymbol{r}\,, \tag{3.20}$$

where $\mathbf{R}_{\boldsymbol{hr}} = \mathbb{E}\{\boldsymbol{h}\boldsymbol{r}^H\}$ and $\mathbf{R}_{\boldsymbol{rr}} = \mathbb{E}\{\boldsymbol{r}\boldsymbol{r}^H\}$ are correlation matrices.

For the received signal in (3.17), we have that

$$\mathbf{R}_{\boldsymbol{hr}} = \mathbf{R}_{\boldsymbol{hh}}\boldsymbol{X}^H \tag{3.21}$$

$$\mathbf{R}_{\boldsymbol{rr}} = \boldsymbol{X}\mathbf{R}_{\boldsymbol{hh}}\boldsymbol{X}^H + \mathbf{R}_{\boldsymbol{ww}}\,, \tag{3.22}$$

where $\mathbf{R}_{\boldsymbol{hh}} = \mathbb{E}\{\boldsymbol{h}\boldsymbol{h}^H\}$ and $\mathbf{R}_{\boldsymbol{ww}} = \sigma_w^2\boldsymbol{I}$. Equation (3.20) then yields,

$$\hat{\boldsymbol{h}}_{\mathrm{MMSE}} = \mathbf{R}_{\boldsymbol{hh}}\left(\mathbf{R}_{\boldsymbol{hh}} + \sigma_w^2(\boldsymbol{X}^H\boldsymbol{X})^{-1}\right)^{-1}\boldsymbol{X}^{-1}\boldsymbol{r}\,. \tag{3.23}$$

As seen from (3.23), the estimator requires knowledge of the channel correlation properties, represented by $\mathbf{R}_{\boldsymbol{hh}}$. For non-stationary channels, this information needs to be updated frequently. By pre-selecting a fixed correlation matrix, the entire estimator can be pre-designed, avoiding this update. It has been shown that a robust choice is to assume the correlation of a channel with uniform power delay profile (PDP) equal to the length of the cyclic prefix [42].

As compared to the LS estimator, the MMSE estimator requires that the received signal is multiplied by an $M \times M$ estimation matrix. Actually, the MMSE estimate can be performed as a filtering of the LS estimate. That is, we can write (3.23) as

$$\hat{\boldsymbol{h}}_{\mathrm{MMSE}} = \mathbf{A}\boldsymbol{X}^{-1}\boldsymbol{r} = \mathbf{A}\hat{\boldsymbol{h}}_{\mathrm{LS}}\,, \tag{3.24}$$

where $\mathbf{A} = \mathbf{R}_{\boldsymbol{hh}}\left(\mathbf{R}_{\boldsymbol{hh}} + \sigma_w^2(\boldsymbol{X}^H\boldsymbol{X})^{-1}\right)^{-1}$. The complexity of the MMSE estimator can be reduced by considering transform based low-rank approximations of the filter $\mathbf{A}$. We discuss such approaches below.

Before that, it should be noted that the LS and MMSE estimators can easily be expanded to incorporate several OFDM symbols by concatenating the different data structures in (3.17). Also, the MMSE estimator can be modified to support pilots which are scattered in time and frequency [43].

### Low-rank MMSE estimators

Simplifications to the MMSE estimation process can be obtained by assuming a low-rank model of the channel frequency response, i.e.,

$$\boldsymbol{h} = \boldsymbol{Q}\boldsymbol{f}\,, \tag{3.25}$$

where $\boldsymbol{Q}$ is an $M \times L$ unitary transform matrix, and $L \ll M$. The optimal low-rank estimator can be shown to use the SVD of the channel correlation matrix [42], $\mathbf{R}_{\boldsymbol{hh}} = \boldsymbol{U}\boldsymbol{\Sigma}\boldsymbol{U}^H$, where $\boldsymbol{\Sigma}$ is collecting the singular values $\{\Sigma_j\}$ on its diagonal. The obtained matrix $\boldsymbol{U}$ is in this case the Karhunen-Loeve transform basis [42]. The optimal low-rank estimator is then given by

$$\hat{\boldsymbol{h}}_{\mathrm{MMSE,LR}} = \boldsymbol{U}\Delta_L\boldsymbol{U}^H\hat{\boldsymbol{h}}_{\mathrm{LS}}\,, \tag{3.26}$$

where $\Delta_L$ is a diagonal matrix with entries

$$\delta_l = \begin{cases} \frac{\Sigma_l}{\Sigma_l + \bar{\gamma}^{-1}}, & \text{if } l = 1, 2, \ldots, L \\ 0 & \text{elsewhere,} \end{cases} \tag{3.27}$$

where $\bar{\gamma}^{-1}$ is the average SNR per symbol. The low-rank estimator, as expressed in (3.26), can be seen as a three stage process. First an LS estimate

is produced, before being transformed to a suitable domain where the energy is concentrated to a few dimensions. The dimensions with insignificant signal energy are then removed. The values which are left would correspond to the vector $\boldsymbol{f}$ in (3.25). Finally, the values are transformed back to the frequency domain. The potential save in complexity, as compared to the MMSE estimator, will depend on the number of required dimensions $L$ needed to obtain acceptable performance. Comparing (3.24) and (3.26), $\boldsymbol{U}\Delta_L\boldsymbol{U}^H$ can be seen as a low-rank approximation of the filter $\boldsymbol{A}$.

As mentioned above, a robust estimator can be obtained by designing for a fixed $\mathbf{R}_{\boldsymbol{hh}}$ corresponding to a channel with a uniform PDP. In that case the transform matrix can be observed to become equivalent to the discrete prolate spheroidal (DPS) sequences [44]. The DPS sequences are commonly referred to as Slepian base functions, and have been the choice for the channel estimation algorithms considered in this thesis. An alternative transform which has been frequently used for low-rank channel estimation is the DFT [45, 46]. The benefit of the DFT is that it can be efficiently implemented through the fast Fourier transform (FFT). The complexity can therefore be reduced as compared to other transforms. On the other hand, as compared to, e.g., the DPS sequences, the energy is not as well concentrated in the transform domain for realistic channels. Therefore, a larger number of transform coefficients are needed for a given estimation error level as, e.g., observed in our paper [47]. In Figure 3.2, originally found in [47], the symbol error rate is shown for an uncoded $4 \times 4$ MIMO-OFDM system using a low-rank channel estimator. The estimator is using either a DFT basis or an SVD (Karhunen-Loeve) transform basis, with different number of coefficients. As can be seen, an error floor is present when using the DFT transform, and for the SVD transform basis with too few transform coefficients.

### Pilot placement

The amount of pilot symbols and their placement depend both on the properties of the wireless channel as well as on the specific system in mind. For OFDM systems, the channel is usually sampled in time and frequency by placing the known pilot symbols at certain subcarrier and OFDM symbol positions. The placement of the pilot symbols can be seen as two-dimensional sampling in time and frequency domain, and as for any sampling the Nyquist sampling criteria has to be met for perfect reconstruction. The distance between two (complex) samples in the time domain $T_s$, and frequency domain $F_s$, is related to the maximum Doppler frequency $\nu_{\max}$ and delay spread $\tau_{\max}$, respectively. More

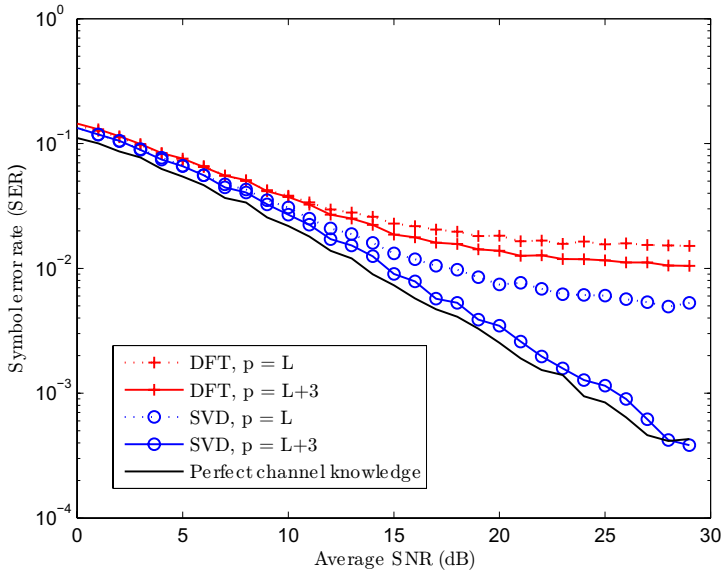


**Figure 3.2:** The performance of an uncoded 4×4 MIMO-OFDM system with channel estimation. The symbol error rate is shown for different types and number of transform coefficients, $p$. SVD refers to a Karhunen-Loeve transform basis. (Figure originally found in [47].)

specific, the sampling needs to fulfill

$$T_s \leq \frac{1}{2\nu_{\max}} \text{ and } F_s \leq \frac{1}{\tau_{\max}}. \tag{3.28}$$

Since the wireless receiver contaminates the samples with noise, oversampling is most often performed in order to facilitate accurate estimates. The sampling can be performed in a number of ways, and system specific requirements have a large affect on the choice of pilot pattern. Design of pilot patterns and sequences are out of the scope of our work, and for those aspects we refer to, e.g., [48].

It should be noted that if iterative decision-directed channel estimation algorithms are used, pilot sampling below the Nyquist rate can be sufficient as, e.g., observed in papers I and V. In that case, the requirement is that the initial pilot sampling leads to a channel estimate which is "good enough", so that the receiver starts to converge. The receiver then provides estimates on the transmitted data symbols, which can be used as additional pilots.

### 3.2.2 Decision-directed channel estimation

To allow for a sufficiently accurate channel estimate at the receiver, a large number of pilot symbols may be required. This will reduce the spectral efficiency of the system, since less data symbols can be transmitted. Ideally, from a spectral efficiency point of view, only data carrying symbols should be transmitted, given that the transmitted information can be retrieved. As mentioned earlier, blind algorithms exist but are impractical in most applications.

A more practical approach is semi-blind algorithms, which only require a small amount of pilot symbols. Iterative algorithms performing joint channel estimation and data detection, exploiting both pilot symbols and estimates of the data symbols, has shown good performance with realizable complexity [49–52]. Similar to iterative decoding, the estimator exploits the turbo principle to produce accurate channel estimates. With such iterative systems, reliable channel estimates can be provided with only a small amount of pilot symbols.

In Figure 3.3, originally found in Paper I, the benefits of using decision-directed channel estimation are shown for a MU-MIMO system with $N = 4$ receive antennas and $K = 4$ users. As the figure illustrates, the potential gain of using an iterative decision-directed channel estimation algorithm is significant. For the investigated receiver, more than 50% of all transmitted symbols have to be pilots if close to single user performance with perfect CSI is to be achieved. For the decision-directed algorithm the same number is 5%.

In most iterative algorithms, channel estimation and data detection are performed sequentially. Initially, the estimator obtains an estimate based on the pilot symbols alone. The detector uses this estimate to produce hard or soft decisions on the transmitted symbols, which are fed back to the estimator and used as additional pilots. If hard decisions are fed back, without any additional information on their reliability, essentially any conventional pilot based estimator can be used. Even though using hard decisions is suboptimal, the performance loss can be small as, e.g., observed in papers I and V.

To illustrate how the soft information can be used in the channel estimator, we revisit the MMSE estimator in (3.20). If prior information on the transmitted symbols $\boldsymbol{X}$ are available, the correlation matrices become

$$\mathbf{R}_{\boldsymbol{hr}} = \mathbb{E}\left\{\boldsymbol{h}(\boldsymbol{X}\boldsymbol{h}+\boldsymbol{w})^H\right\} = \mathbf{R}_{\boldsymbol{hh}}\mathbb{E}\left\{\boldsymbol{X}^H\right\} \tag{3.29}$$

$$\begin{aligned}\mathbf{R}_{\boldsymbol{rr}} &= \mathbb{E}\left\{(\boldsymbol{X}\boldsymbol{h}+\boldsymbol{w})(\boldsymbol{X}\boldsymbol{h}+\boldsymbol{w})^H\right\} = \\ &= \mathbb{E}\left\{\boldsymbol{X}\boldsymbol{h}\boldsymbol{h}^H\boldsymbol{X}^H\right\} + \mathbb{E}\left\{\boldsymbol{w}\boldsymbol{w}^H\right\} = \mathbf{R}_{\boldsymbol{hh}} \odot \mathbf{R}_{\boldsymbol{xx}} + \sigma_w^2\boldsymbol{I}\,,\end{aligned} \tag{3.30}$$

where $\mathbf{R}_{\boldsymbol{xx}} = \mathbb{E}\{\boldsymbol{x}\boldsymbol{x}^H\}$, and $\boldsymbol{x} = diag(\boldsymbol{X})$. The soft information based MMSE channel estimate can therefore be written as

$$\hat{\boldsymbol{h}}_{\text{MMSE}} = \mathbf{R}_{\boldsymbol{hh}}\mathbb{E}\left\{\boldsymbol{X}^H\right\}\left(\mathbf{R}_{\boldsymbol{hh}} \odot \mathbf{R}_{\boldsymbol{xx}} + \sigma_w^2\boldsymbol{I}\right)^{-1}\boldsymbol{r}\,. \tag{3.31}$$

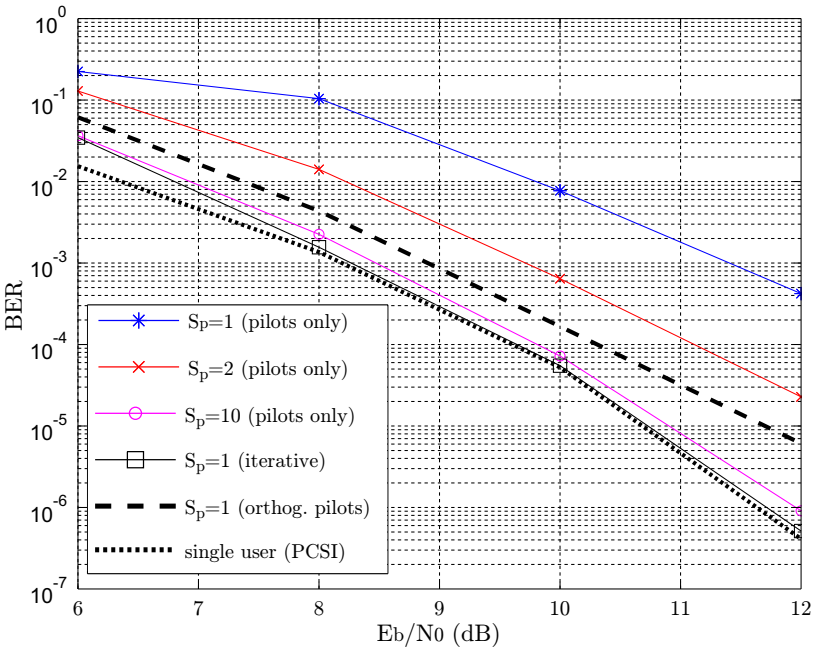


**Figure 3.3:** The BER at different SNR for a MU-MIMO system with $N = 4$ receive antennas and $K = 4$ users. Different number of pilot OFDM symbols are used, $S_p = 1, 2$ and 10, where the total number of symbols is $S = 20$. Also shown is the performance obtained when using the channel estimator in the loop of the iterative receiver, as well as single user performance when the channel is perfectly known, and the case of orthogonal boosted pilots. (From Paper I.)

Assuming that the symbols on different subcarriers are independent, the entries of $\mathbf{R}_{\boldsymbol{xx}}$ equal

$$r_{ij} = \begin{cases} \mathbb{E}\{x[i]x^*[i]\} & \text{if } i = j\,, \\ \mathbb{E}\{x[i]\}\mathbb{E}\{x^*[j]\} & \text{if } i \neq j\,, \end{cases} \tag{3.32}$$

where $(\cdot)^*$ denotes the complex conjugate operation. If we for simplicity assume BPSK signaling, the detector provides the symbol probabilities $p_{0,i} = p(x[i] = -1|\boldsymbol{r}, \hat{\boldsymbol{h}})$ and $p_{1,i} = p(x[i] = +1|\boldsymbol{r}, \hat{\boldsymbol{h}})$. In that case, (3.32) becomes

$$r_{ij} = \begin{cases} (-1)^2 \cdot p_{0,i} + (1)^2 \cdot p_{1,i} = 1 & \text{if } i = j\,, \\ \left((-1) \cdot p_{0,i} + 1 \cdot p_{1,i}\right)\left((-1) \cdot p_{0,j} + 1 \cdot p_{1,j}\right) & \text{if } i \neq j\,. \end{cases} \tag{3.33}$$

The same type of calculations can be performed for higher order constellation types, but leads to more complex expressions.

### 3.2.3 Multi-user and Multi-antenna channel estimation

So far we have only discussed channel estimation in the case of single antenna systems. For multiple antenna and multi-user systems, which are considered in this thesis, the challenges for estimating the channel increases. For example, the number of channel parameters to estimate increases linearly with the number of users. A large number of estimation algorithms have been proposed, exploiting various properties of the specific systems. Here, we will restrict the discussion to OFDM systems, where all users transmit synchronously and simultaneously. For practical systems, perfect synchronization can be difficult to obtain. Fortunately, OFDM is insensitive to time synchronization errors which are smaller than the CP minus the maximum channel delay.

If multiple antennas are used, and are assumed independent, per antenna estimates are optimal. Algorithms for the single receive antenna case can then directly be applied to multiple receive antenna systems. Furthermore, for the design of channel estimation algorithms such assumption is a robust choice, since the true spatial correlation of the channel is unknown in the general case. Due to this, we restrict the presentation to the single receive antenna case.

We will in this section discuss two types of estimation approaches; joint estimation of all user channels, and per user estimation obtained through interference cancellation.

#### Joint estimation

The presentation in the previous sections for the single transmit antenna case can be extended to the multi-user channel in a straightforward way. By expressing the received signal, for $S$ consecutive OFDM symbols from $K$ users, using the classical linear model [41] we have that

$$\begin{bmatrix} \boldsymbol{r}[1] \\ \vdots \\ \boldsymbol{r}[S] \end{bmatrix} = \begin{bmatrix} [\boldsymbol{X}_1[1], \ldots, \boldsymbol{X}_K[1]] & 0 & \cdots & 0 \\ 0 & \ddots & & \vdots \\ \vdots & & \ddots & 0 \\ 0 & \cdots & 0 & [\boldsymbol{X}_1[S], \ldots, \boldsymbol{X}_K[S]] \end{bmatrix} \begin{bmatrix} \boldsymbol{h}_1[1] \\ \vdots \\ \boldsymbol{h}_K[1] \\ \boldsymbol{h}_1[2] \\ \vdots \\ \boldsymbol{h}_K[S] \end{bmatrix} + \begin{bmatrix} \boldsymbol{w}[1] \\ \vdots \\ \boldsymbol{w}[S] \end{bmatrix} \tag{3.34}$$

where $\boldsymbol{X}_k[s]$ are diagonal matrices corresponding to the transmitted OFDM symbols, and $\boldsymbol{h}_k[s]$ is the frequency response, of user $k$ at time instance $s$.

Furthermore, $\boldsymbol{r}[s]$ and $\boldsymbol{w}[s]$ collect the received signal and noise, respectively, on all subcarriers at time instance $s$. In a more compact form (3.34) can be written as

$$\bar{\boldsymbol{r}} = \bar{\boldsymbol{X}}\bar{\boldsymbol{h}} + \bar{\boldsymbol{w}}\,, \tag{3.35}$$

where $\bar{\boldsymbol{r}}$, $\bar{\boldsymbol{X}}$, $\bar{\boldsymbol{h}}$ and $\bar{\boldsymbol{w}}$ correspond to the vectors and the matrix in (3.34).

Using the model in (3.35), we can apply the same channel estimation approaches as in the single antenna case, e.g., the estimators in (3.23) and (3.31). A large number of joint channel estimation algorithms have been proposed in the literature [47, 51, 53, 54], and in papers I, II, IV and V a joint MMSE estimator of this type is evaluated as part of an iterative receiver structure.

### Separate estimation

Performing a joint estimate for all users can be a highly complex task. A simpler approach is to first separate the users, and then perform per user estimates. Since the channel needs to be known in order to separate the users, iterative algorithms are needed.

In order to see how such estimation can be performed, (3.35) may be rewritten as a sum of the per user signal components, i.e.,

$$\bar{\boldsymbol{r}} = \bar{\boldsymbol{X}}_j\bar{\boldsymbol{h}}_j + \sum_{k\neq j}\bar{\boldsymbol{X}}_k\bar{\boldsymbol{h}}_k + \bar{\boldsymbol{w}}\,, \tag{3.36}$$

where $\bar{\boldsymbol{X}}_k$ are block-diagonal matrices with entries $\boldsymbol{X}_k[s]$, for $s = 1, \ldots, S$, and $\bar{\boldsymbol{h}}_k = [\boldsymbol{h}_k^T[1], \ldots, \boldsymbol{h}_k^T[S]]$. Furthermore, we have separated out the signal component of the $j$:th user. The second term on the right hand side of (3.36) is the sum of all interfering users, with respect to user $j$. If this interference can be canceled perfectly, the channel of user $j$ can be estimated with single user performance.

For the problem at hand, one algorithm which indirectly performs such interference cancellation is the expectation maximization (EM) algorithm [55]. The EM algorithm is an efficient iterative method for computing the ML estimate in the presence of hidden data. In our case, the hidden data is the received signal components for the different users, i.e., $\bar{\boldsymbol{S}}_k \triangleq \bar{\boldsymbol{X}}_k\bar{\boldsymbol{h}}_k$. Each iteration of the EM algorithm consists of two steps; the expectation, or E-step, and maximization, or M-step. In the E-step, the missing data is estimated given the observed data and the current estimate of the model parameters. This is achieved using conditional expectation. In the M-step, the likelihood function is maximized under the assumption that the estimates of missing data correspond to the true values.

For the model in (3.36), the $i$:th iteration of the EM algorithm can be shown to yield [55, 56]

- E-step: *for* $k = 1, \ldots, K$

$$\hat{\bar{\boldsymbol{S}}}_k^{(i)} = \bar{\boldsymbol{X}}_k \hat{\bar{\boldsymbol{h}}}_k^{(i)} \tag{3.37}$$

$$\hat{\bar{\boldsymbol{r}}}_k^{(i)} = \hat{\bar{\boldsymbol{S}}}_k^{(i)} + \beta_k \left( \bar{\boldsymbol{r}} - \sum_{k=1}^{K} \hat{\bar{\boldsymbol{S}}}_k^{(i)} \right) \tag{3.38}$$

- M-step: *for* $k = 1, \ldots, K$

$$\hat{\bar{\boldsymbol{h}}}_k^{(i+1)} = \arg\min_{\bar{\boldsymbol{h}}_k} \left\{ \left\| \hat{\bar{\boldsymbol{r}}}_k^{(i)} - \bar{\boldsymbol{X}}_k \bar{\boldsymbol{h}}_k \right\|^2 \right\} . \tag{3.39}$$

In (3.38), $\beta_k$ are real-valued scaling parameters, satisfying $\sum_{k=1}^{K} \beta_k = 1$, often conveniently chosen as $\beta_k = 1/K$. The algorithm also requires an initial estimate, or guess, $\hat{\bar{\boldsymbol{h}}}_k^{(0)}$, of the different user channels. The accuracy of the initial guess influences the speed on convergence as, e.g., illustrated in Paper V where we look at a few initial estimators with different complexity for an OFDM-IDMA system.

Looking at the expression in (3.38), it can be seen as an interference cancellation operation. Thus, for this specific problem at hand, the EM algorithm can be interpreted as performing a parallel interference cancellation, followed by a per user ML estimation. An alternative version of the EM algorithm is the space alternating generalized EM (SAGE) algorithm [57], which has shown to have better convergence properties. The SAGE algorithm performs the estimates of the individual users sequentially, with the most resent channel estimates being used in each step for the interference cancellation process. As compared to the EM algorithm, SAGE can be interpreted as performing successive interference cancellation, where a per user ML estimate is performed at each stage.

In the derivation above, we have assumed that $\{\bar{\boldsymbol{X}}_k\}$ are perfectly known through the transmission of pilot symbols. Decision-directed channel estimation can, e.g., be performed in a straightforward way through the use of hard decisions. In papers I and V, we compare estimators based on SAGE with other types of estimators, for the use in an iterative receiver. Furthermore, in Paper V we propose a modified SAGE based algorithms in order to incorporate the use of soft symbol decisions. This is done by changing from an ML estimate to an MMSE estimate in the M-step of (3.39).

## 3.3 An iterative multi-user receiver structure

So far in this chapter we have discussed both multi-user detection and channel estimation for the considered uplink system. A receiver needs to perform both

these tasks, along with decoding of an error correcting code. Optimally, these three tasks should be performed jointly, but such an operation is not tractable for most practical systems. Therefore this task is commonly solved iteratively, by exchanging information between the three receiver components. This ad-hoc way of iteratively performing joint multi-user detection and channel estimation has become a de facto standard approach [50, 51, 58]. This approach is also adopted for the iterative receivers investigated in this thesis.

Many receiver structures in the literature rely on a separate channel estimator [46, 48, 53, 56], providing reliable estimates based on pilot symbols only. But, as discussed in the previous section, decision-directed channel estimation can help to improve system performance and spectral efficiency. Ideally, the channel estimator should provide information about the reliability of the channel estimate, which could be used by the MUD. Even though such algorithms exist [50, 59], we have not considered the exchange of such information for the investigated receivers in this thesis.

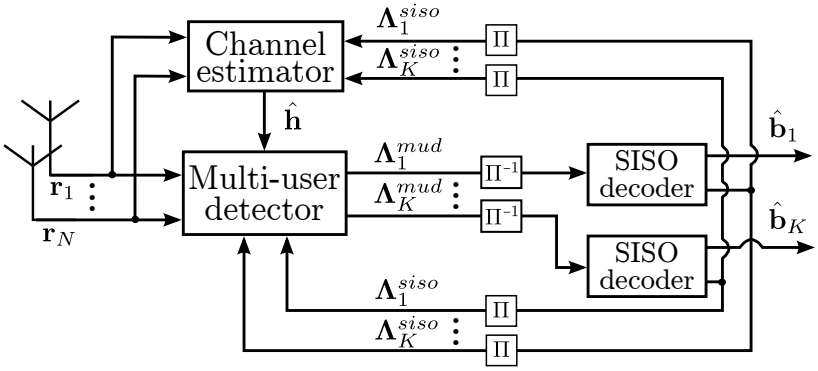


**Figure 3.4:** An iterative receiver structure with channel estimation

The principle of an iterative receiver as discussed above is shown in Figure 3.4. Going through the receiver, an initial channel estimate is first obtained based on the transmitted pilot symbols. With this initial channel estimate, the MUD performs user separation and delivers extrinsic LLR values ($\mathbf{\Lambda}_k^{\mathrm{mud}}$) as input to the channel decoders, after deinterleaving. The interleaver between the two is needed in order to break up dependencies between symbols. The channel decoders then decode the received sequences, and produce extrinsic LLR values ($\mathbf{\Lambda}_k^{\mathrm{siso}}$) which are fed back to the MUD and channel estimator[1],

[1]In Paper IV, the channel estimator is fed *a posteriori* LLR values, as proposed in [51]. But as we observed in Paper II, feeding back extrinsic values has a negligible impact on performance.

after reinterleaving. The channel estimator then computes an updated estimate, which is fed to the MUD which performs a new user separation with the updated information. The iterations then continue up till a maximum number, or until a stopping criterion is met. After that, the channel decoder produces hard decisions on the transmitted information bits.

# Chapter 4

# Performance and complexity evaluations

The purpose of this chapter is to provide a brief overview of, and a discussion on, the tools and models which have been used and proposed in the included papers. We start by considering the choice of channel model, and also discuss the alternative approach of using channel measurement data. The latter is further discussed in Paper III. We then continue by discussing how convergence analysis of iterative receivers can be performed, before we look at how the algorithm complexity can be estimated. The relation between convergence and complexity is, e.g., investigated in papers I and V, where we consider the performance versus complexity tradeoff for different iterative receivers.

## 4.1 Channel models and measurement data

When evaluating receiver algorithms, appropriate channel models need to be chosen, which capture the properties of the wireless channel. An inappropriate choice can lead to inaccurate algorithm performance, potentially leading to bad design choices. For example, when designing channel estimation algorithms, assumptions on the channel statistics is often exploited. If the chosen channel model does not have the same statistics as the real channel, but the same as falsely assumed by the algorithm, the simulations could deceitfully show a good estimation performance.

When it comes to choosing a channel model, a large number of them exists (see, e.g., [60,61]), often designed with specific systems in mind. They typically model the behavior of the channel in terms of path loss, shadowing, multipath,

Doppler spread and spatial statistics. If we restrict the discussion to wideband models, the European cooperation in science and technology (COST) and the International telecommunications union (ITU) have provided a number of industrial standard channel models. Amongst these we have, the COST 207 model used in GSM, COST 231 and ITU-R used for UMTS, and extended ITU models for LTE [62, 63].

The multi-user systems which we are investigating in this thesis are assumed to be operating over large bandwidths in indoor environments, where we can expect rich scattering, small time variations and large frequency correlation. We also assume that line-of-sight is generally blocked which, together with the rich scattering, leads to a low spatial correlation. Additionally, we assume that appropriate power control is performed, leading to equal average power amongst the users.

Even though the latest channel models, e.g., COST 2100, have support for multiple antenna terminals and multiple base stations, we have in papers I, II and V adopted a simpler and more tractable channel model suitable for the considered systems. As for most of the standardized models, we adopt a tapped-delay line model with wide sense stationary uncorrelated scattering [64], whos impulse response is given by

$$g(\tau) = \sum_{p=0}^{P-1} \alpha_p \delta(\tau - \tau_p)\,, \tag{4.1}$$

where $\{\alpha_p\}$ are zero-mean complex Gaussian random variables with an exponential PDP, $\mathbb{E}\{|\alpha_p|^2\} = Ce^{-\tau_p/\tau_{\text{rms}}}$, where $C$ is a normalization constant, and the delays $\{\tau_p\}$ are uniformly distributed between zero and a maximum channel delay $\tau_{\max}$. For a large $P$, the model describes a rich scattering environment, and a strong frequency correlation is given if $\tau_{\max}$ or $\tau_{\text{rms}}$ are small, as compared to the symbol length. Furthermore, using the assumption of low spatial correlation, the different user/antenna channels are generated independently of each other. We also assume transmission of short data packets, so that Doppler effects can be neglected, thus leading to a block fading channel.

An alternative to using a statistical model of the wireless channel is to use channel measurements performed in a relevant environment. Channel measurements are often performed in order to gain understanding of the properties of the propagation channel, and are the basis of channel modeling. One of the benefits of using measurement data, rather than a channel model, is that they provide a snapshot of the true environment without any underlaying assumptions on the channel properties. Furthermore, in the early design phase of novel wireless systems, models may not be available or properly verified. The use of measurements can therefore speed up the design process. At the same time,

there are a number of measurement related issues which needs to be commented on. Measurement imperfections can reduce validity of the measured channel. These include the presence of measurement noise, and synchronization errors. Measurement noise leads to reduced correlation in the channel, which can lead to erroneous performance evaluations. In Paper III the use of measurements for system evaluations are discussed in more detail, and the impact of a number of issues is illustrated through system simulations. Additionally, we perform a system evaluation based on unique dynamic dual-link MIMO measurements in Paper IV.

## 4.2 Receiver convergence and complexity analysis

For iterative systems, evaluating the convergence properties is of importance. From a receiver algorithm design point of view, it is important to understand when, and how, the algorithm converges. Furthermore, slow convergence can increase processing latency, computational effort and power consumption, which grow with the number of iterations. The convergence speed, in combination with the per iteration algorithm complexity, therefore have an impact on the algorithm choices. In this section we provide a brief overview of the tools we have used for convergence evaluation, as well as for complexity analysis. More details can be found in papers I and V, where the convergence properties of different multi-user receivers are evaluated. In the papers, the impact of convergence on the receiver complexity is discussed, with the aim of finding the receiver with the lowest overall complexity.

### 4.2.1 Convergence analysis

Analytical evaluations on performance can be performed for simplified and idealized receivers, but for more advanced receiver designs such evaluations are in general infeasible. We therefore need to resort to computer based system simulations. The convergence properties of a receiver can be visualized, e.g., by looking at the evolution of the BER and estimation MSE with iterations. This is a good tool for comparing the performance of different receiver algorithms, and shows the overall performance. An alternative tool which has become popular for the design and evaluation of iterative algorithms is extrinsic information transfer (EXIT) charts [65]. These charts provide additional information on the interactions between the involved components of the receiver.

EXIT charts have shown to be helpful tools for visualizing convergence behavior and aid the design and performance evaluation of iterative systems.

These charts were initially proposed for the evaluation of concatenated codes, and visualize the exchange of mutual information between the components of an iterative decoder. They have also shown useful for visualizing the exchange of soft information between other receiver components, such as channel equalizer [66], MUD [67] and channel estimator [59]. Even though EXIT charts are derived under certain limiting assumptions, such as perfect interleaving and Gaussian distribution of LLRs, they have been shown to model the behavior of practical systems quite well.

In order to produce an EXIT chart, information transfer functions of the receiver components have to be produced. Each unit is seen as an LLR transformer ($\Lambda_{\mathrm{a}} \rightarrow \Lambda_{\mathrm{ext}}$), where the transfer function measures the improvement of the LLR-transformation in terms of mutual information between the LLRs and the underlying variables, i.e.,

$$I_{\mathrm{ext}} = T\left(I_{\mathrm{a}}\right), \tag{4.2}$$

where $I_{\mathrm{a}} = I(x; \Lambda_{\mathrm{a}})$ and $I_{\mathrm{ext}} = I(x; \Lambda_{\mathrm{ext}})$ are the input *a priori* mutual information and output extrinsic mutual information, respectively. The extrinsic information of one unit then becomes the *a priori* input for the other.

Once the transfer functions for the components have been obtained, their exchange of information can be visualized in a graph. Figure 4.1, which is based on the results in Paper I, shows an EXIT chart for an MU-MIMO-OFDM system for the case of $N = 4$ receive antennas, $K = 4$ users. The upper curve is the transfer function of the MUD and channel estimator part of the receiver, while the lower curve is the inverse of the transfer function of the soft-input soft-output (SISO) data decoder. The zig-zag line shows how the two components exchange information, and provides an estimate of the convergence behavior of the iterative receiver. The receiver is estimated to converge to its final value in around five iterations for the given scenario.

In the above presentation, we have omitted the discussion on how one would actually produce the transfer functions. Instead, we refer to papers I or II for an introduction. In Paper II, we also present a multi-dimensional EXIT chart model for an iterative receiver structure for MIMO-OFDM systems. Alternatively, the reader may consult tutorial papers on EXIT charts, such as [68].

### 4.2.2 Receiver complexity

As we have mentioned, the algorithm complexity is an important aspect in receiver design. In the quest for increased system performance and bandwidth utilization, the receiver algorithms inevitably become more and more complex. The complexity represents itself in terms of an increased chip area and power consumption of the final hardware. For the design of iterative receivers, which

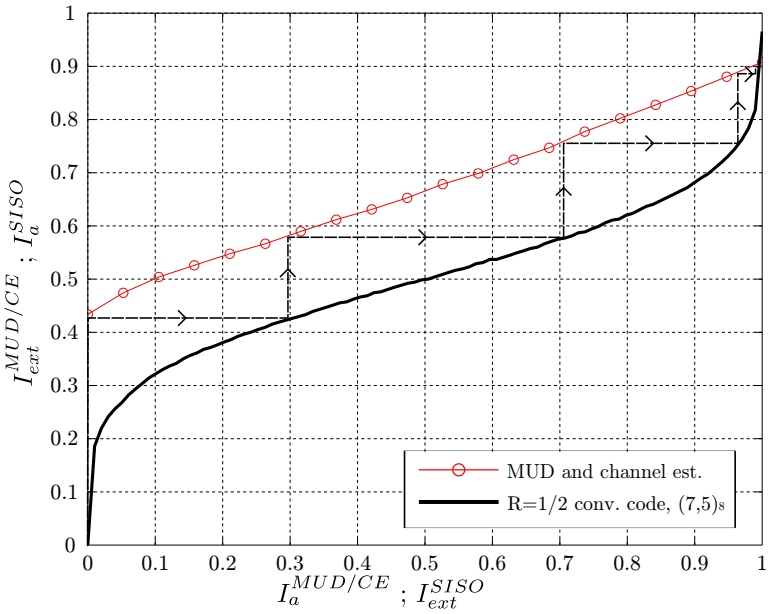


**Figure 4.1:** EXIT chart for a MU-MIMO-OFDM system for the case of $N = 4$ receive antennas, $K = 4$ users. The chart shows the exchange of information between the MUD with channel estimation, and the data decoders. (See Paper I for more details.)

is the objective in this thesis, the complexity will depend on the choice of the individual components. As mentioned, the convergence speed of the receiver also plays an important role in the overall computational complexity of the receiver. In papers I and V, we investigate the performance versus complexity tradeoff for different systems and receiver configurations. An ultimate tradeoff analysis would require implementing the algorithms on a hardware platform, requiring a huge work effort not allowed by the time frame of this thesis. An estimate of the complexity can be obtained by counting the required number of arithmetic operations. Amongst these, additions and multiplications are most commonly encountered, and thus have a central role. Furthermore, since the complexity of the multiplier is significantly larger than that of the adder [69], the multiplications tend to dominate the overall complexity. To get a tractable and reliable measure of complexity when performing the tradeoff analysis in the included papers, we therefore restrict to the required number of (complex) multiplications.

# Chapter 5

# Contributions and discussion

This chapter provides a summary of my contributions to the research field. In a separate section, we also give some concluding remarks and comments on future work. To begin with, the five papers, which constitutes the core of this theses, are summarized and the contributions highlighted. The papers are not listed in a chronological order, but are ordered based on on their content. For all of these papers, I am the main contributor, and was taking part in all steps in the scientific process: implementing algorithms, performing simulations, evaluating the results and writing the papers.

## 5.1 Research contributions

### 5.1.1 Paper I: "Iterative Receivers with Channel Estimation for Multi-User MIMO-OFDM: Complexity and Performanc"

In the first of the included papers, an evaluation of iterative receiver structures for an uplink multi-user MIMO-OFDM systems is conducted. The considered receivers are composed of three main components; a MUD unit, a channel estimation unit and a SISO data decoder. Three different MUD algorithms and three channel estimation algorithms are considered, and compared on an equal footing. The paper studies the trade-off between complexity and performance for different combinations of these algorithms. The investigation is restricted to the case of $N = 4$ receive antennas, and single antenna users. The main

contributions are summarized as follows:

- A tradeoff analysis between complexity and performance is performed. Three transform based channel estimation algorithms are considered; one based on SAGE, one performing a joint MMSE estimation of all user channels, and one low-complexity approximation of the joint MMSE estimator based on a Krylov subspace projection method. The latter is, to the best of our knowledge, evaluated for the first time in a MIMO-OFDM system. Three MUDs are considered; two PIC based detectors and one full maximum a-posteriori probability (MAP) detector. The latter being a natural performance benchmark.
- In the tradeoff analysis, the total complexity, in terms of complex multiplications, required to reach a given bit error rate is computed for all algorithm combinations. The analysis is performed for different SNRs, and for different number of users. The total complexity is given by the sum of the derived complexities of the receiver components, multiplied by the number of required iterations obtained through system simulations.
- The convergence of the different receiver configurations are investigated by looking at the system BER, estimator MSE, and an EXIT chart.

Our results show that low-complexity receiver components can be competitive when looking at the total complexity versus performance tradeoff. Despite having a slower convergence, the overall computational effort is lower in most of the considered scenarios. Furthermore, our investigations also show that the proposed low-complexity Krylov subspace based estimator shows performance close to that of the joint MMSE algorithm, but with significantly lower complexity.

### 5.1.2 Paper II: "EXIT Chart Evaluation of a Receiver Structure for Multi-User Multi-Antenna OFDM Systems"

In this paper an iterative receiver for multi-user MIMO-OFDM systems, incorporating iterative MUD and channel estimation (CE), is evaluated. The evaluation is performed through the use of EXIT charts, which model the flow of mutual information between the components of the receiver, in our case between the data decoders and the combined MUD/CE. In the paper we restrict the evaluation to the case of two single antenna users and a receiver with two antennas. The contributions of the paper are as follows:

- We illustrate how the convergence properties of the multi-user receiver can be modeled through the use of multi-dimensional EXIT charts. For the given system configurations, paired 3D EXIT charts illustrate the exchange of information between the two SISO decoders and and the combined MUD/CE.
- A modification of the receiver is also proposed, where the SISO decoders feed back extrinsic, rather than *a posteriori* LLRs, as earlier proposed, to the CE. An insignificant performance loss is observed. The modification removes the dependencies between the transfer functions of the SISO decoders and the MUD/CE, which simplifies EXIT chart based receiver design.

The results illustrate a good correspondence between the EXIT chart prediction and the true decoding trajectory. The charts provide an improved understanding of the convergence behavior of the iterative receiver, and can, e.g., be used for investigations on iteration scheduling between the involved components.

### 5.1.3 Paper III: "Using Measured Channels in Performance Evaluation of Multi-User OFDM Systems"

The paper provides a tutorial overview of the use of channel measurement data in wireless communication system evaluations. Channel measurements are generally used as a basis for generating channel models, but can also be used directly in system simulations to provide a close to reality channel scenario. With this paper we summarize our experiences gained from using channel measurement data in system simulations, and we also provide illustrative examples of certain aspects. The focus is on wideband multi-user MIMO systems, but most observations are applicable to other scenarios and systems. The main contributions are as follows:

- A number of measurement specific issues related to the data is described, and ways to alleviate these problems are discussed. The issues include, e.g., the presence of measurement noise, directive antennas, and propagation delay.
- Illustrations of a number of the issues are provided, e.g., by looking at the performance of an iterative receiver for a MU-MIMO-OFDM system with cooperative base stations. For the evaluation, the performance obtained with the true channel is compared with that of a measurement impaired channel. The true channel is given as the output of the COST 2100

dynamic multi-link MIMO channel model. In the case of measurement noise, we illustrate that both improved as well as reduced performance can be obtained, depending on the considered system.

Due to the discussed issues, measurements need to be handled with care if used for system evaluations. If doing so, being aware of the problems, measurement data can be a good alternative for system evaluations. Especially in the early design phase of novel wireless systems, before appropriate models have been made available.

### 5.1.4 Paper IV: "On the Performance of Iterative Receivers for Interfering MIMO-OFDM Systems in Measured Channels"

This paper presents the first ever evaluation of a MU-MIMO system based on real measurement data from a dual link MIMO scenario. In the paper, which was performed in the early part of my Ph.D. studies, we investigate the gains that can be harvested through base station cooperation in an uplink multi-user MIMO-OFDM system in a real environment. The system is comprised of two mobile users and two base stations, all equipped with two antennas, where the receivers either perform iterative joint multi-user detection incorporating channel estimation, or independent processing for each base station and user pair. The performance is evaluated using unique channel measurements from an indoor dual-link mobile MIMO measurement campaign.

The contributions of the paper are as follows:

- The performance of base station cooperation in a MU-MIMO system is investigated through the use of real indoor mobile dual-link MIMO measurements. System simulations are performed over 700 measurement points along the routes of the two mobile users. In the results we illustrate the large gain that can be achieved through cooperation, where interfering power is turned into useful power. The BER performance at different signal-to-interference ratios (SIR) is also presented.

- We also exemplify the benefits of using soft estimates of the transmitted data symbols as additional pilot symbols, where the BER performance is seen to improve by orders of magnitude as compared to when using pilots only.

This paper point at the large gains which can be obtained through base station cooperation, when used in a real multi-link MIMO environment, represented by channel measurements. Furthermore, it also illustrates that decision-

directed channel estimation can help to significantly improve the performance of these systems.

### 5.1.5 Paper V: "Overview of Channel Estimation Algorithms for OFDM-IDMA: Complexity and Performance"

This paper presents a study of a number of channel estimation algorithms suitable for single antenna, uplink OFDM-IDMA systems. The considered algorithms cover both an initial pilot based estimation, as well as the following iterative decision-directed channel estimation. The presented estimation algorithms, ranging from simple per user LS to joint multi-user MMSE estimators, are mainly modifications of previously presented algorithms, but a more novel SAGE based approach is also presented. In a similar way as in Paper I, a performance versus complexity tradeoff analysis is performed.

The contributions of the paper are as follows:

- Three different transform based decision-directed channel estimation algorithms are compared in an OFDM-IDMA system for the first time. One of the algorithms jointly estimates the channels for all users, while the others perform per-user estimates based on the SAGE algorithm.
- In one of the estimation algorithms we propose a novel approach to incorporate the use of soft decisions into the SAGE framework, where an MMSE estimate is performed in the M-step instead of an ML estimate.
- Different algorithms for obtaining an initial pilot based channel estimate, which provide a starting point for the iterative receiver, are also evaluated. The algorithms effect on the overall system performance and convergence is studied, along with their complexities.
- A complexity versus performance analysis is performed, where the total number of complex multiplications needed to reach a bit error rate (BER) target is evaluated. For the evaluation, the complete receiver complexity incorporating channel estimation, MUD and data decoding is considered. The analysis is performed at different SNRs, and for different user loads.

In the paper we have presented a number of suitable decision-directed channel estimation algorithms for OFDM-IDMA systems, and compared them on an equal footing. The tradeoff analysis indicate that low-complexity channel estimation algorithm can be competitive alternatives. Despite leading to a slower receiver convergence, the overall computational effort required by the receiver can be decreased.

## 5.2 Discussion and future work

As mentioned in the beginning of the thesis, the question that we are trying to shed some light on is: How can we design efficient iterative receivers incorporating channel estimation? The answer to that question depends very much on the specific system under consideration. In this thesis we have considered algorithms both for MU-MIMO-OFDM (papers I, II and IV), as well as OFDM-IDMA systems (Paper V), transmitting over block fading channels. For both systems we have seen that by using algorithms with relatively low complexity, receivers can be designed which have competitive performance. The considered algorithms with reduced complexity will in general lead to more receiver iterations, but still require less total computational effort.

Even though the presented receiver algorithms show good performance in the investigated systems, there are a number of underlying assumptions and limitations which deserve to be discussed. In the rest of this section we therefore reflect over the following aspects: time fading channels, symbol constellation sizes, time and frequency synchronization, unequal user powers and hardware implementation aspects.

To start with, we have limited this thesis to communication over block fading channels. This choice is motivated by the fact that we mainly consider indoor communications. The degree of channel variations is highly coupled to the terminal velocities. For indoor environments, these velocities can be assumed to be small, which implies that the channel variations occurs slowly in comparison to the symbol rate. Hence, making the block fading assumption valid. For outdoor environments and at high terminal velocities, channel variations within a block can occur. In such scenario the presented channel estimation techniques need to be modified accordingly, and the resulting performance has to be investigated. Further on, we have restricted the scope of this thesis to QPSK signaling, and instead achieve spectral efficiency through, e.g., spatial multiplexing. For systems aiming at higher spectral efficiencies, larger constellation sizes are required. An extension of the presented algorithms is conceptually straightforward, but would inevitably lead to increased algorithm complexities. For the case of larger constellations, we still expect that low complexity approaches would be competitive. With this in mind, a natural extension of our work would therefore be to consider algorithms supporting large constellations and time varying channels.

Furthermore, we have assumed that the users are well synchronized in time and frequency. Achieving this can be both challenging and may require considerable signaling overhead, reducing the efficiency of the system. Synchronization can, e.g., be obtained through dedicated signals transmitted regularly from the base station, in combination with individual timing information (timing ad-

vance). If large enough synchronization errors exist, performance degradation will occur since the orthogonality between subcarriers and consecutive OFDM symbols are lost. Further on, we have assumed that the received power from all users are equal. In general, large power variations amongst users can occur due to difference in path loss. Power control, where the base station informs the users how to adjust their transmit power, can partly compensate for these imbalances.

Finally, as indicated in Section 4.2.2, counting the number of required multiplications only provide a rough estimate of the hardware complexity. The actual complexity will depend on the final hardware design, where the choice of architecture, memory usage, word lengths, and hardware reuse are important parameters. Implementing the investigated algorithms on a hardware platform, to more thoroughly investigate their properties and implementation complexities would be an interesting extension of our work.

# References


[1] T. Sarkar, A. Oliner, R. Mailloux, M. Salazar-Palma, and D. Sengupta, *History of wireless*. John Wiley & Sons ltd., 2006.

[2] F. O. B. Initiative, "Mobile broadband: The benefits of additional spectrum," tech. rep., US Federal Communications Commission, Oct. 2010.

[3] J. Winters, "On the capacity of radio communication systems with diversity in a Rayleigh fading environment," *IEEE Journal on Selected Areas in Communications*, vol. 5, pp. 871 – 878, jun 1987.

[4] G. Foschini and M. Gans, "On limits of wireless communications in a fading environment when using multiple antennas," *Wireless Personal Communications*, vol. 6, pp. 311–335, 1998.

[5] C. Berrou, A. Glavieux, and P. Thitimajshima, "Near shannon limit error-correcting coding and decoding: Turbo-codes (1)," in *Proc. IEEE International Conference on Communications*, vol. 2, pp. 1064–1070, May. 1993.

[6] J. Hagenauer, "The turbo principle in mobile communications," *Proc. International Symposium on Nonlinear Theory and its Applications*, Oct. 2002.

[7] S. Weinstein and P. Ebert, "Data transmission by frequency-division multiplexing using the discrete fourier transform," *IEEE Transactions on Communication Technology*, vol. 19, pp. 628–634, Oct. 1971.

[8] A. Paulraj, R. Nabar, and D. Gore, *Introduction to space-time wireless communications*. Cambridge University Press, 2003.

[9] H. Beverage and H. Peterson, "Diversity receiving system of R.C.A. Communications, Inc., for radiotelegraphy," *Proceedings of the Institute of Radio Engineers*, vol. 19, pp. 529 – 561, Apr. 1931.

[10] E. Telatar, "Capacity of multi-antenna Gaussian channels," tech. rep., AT&T-Bell Labs Internal Tech. Memo., Jun. 1995.

[11] L. Zheng and D. Tse, "Diversity and multiplexing: A fundamental tradeoff in multiple-antenna channels," *IEEE Transactions on Information Theory*, vol. 49, pp. 1073–1096, May 2003.

[12] E. Larsson and P. Stoica, *Space-time block coding for wireless communications*. Cambridge University Press, 2003.

[13] S. Alamouti, "A simple transmit diversity technique for wireless communications," *IEEE Journal on Selected Areas in Communications*, vol. 16, pp. 1451–1458, Oct. 1998.

[14] E. Telatar, "Capacity of multi-antenna gaussian channels," *European Transactions on Telecommunications*, vol. 10, no. 6, pp. 585–595, 1999.

[15] E. Dahlman, S. Parkvall, J. Sköld, and P. Beming, *3G Evolution HSPA and LTE for Mobile Broadband*. Academic Press, 2nd ed., 2008.

[16] J. Massey, "Information theory aspects of spread-spectrum communications," in *IEEE Third International Symposium on Spread Spectrum Techniques and Applications*, vol. 1, pp. 16–21, Jul. 1994.

[17] S. Hara and R. Prasad, "Overview of multicarrier cdma," *IEEE Communications Magazine*, vol. 35, pp. 126–133, Dec. 1997.

[18] S. Verdu, *Multiuser detection*. Cambridge University Press, 1998.

[19] M. E. Honig, *Advances in Multiuser Detection*. John Wiley & Sons, Inc., 2009.

[20] A. Viterbi, "Very low rate convolution codes for maximum theoretical performance of spread-spectrum multiple-access channels," *IEEE Journal on Selected Areas in Communications*, vol. 8, pp. 641–649, May 1990.

[21] P. Frenger, P. Orten, and T. Ottosson, "Code-spread CDMA using maximum free distance low-rate convolutional codes," *Communications, IEEE Transactions on*, vol. 48, pp. 135–144, jan 2000.

[22] S. Verdu and S. Shamai, "Spectral efficiency of CDMA with random spreading," *IEEE Transactions on Information Theory*, vol. 45, pp. 622–640, Mar. 1999.

[23] L. Ping, L. Liu, and W. Leung, "A simple approach to near-optimal multiuser detection: Interleave-division multiple-access," in *Proc. IEEE Wireless Communications and Networking Conference*, vol. 1, pp. 391–396, 2003.

[24] J. Winters, "Smart antennas for wireless systems," *IEEE Personal Communications*, vol. 5, pp. 23–27, Feb. 1998.

[25] A. Goldsmith, S. Jafar, N. Jindal, and S. Vishwanath, "Capacity limits of MIMO channels," *IEEE Journal on Selected Areas in Communications*, vol. 21, pp. 684–702, Jun. 2003.

[26] Q. Spencer, C. Peel, A. Swindlehurst, and M. Haardt, "An introduction to the multi-user MIMO downlink," *IEEE Communications Magazine*, vol. 42, pp. 60–67, Oct. 2004.

[27] M. Jiang and L. Hanzo, "Multiuser MIMO-OFDM for next-generation wireless systems," *Proceedings of the IEEE*, vol. 95, pp. 1430–1469, july 2007.

[28] D. Gesbert, M. Kountouris, R. Heath, C.-B. Chae, and T. Salzer, "Shifting the MIMO paradigm," *IEEE Signal Processing Magazine*, vol. 24, pp. 36–46, Sept. 2007.

[29] J. Anderson, *Digital transmission engineering*. IEEE Series on Digital & Mobile Communication, IEEE Press, 2005.

[30] S. Lin and D. Costello, *Error control coding: Fundamentals and applications*. Pearson-Prentice Hall, 2004.

[31] E. Larsson, "MIMO detection methods: How they work," *IEEE Signal Processing Magazine*, vol. 26, no. 3, pp. 91–95, 2009.

[32] B. Hassibi and H. Vikalo, "On the sphere-decoding algorithm I. Expected complexity," *IEEE Transactions on Signal Processing*, vol. 53, pp. 2806–2818, Aug. 2005.

[33] J. Jalden and B. Ottersten, "On the complexity of sphere decoding in digital communications," *IEEE Transactions on Signal Processing*, vol. 53, pp. 1474–1484, Apr. 2005.

[34] X. Wang and H. Poor, "Iterative (turbo) soft interference cancellation and decoding for coded CDMA," *IEEE Transactions on Communications*, vol. 47, no. 7, pp. 1046–1061, 1999.

[35] L. Ping, L. Liu, K. Wu, and W. Leung, "Interleave-division multiple-access," *IEEE Transactions on Wireless Communications*, vol. 5, no. 4, pp. 938–947, 2006.

[36] I. Mahafeno, C. Langlais, and C. Jego, "OFDM-IDMA versus IDMA with ISI cancellation for quasistatic Rayleigh fading multipath channels," *Proc. 4th International Symposium on Turbo Codes and Related Topics*, pp. 1–6, Apr. 2006.

[37] C. Novak, F. Hlawatsch, and G. Matz, "MIMO-IDMA: Uplink multiuser MIMO communications using interleave-division multiple access and low-complexity iterative receivers," in *Proc. IEEE International Conference on Acoustics, Speech, and Signal Processing*, vol. 3, pp. 225–228, Apr. 2007.

[38] K.-H. Chang and C. Georghiades, "Iterative joint sequence and channel estimation for fast time-varying intersymbol interference channels," in *Proc. IEEE International Conference on Communications*, vol. 1, pp. 357–361, Jun. 1995.

[39] G. Giannakis, "Filterbanks for blind channel identification and equalization," *IEEE Signal Processing Letters*, vol. 4, pp. 184–187, Jun. 1997.

[40] C. Shin, R. Heath, and E. Powers, "Blind channel estimation for MIMO-OFDM systems," *IEEE Transactions on Vehicular Technology*, vol. 56, pp. 670–685, Mar. 2007.

[41] S. M. Kay, *Fundamentals of Statistical Signal Processing, Volume I: Estimation Theory*. Prentice Hall, 1993.

[42] O. Edfors, S. Wilson, and P. Börjesson, "OFDM channel estimation by singular value decomposition," *IEEE Transactions on Communications*, vol. 46, no. 7, pp. 931–939, 1998.

[43] P. Hoeher, S. Kaiser, and P. Robertson in *Proc. IEEE International Conference on Acoustics, Speech, and Signal Processing*.

[44] D. Slepian, "Prolate spheroidal wave functions, Fourier analysis, and uncertainty - V: The discrete case," *Bell System Technical Journal*, vol. 57, pp. 1371–1430, May/Jun. 1978.

[45] Y. Li, N. Seshadri, and S. Ariyavisitakul, "Channel estimation for OFDM systems with transmitter diversity in mobile wireless channels," *IEEE Journal on Selected Areas in Communications*, vol. 17, pp. 461–471, Mar. 1999.

[46] O. Edfors, M. Sandell, J.-J. van de Beek, S. Wilson, and P. Bö rjesson, "Analysis of dft-based channel estimators for ofdm," *Wireless Personal Communications*, vol. 12, pp. 55–70, 2000. 10.1023/A:1008864109605.

[47] P. Hammarberg and O. Edfors, "A comparison of DFT and SVD based channel estimation in MIMO OFDM systems," in *Proc. IEEE International Symposium on Personal, Indoor and Mobile Radio Communications*, pp. 1–5, Sept. 2006.

[48] I. Barhumi, G. Leus, and M. Moonen, "Optimal training design for MIMO OFDM systems in mobile wireless channels," *IEEE Transactions on Signal Processing*, vol. 51, pp. 1615–1624, Jun. 2003.

[49] M. Sandell, C. Luschi, P. Strauch, and R. Yan, "Iterative channel estimation using soft decision feedback," in *Proc. IEEE Global Communications Conference*, vol. 6, pp. 3728–3733, Nov. 1998.

[50] A. Kocian and B. Fleury, "EM-based joint data detection and channel estimation of DS-CDMA signals," *IEEE Transactions on Communications*, vol. 51, pp. 1709–1720, Oct. 2003.

[51] T. Zemen, C. Mecklenbrauker, J. Wehinger, and R. Muller, "Iterative joint time-variant channel estimation and multi-user detection for MC-CDMA," *IEEE Transactions on Wireless Communications*, vol. 5, pp. 1469–1478, Jun. 2006.

[52] M. Nicoli, S. Ferrara, and U. Spagnolini, "Soft-iterative channel estimation: Methods and performance analysis," *IEEE Transactions on Signal Processing*, vol. 55, pp. 2993–3006, Jun. 2007.

[53] Y. Li, "Simplified channel estimation for OFDM systems with multiple transmit antennas," *IEEE Transactions on Wireless Communications*, vol. 1, pp. 67–75, Jan. 2002.

[54] P. Rossi, R. Müller, and O. Edfors, "Slepian-based serial estimation of time-frequency variant channels for MIMO-OFDM systems," in *Proc. IEEE Global Communications Conference*, pp. 1–6, 2009.

[55] M. Feder and E. Weinstein, "Parameter estimation of superimposed signals using the EM algorithm," *IEEE Transactions on Acoustics, Speech, and Signal Processing*, vol. 36, pp. 477–489, Apr. 1988.

[56] Y. Xie and C. Georghiades, "Two EM-type channel estimation algorithms for OFDM with transmitter diversity.," *IEEE Transactions on Communications*, vol. 51, no. 1, pp. 106–116, 2003.

[57] J. Fessler and A. Hero, "Space-alternating generalized expectation-maximization algorithm," *IEEE Transactions on Signal Processing*, vol. 42, pp. 2664 –2677, Oct. 1994.

[58] M. Kobayashi, J. Boutros, and G. Caire, "Successive interference cancellation with SISO decoding and EM channel estimation," *IEEE Journal on Selected Areas in Communications*, vol. 19, pp. 1450–1460, Aug. 2001.

[59] D. Shepherd, Z. Shi, M. Anderson, and M. Reed, "EXIT chart analysis of an iterative receiver with channel estimation," *Proc. IEEE Global Communications Conference*, pp. 4010–4014, Nov. 2007.

[60] P. Almers, E. Bonek, A. Burr, N. Czink, M. Debbah, V. Degli-Esposti, H. Hofstetter, P. Kyösti, D. Laurenson, G. Matz, A. F. Molisch, C. Oestges, and H. Özcelik, "Survey of channel and radio propagation models for wireless MIMO systems," *EURASIP Journal on Wireless Communications and Networking*, vol. 2007, pp. 56–56, Jan. 2007.

[61] R. Ertel, P. Cardieri, K. Sowerby, T. Rappaport, and J. Reed, "Overview of spatial channel models for antenna array communication systems," *IEEE Personal Communications*, vol. 5, pp. 10 –22, Feb. 1998.

[62] A. Molisch, *Wireless Communications*. John Wiley & Sons ltd., 2nd ed., 2011.

[63] L. Song and J. Shen, *Evolved Cellular Network Planning and Optimization for UMTS and LTE*. CRC Press, 2011.

[64] P. Hoeher, "A statistical discrete-time model for the WSSUS multipath channel," *IEEE Transactions on Vehicular Technology*, vol. 41, pp. 461–468, Nov. 1992.

[65] S. ten Brink, "Convergence of iterative decoding," *IEEE Electronics Letters*, vol. 35, pp. 806–808, May 1999.

[66] M. Tuchler, R. Koetter, and A. Singer, "Turbo equalization: principles and new results," *IEEE Transactions on Communications*, vol. 50, pp. 754–767, May 2002.

[67] K. Li and X. Wang, "EXIT chart analysis of turbo multiuser detection," *IEEE Transactions on Wireless Communications*, vol. 4, pp. 300–311, Jan. 2005.

[68] J. Hagenauer, "The EXIT chart - introduction to extrinsic information transfer in iterative processing," *Proc. European Signal Processing Conference*, pp. 1541–1548, Sept. 2004.

[69] J. Rabaey, *Digital Integrated Circuits*. Prentice Hall, 2nd ed., 2003.

# Part II

# Included Papers

# *Paper I*

# Iterative receivers with channel estimation for multi-user MIMO-OFDM: Complexity and performance

**Abstract**

A family of iterative receivers is evaluated in terms of complexity and performance for the case of an uplink multi-user (MU) multiple-input multiple-output orthogonal frequency division multiplexing (MIMO-OFDM) system. The transmission over block fading channels is considered. The analyzed class of receivers is performing channel estimation inside the iterative detection loop, which has been shown to improve estimation performance. As part of our results we illustrate the ability of this type of receiver to reduce the required amount of pilot symbols. A remaining question to ask is which combinations of estimation and detection algorithms that provide the best trade-off between performance and complexity. We address this issue by considering MU detectors and channel estimators, with varying algorithm complexity. For MU detection, two algorithms based on parallel interference cancellation (PIC) are considered and compared with the optimal symbol-wise maximum a-posteriori probability (MAP) detector. For channel estimation, an algorithm performing joint minimum mean square error (MMSE) estimation is considered along with a low complexity replica making use of a Krylov subspace method. An estimator based on the space alternating generalized expectation-maximization (SAGE) algorithm is also considered. Our results show that low-complexity algorithms provide the best trade-off, even though more receiver iterations are needed to reach a desired performance.

---


P. Hammarberg, F. Rusek and O. Edfors,
"Iterative Receivers with Channel Estimation for Multi-User MIMO-OFDM: Complexity and Performance,"
to appear in *EURASIP Journal on Wireless Communications and Networking*.

# 1 Introduction

In future wireless systems high data rate transmissions need to be supported, requiring larger bandwidths to be used. At the same time, spectral efficiency is becoming increasingly important. A technology that has become popular in later years, and also found its way into many wireless standards such as, e.g. LTE [1], is the use of multiple-input multiple-output (MIMO) antenna systems in combination with orthogonal frequency division multiplexing (OFDM). OFDM is used to efficiently combat inter-symbol interference (ISI), inherent in broadband transmissions, while MIMO is used for improving the channel spectral efficiency and/or suppress interference.

Introducing multiple users (MU) into such systems, a MU-MIMO-OFDM system is created. In the uplink, accurate multi-user receivers are needed to harvest the available gains. A significant number of algorithms, with varying complexity, have been proposed for this task; ranging from the simple zero-forcing detector to the high complexity maximum-likelihood (ML) detector. Please refer [2] for an overview.

The degree of channel state information (CSI) available at the receiver plays an important role in the design of the receiver structure. While it is convenient for theoretical investigations to assume that perfect CSI is available, practical receivers need to obtain CSI via, e.g. noisy pilot symbol observations. In the case of a large coherence time, the accuracy of the channel estimate can be made high since many symbols can be dedicated for pilot information without any significant effect on the spectral efficiency. In fast fading environments, or packet-based systems, the number of pilot symbols must, however, be kept small to maintain a reasonable spectral efficiency. To this end, other more sophisticated transceiver structures have been developed [3–5]. These receivers jointly detect the data symbols and estimate the transmission channel, which allows for a lower number of inserted pilot symbols as compared to traditional pilot based transceiver systems. While the prospect of reducing the number of pilot symbols is important, these receivers are of limited utility since they have grossly larger computational complexity than traditional pilot based receivers. This complexity amplifies dramatically if the data is coded.

The discovery of the turbo principle [6] brought radical changes to the entire communication field. It is today understood that highly complex problems, such as jointly detecting coded data and estimating the underlying transmission channel, can be efficiently handled by iteratively solving much simpler sub-problems. In particular, during the last decade there has been a growing interest in iteratively solving the joint coded data detection and channel estimation problem [7–10]. The receiver is alternating between decoding of the outer error correcting code, performing multi-user detection (MUD), and esti-

mation the transmission channel, in an iterative manner. In [10], a theoretical framework is presented for this, elsewhere ad-hoc, choice of receiver design; strengthening the motive for this choice.

Even though iterative algorithms can reduce the complexity of the digital receiver, they may still be of prohibitive complexity in many practical scenarios; representing itself in a large chip area and high power consumption. It is therefore important to find low-complexity algorithms that are both power efficient and can deliver performance required to reach high spectral efficiencies.

In the current literature, an impressive number of low-complexity algorithms have been proposed for the different components of an iterative receiver, see e.g. [11]. However, few have studied the trade-off between complexity and performance for the entire receiver, including MUD, channel estimation and channel decoder. One exception being [12], where the complexity and performance of a set of receiver algorithms for MIMO multi-carrier code division multiple access (MC-CDMA) systems are investigated. In contrast to [12], this paper evaluates a family of iterative receivers for an uplink MU MIMO-OFDM system, operating over block fading channels. Furthermore, we have tried to place a greater focus on the convergence properties of the different receiver configurations. The convergence speed is important since more iterations require a larger computational effort. Also worth mentioning is the work in [13], where a performance-complexity comparison of receivers for down-link MIMO-OFDM systems is performed. Unlike in our comparison, the investigated receivers does not contain any channel estimator.

In our evaluation, the complexity of all the building blocks of the iterative receiver is derived, and related to the system performance. Our results show that low-complexity algorithms are generally sufficient, but more complex schemes may be needed if convergence speed, measured in iterations, is at focus. The main contributions are summarized as follows

- A tradeoff analysis between complexity and performance is performed for a MU MIMO-OFDM system incorporating iterative channel estimation and MUD. Two popular channel estimation algorithms, one based on expectation maximization [14], and one performing a joint MMSE estimation of all user channels [8,9], are evaluated. A low-complexity approximation of the latter based on a Krylov subspace projection method, as presented in [12], is also evaluated. Three popular MUDs are considered; two parallel interference cancellation based detectors and one full maximum a-posteriori probability (MAP) detector. The latter being a natural performance benchmark.

- In the tradeoff analysis, the total complexity, in terms of complex multiplications, required to reach a given bit error rate is derived for all

algorithm combinations at different signal-to-noise ratios and number of users. The results show that low-complexity schemes are generally providing the best tradeoff.

- The convergence properties of the different receiver combinations are presented, both in terms of bit error rate, mean square estimation error, and through the use of extrinsic information transfer (EXIT) charts [15]. The EXIT charts visualize the exchange of extrinsic information between the outer code and the rest of the receiver incorporating channel estimation and MUD.

The rest of this paper is organized as follows. In Section 2, a description of the considered MU-MIMO-OFDM system is given. The algorithms for obtaining the channel estimate are presented in Section 3, and the MUD algorithms in Section 4. In Section 5 the complexity of the algorithms is discussed, and in Section 6 the performance of different algorithm combinations is investigated. A complexity versus performance analysis is performed in Section 7, before the paper is summarized in Section 8.

# 2 System Description

## 2.1 MU-MIMO-OFDM system overview

The MU-MIMO-OFDM system under consideration is shown in Fig. 1. It consists of $K$ single-antenna users, transmitting to a receiver (the base-station) equipped with $N$ antennas. The users transmit blocks of $S$ OFDM symbols, each containing $M$ sub-carriers. The first $S_p$ OFDM symbols are reserved for pilot symbols, which are known to the receiver. The following $S_d = S - S_p$ OFDM symbols contain coded data. The total number of information bearing signal constellation points per block, transmitted from each user, then becomes $L = S_d M$. A forward error correcting code (FEC) with rate $R$ is used to generate codewords, which after interleaving, are mapped onto the $L$ signal constellation points. We restrict our investigations to the case of QPSK. An extension to other constellations is conceptually straightforward, but in general non-trivial [16].

After OFDM modulation and pilot insertion, the users transmit their signals over a frequency selective block fading channel, where the different multi-antenna links are independent and identically distributed (IID). The block fading assumption holds if the transmitted data blocks are much shorter than the channel coherence time. Thus, a system with short data blocks transmitted over a channel with moderate Doppler spread is considered. Furthermore, to

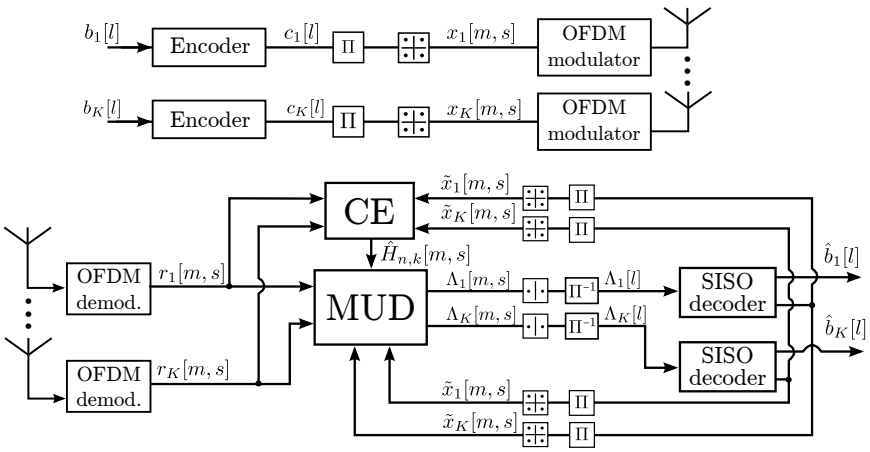


**Figure 1:** A baseband model of a MIMO-OFDM system with $K$ users. The receiver implements an iterative multi-user receiver with channel estimation (CE), multi-user detection (MUD) and a bank of SISO decoders.

allow for correct OFDM demodulation at the receiver, the users are assumed to be synchronized both in time and frequency. In frequency, the synchronization requirement is strict, but due to the use of a cyclic prefix, the time requirement is somewhat relaxed to the case where the difference in arrival times is less than the duration of the cyclic prefix minus the channel delay spread.

At the receiver, the signal is demodulated into the complex baseband, where an iterative receiver is implemented. The complexity-performance trade-off of this receiver is the focal point of this paper. The receiver consists of three blocks; a channel estimator, a MUD, and a bank of soft-input-soft-output (SISO) channel decoders. First, an initial channel estimation is done, based on the transmitted pilot symbols. This estimate is then used in the MUD to separate the different user streams, which are then fed to the SISO decoders. The output of the decoders are then used in the next iteration to update the channel estimate, and to further improve the user separation in the MUD. Multiple iterations are then performed in the same way. The different components are described in detail in later sections.

## 2.2 Input-output relationship of the channel

Next we turn the attention to a description of the input-output relationship of the channel used in this paper. The notation introduced here will also be

used for the description of the various algorithms. Furthermore, a low-rank description of the channel, being used by the channel estimation algorithms, is also introduced in section.

Under the assumption of block-faded channels, the discrete-time model for the received signal at the $m$th subcarrier, during the transmission of OFDM symbol $s$, can be written as

$$\boldsymbol{r}[m,s] = \boldsymbol{H}[m]\boldsymbol{x}[m,s] + \boldsymbol{w}[m,s] \; . \tag{1}$$

where $\boldsymbol{H}[m]$ denotes the composite $N \times K$ channel matrix

$$\boldsymbol{H}[m] \;\; = \;\; \begin{pmatrix} h_{1,1}[m] & \dots & h_{1,K}[m] \\ \vdots & \ddots & \vdots \\ h_{N,1}[m] & \dots & h_{N,K}[m] \end{pmatrix} \; ,$$

from the $K$ autonomous users to the $N$-antenna base-station at subcarrier $m$. For later use, we define $\boldsymbol{h}_{:,k}[m] = [h_{1,k}[m], \dots, h_{N,k}[m]]^{\mathrm{T}}$ and similarily for $\boldsymbol{h}_{n,:}[m]$ and $\boldsymbol{h}_{n,k}[:]$ [1]. Note that due to the block-fading assumption, the matrix $\boldsymbol{H}[m]$ does not depend on $s$. Furthermore, $\boldsymbol{r}[m,s]$, $\boldsymbol{x}[m,s]$, and $\boldsymbol{w}[m,s]$ are column vectors which contain the received signal, the composite transmitted vector from the $K$ users, and the noise vector ($\sim \mathcal{CN}(\boldsymbol{0}, \sigma_w^2 \boldsymbol{I})$ distributed) respectively, at subcarrier $m$ and OFDM symbol $s$.

Let $r_n[m,s]$ denote the $n$th element of the vector $\boldsymbol{r}[m,s]$. For later use, we define the vector

$$\boldsymbol{r}_n[s] = [r_n[1,s],\, r_n[2,s],\, \dots, r_n[M,s]]^{\mathrm{T}},$$

which collects the received signals at antenna $n$ and OFDM symbol $s$, across all subcarriers. Further, this vector equals

$$\boldsymbol{r}_n[s] = \sum_{k=1}^{K} \boldsymbol{X}_k[s]\boldsymbol{h}_{k,n}[:] + \boldsymbol{w}_n[s] \; , \qquad 1 \le n \le N, \tag{2}$$

where $\boldsymbol{X}_k[s] \in \mathbb{C}^{M \times M}$ is a diagonal matrix which contains user $k$'s transmitted data in OFDM symbol $s$ along its diagonal, and $\boldsymbol{w}_n[s] \in \mathbb{C}^{M \times 1}$ is a vector collecting the noise at receive antenna $n$ across subcarriers.

All channel estimation algorithms to be evaluated in this paper are based on low rank approximations of the wireless channel. The assumption made is that the channel is limited in the delay domain, and can therefore be accurately

[1] In general the notation will be that sub-indices state which user and receive antenna is considered, while the time and frequency position will be given in brackets.

represented by a relatively small number of base functions. The optimal set of base functions are presented in [17], and are known under the name *discrete prolate spheroidal* (DPS) sequences. Their use for low-complexity channel estimation were proposed in [18], and estimators using the same type of base functions have also been proposed in, e.g. [19].

Forming a base with $I$ base functions, the frequency response between user $k$ and antenna $n$ of the block fading channel may be expressed as

$$\boldsymbol{h}_{k,n}[:] = \boldsymbol{U}\boldsymbol{\psi}_{k,n} \,, \tag{3}$$

in a notation similar to the one used in [19], where $\boldsymbol{U} \in \mathbb{C}^{M\times I}$ is a matrix collecting $I$ orthonormal base functions in its columns and $\boldsymbol{\psi}_{k,n} \in \mathbb{C}^{I\times 1}$ is a vector containing the corresponding channel DPS coefficients. Note that $\boldsymbol{\psi}_{k,n}$ can be interpreted as the impulse response of the channel, though not mathematically correct unless $\boldsymbol{U}$ is the Fourier base. Using this model of the channel, the received signal in (2) may be expressed as

$$\boldsymbol{r}_n[s] = \sum_{k=1}^{K} \boldsymbol{X}_k[s]\boldsymbol{U}\boldsymbol{\psi}_{k,n} + \boldsymbol{w}_n[s] \,. \tag{4}$$

Now, by collecting the received signal for all $S$ OFDM symbols, and all receive antennas, in a vector, and in a similar way collecting the channel coefficients, $\boldsymbol{\psi}_{k,n}$, for all users and antennas, the received signal may be expressed using the classical linear model [8, 20]. It then becomes

$$\boldsymbol{r} = \bar{\boldsymbol{X}}_N\bar{\boldsymbol{U}}_N\boldsymbol{\psi} + \boldsymbol{w} = \boldsymbol{\Xi}\boldsymbol{\psi} + \boldsymbol{w} \,, \tag{5}$$

where $\boldsymbol{r} \in \mathbb{C}^{SMN\times 1}$ is collecting the received signal in all time-frequency positions and at all receive antennas, $\boldsymbol{\Xi} \in \mathbb{C}^{SMN\times KNI}$ is an observation matrix collecting the transmitted symbols and channel base functions, $\boldsymbol{\psi} \in \mathbb{C}^{KNI\times 1}$ is collecting the channel coefficients for all users, and $\boldsymbol{w} \in \mathbb{C}^{SMN\times 1}$ is collecting noise. More explicitly, the data structures are given by: $\boldsymbol{r} = \left(\boldsymbol{r}^{\mathrm{T}}[1], \ldots, \boldsymbol{r}^{\mathrm{T}}[S]\right)^{\mathrm{T}}$, $\boldsymbol{r}[s] = \left(\boldsymbol{r}^{\mathrm{T}}[1, s], \ldots, \boldsymbol{r}^{\mathrm{T}}[M, s]\right)^{\mathrm{T}}$, $\boldsymbol{\Xi} = \bar{\boldsymbol{X}}_N\bar{\boldsymbol{U}}_N$, $\bar{\boldsymbol{X}}_N = \bar{\boldsymbol{X}} \otimes \boldsymbol{I}_N$, $\bar{\boldsymbol{X}} = (\boldsymbol{X}_1, \ldots, \boldsymbol{X}_K)$, $\boldsymbol{X}_k = \left(\boldsymbol{X}_k^T[1], \ldots, \boldsymbol{X}_k^T[s]\right)^T$, $\bar{\boldsymbol{U}}_N = \boldsymbol{U} \otimes \boldsymbol{I}_{NK}$, $\boldsymbol{\psi} = \left(\boldsymbol{\psi}_1^{\mathrm{T}}, \ldots, \boldsymbol{\psi}_N^{\mathrm{T}}\right)^{\mathrm{T}}$, $\boldsymbol{\psi}_n = \left(\boldsymbol{\psi}_{n,1}^{\mathrm{T}}, \ldots, \boldsymbol{\psi}_{n,K}^{\mathrm{T}}\right)^{\mathrm{T}}$.

The DPS base functions are obtained from solving the eigenvalue equation [8, 17, 19], $\boldsymbol{C}\boldsymbol{u}_i = \lambda_i\boldsymbol{u}_i$, where $\boldsymbol{C} \in \mathbb{C}^{M\times M}$ is a channel correlation matrix. For later use, the eigenvalues $\lambda_i$ are collected in a vector, $\boldsymbol{\lambda} = [\lambda_1, \ldots, \lambda_I]^{\mathrm{T}}$. For $I \geq \lceil \tau_{\max} M \rceil + 1$, the energy of the eigenvalues are small and can in general be neglected [17]. This value sets a bound on the number of DPS sequences that are needed to represent the channel in an accurate way.

# 3 Channel estimation algorithms

In order to achieve satisfactory detection performance, high-accuracy channel estimates need to be made available at the receiver. A large number of appropriate algorithms has been proposed in the literature. Amongst these, two popular families of algorithms have received a great deal of attention; algorithms performing joint estimation for all users [8,21,22], and algorithms based on interference cancellation [14,23]. In this paper, two algorithm from the first, and one from the second family is considered. The algorithms make use of the transmitted pilot symbols, as well as decoded data symbols. Thus, they are all using the turbo principle to iteratively improve the channel estimate as the reliability of the decoded data symbols increases. Furthermore, the algorithms have in common that they all use the same underlying low-rank channel model, the one given in Section 2.2.

The first algorithm, previously presented for MC-CDMA systems in [8, 24] and later for MIMO-OFDM in [21], performs a joint minimum-mean-square-error (MMSE) estimate of the composite channel matrices $\boldsymbol{H}[m]$ based on the model in (3). The second algorithm, presented in [12], uses a Krylov subspace method to approximate a costly matrix inverse in the joint MMSE estimator. The third algorithm, based on [14], is using the expectation maximization (EM) framework, and iteratively performs per-user channel estimation, *i.e.*, estimates of the columns of $\boldsymbol{H}[m]$. We slightly modify the second algorithm by using the improved space alternating generalized EM (SAGE) [25] algorithm. The three algorithms are described below.

## 3.1 Joint MMSE estimator using soft decisions (Joint MMSE)

The optimal channel estimation approach is to estimate all user channels jointly, making use of both pilots and soft estimates of the transmitted symbols, along with the channel correlation properties. Based on the model for the received signal given in (5), the optimal estimate of the channel coefficients $\boldsymbol{\psi}$ (in the MMSE sense) can be derived as [9]

$$\hat{\boldsymbol{\psi}} = \left(\hat{\boldsymbol{\Xi}}^{\mathrm{H}}\boldsymbol{\Delta}^{-1}\hat{\boldsymbol{\Xi}} + \boldsymbol{C}_{\psi}^{-1}\right)^{-1}\hat{\boldsymbol{\Xi}}^{\mathrm{H}}\boldsymbol{\Delta}^{-1}\boldsymbol{r}\,, \tag{6}$$

where $\hat{\boldsymbol{\Xi}}$ has the same structure as $\boldsymbol{\Xi}$, but contains both known pilot symbols and soft estimates of the transmitted data carrying symbols; $\boldsymbol{\Delta} = \mathrm{diag}(\boldsymbol{\vartheta}) + \sigma_w^2\boldsymbol{I}_{NMS}$, with $\boldsymbol{\vartheta} = \left(\boldsymbol{\vartheta}^{\mathrm{T}}[1], \ldots, \boldsymbol{\vartheta}^{\mathrm{T}}[S]\right)^{\mathrm{T}}$, $\boldsymbol{\vartheta}[s] = \left(\boldsymbol{\vartheta}[1,s], \ldots, \boldsymbol{\vartheta}[M,s]\right)^{\mathrm{T}}$, $\boldsymbol{\vartheta}[m,s] = \left(\sum_{k=1}^{K}\left(1 - |\hat{x}_k[m,s]|^2\right)\right)\mathbf{1}_N$, and $\hat{x}_k[m,s]$ are either pilots or soft

symbol outputs from the decoder, and $\mathbf{1}_N$ is the all-ones column vector of length $N$. Further, note that $\text{diag}(\boldsymbol{\vartheta}) = \mathbb{E}\{\boldsymbol{\Xi}\boldsymbol{\psi}\boldsymbol{\psi}^H\boldsymbol{\Xi}^H\} - \hat{\boldsymbol{\Xi}}\boldsymbol{C}_\psi\hat{\boldsymbol{\Xi}}^H$, and $\boldsymbol{C}_\psi$ is the covariance matrix of the DPS sequences.

Due to the sizes of the matrices involved in (6), the computational complexity can be expected to be significant. The computational burden is significantly decreased, but still large, if the sparsity and regularity of $\hat{\boldsymbol{\Xi}}$ is taken into account. We will elaborate more on this in Section 5.

## 3.2 Krylov subspace reduced joint MMSE estimator using soft decisions (Krylov MMSE)

As mentioned above the implementation of the joint MMSE estimator embeds a significant computational cost. Multiplication of matrices of large dimensions, along with a costly matrix inversion, adds greatly to the receiver complexity. In [12] an approach to reduce these costs was proposed. The algorithm is making use of a Krylov subspace method, more precisely the unconditional conjugate gradient method [26], to iteratively solve (6). The method iteratively finds the solution to the linear equation system $\boldsymbol{x} = \boldsymbol{A}\boldsymbol{b}$, based on an initial guess $x_0$, using that $\boldsymbol{A}^{-1} = \sum_{r=1}^{R} a_r \boldsymbol{A}^r \approx \sum_{r=1}^{S_K} a_r \boldsymbol{A}^r$. The number of terms $S_K$ gives the dimensionality of the Krylov subspace, and equals the number of iterations in the algorithm.

Looking at (6), it can be rewritten as $\boldsymbol{b} = \boldsymbol{A}\hat{\boldsymbol{\psi}}$, where $\boldsymbol{b} = \hat{\boldsymbol{\Xi}}^{\mathrm{H}}\boldsymbol{\Delta}^{-1}\boldsymbol{r}$ and $\boldsymbol{A} = \hat{\boldsymbol{\Xi}}^{\mathrm{H}}\boldsymbol{\Delta}^{-1}\hat{\boldsymbol{\Xi}} + \boldsymbol{C}_\psi^{-1}$. Without going into any further details, the algorithm for obtaining the approximate solution $\hat{\boldsymbol{\psi}}_s$, based on an initial guess $\hat{\boldsymbol{\psi}}_0$ and the subspace order $S_k$, is outlined in Table 1 as given in [26]. In the first receiver iteration, $\hat{\boldsymbol{\psi}}_0$ is set to be the all one vector, while in the following iterations, the estimate from the previous receiver iteration is used. Note that the subspace order can either be fixed, or an error threshold $\epsilon$ could be used as a stopping criteria. The former is chosen here in order to get a fixed algorithm runtime and complexity.

## 3.3 SAGE based estimator (SAGE ML)

Even though the Krylov subspace method can significantly reduce the complexity of the joint MMSE estimator, the complexity is still high, since large matrix-vector multiplications are required in each Krylov iteration. A low-complexity alternative, which has shown good performance, is to use an algorithm based on EM/SAGE. In SAGE, given a received signal, the ML solution is iteratively generated based on an underlying subspace model of the data. In [14] one such algorithm was presented, producing an optimal low-rank MMSE estimate of the

**Table 1:** Outline of the Krylov subspace projection method.

| Steps |
|---|
| Input: $\boldsymbol{A}$, $\boldsymbol{b}$ and $\hat{\boldsymbol{\psi}}_0$ |
| $\boldsymbol{r} = \boldsymbol{b} - \boldsymbol{A}\hat{\boldsymbol{\psi}}_0$ |
| $\rho_0 = \boldsymbol{r}^{\mathrm{H}}\boldsymbol{r}$ |
| $\boldsymbol{p} = \boldsymbol{r}$ |
| $\boldsymbol{q} = \boldsymbol{A}\boldsymbol{p}$ |
| $\alpha = \rho_0 / \boldsymbol{p}^{\mathrm{H}}\boldsymbol{q}$ |
| $\hat{\boldsymbol{\psi}}_1 = \hat{\boldsymbol{\psi}}_0 + \alpha\boldsymbol{p}$ |
| $\boldsymbol{r} = \boldsymbol{r} - \alpha\boldsymbol{q}$ |
| for $s = 2, \ldots, S_k$ (or while $\rho_s > \epsilon$) |
| $\rho_s = \boldsymbol{r}^{\mathrm{H}}\boldsymbol{r}$ |
| $\beta = \rho_s / \rho_{s-1}$ |
| $\boldsymbol{p} = \boldsymbol{r} + \beta\boldsymbol{p}$ |
| $\boldsymbol{q} = \boldsymbol{A}\boldsymbol{p}$ |
| $\alpha = \rho_s / \boldsymbol{p}^{\mathrm{H}}\boldsymbol{q}$ |
| $\hat{\boldsymbol{\psi}}_s = \hat{\boldsymbol{\psi}}_{s-1} + \alpha\boldsymbol{p}$ |
| $\boldsymbol{r} = \boldsymbol{r} - \alpha\boldsymbol{q}$ |
| end |
| Output: $\hat{\boldsymbol{\psi}}_{S_k}$ |

channel. The details of that algorithm are outlined below, where a conversion from EM to SAGE has been performed.

The algorithm is processing one receive antenna channel at the time, based on the following underlying model for the channel between user $k$ and receive antenna $n$,

$$\boldsymbol{r}_{k,n}[s] = \boldsymbol{X}_k[s]\boldsymbol{U}\boldsymbol{\psi}_{k,n} + \boldsymbol{w}_k[s], \qquad k = 1, 2, ..., K \ , \tag{7}$$

where $\boldsymbol{w}[s] = \sum_k \boldsymbol{w}_k[s]$ is the complete noise vector. As can be seen, $\boldsymbol{r}_{k,n}[s]$ is the signal contribution from user $k$, and summing over all users gives (2). For the problem at hand, the SAGE algorithm is formulated as [25]

- Initialization: For all $k$ and $s$

$$\hat{\boldsymbol{s}}_{k,n}^{(0)}[s] = \tilde{\boldsymbol{X}}_k[s]\boldsymbol{U}\hat{\boldsymbol{\psi}}_{k,n}^{(0)}. \tag{8}$$

- For each iteration $i$:

for $k = 1 + [i \text{ modulo } K]$, and for all $s$, compute

$$\text{E-step:} \qquad \hat{\boldsymbol{r}}_{k,n}^{(i)}[s] = \hat{\boldsymbol{s}}_{k,n}^{(i)}[s] + \left( \boldsymbol{r}_n[s] - \sum_{j=1}^{K} \hat{\boldsymbol{s}}_{j,n}^{(i)}[s] \right) \tag{9}$$

$$\text{M-step:} \qquad \hat{\boldsymbol{\psi}}_{k,n}^{(i+1)}[s] = \arg \min_{\boldsymbol{\psi}_{k,n}[s]} \left( \left\| \hat{\boldsymbol{r}}_{k,n}^{(i)}[s] - \boldsymbol{X}_k[s] \boldsymbol{U} \boldsymbol{\psi}_{k,n}[s] \right\|^2 \right) \tag{10}$$

$$= \Delta_m \boldsymbol{U}^H \hat{\boldsymbol{X}}_k^H[s] \hat{\boldsymbol{r}}_{k,n}^{(i)}[s], \tag{11}$$

$$\hat{\boldsymbol{\psi}}_{k,n}^{(i+1)} = \frac{1}{S} \sum_{s=0}^{S-1} \hat{\boldsymbol{\psi}}_{k,n}^{(i+1)}[s] = \frac{1}{S} \Delta_m \boldsymbol{U}^H \sum_{s=0}^{S-1} \hat{\boldsymbol{X}}_k^H[s] \hat{\boldsymbol{r}}_{k,n}^{(i)}[s], \tag{12}$$

$$\hat{\boldsymbol{s}}_{k,n}^{(i+1)}[s] = \tilde{\boldsymbol{X}}_k[s] \boldsymbol{U} \hat{\boldsymbol{\psi}}_{k,n}^{(i+1)}. \tag{13}$$

for all $j$, $j \neq k$,

$$\hat{\boldsymbol{s}}_{j,n}^{(i+1)}[s] = \hat{\boldsymbol{s}}_{j,n}^{(i)}[s]. \tag{14}$$

In (11), the matrix $\Delta_m = \text{diag}(\frac{\lambda_1}{\lambda_1+\sigma_w^2}, \ldots, \frac{\lambda_I}{\lambda_I+\sigma_w^2})$ stems from the low-rank MMSE estimator, and in (12) averaging is performed to make use of the assumption that the channel is static over one block.

The value of $\boldsymbol{X}_k[s]$ is only perfectly known at time instances where pilots are transmitted. On all other positions, symbol estimates must be used. The estimates are updated by the SISO decoders in every iteration, using the most recent channel estimate. Here, hard decisions $\hat{\boldsymbol{X}}_k[s] = \text{sign}(\tilde{\boldsymbol{X}}_k[s])$ of the decoded soft symbols are used for channel estimation, and soft for interference cancellation.

At the very first receiver iteration, no channel estimate is available. Therefore, the algorithm is initialized with $\hat{\boldsymbol{s}}_{k,n}^{(0)}[s] = \boldsymbol{X}_k[s]\boldsymbol{1}_M$. Furthermore, to improve the accuracy of the initial estimate, several internal iterations can be performed within the estimator itself. This can be seen as the algorithm being reinitialized with its own updated channel estimate, without waiting for updates on the symbol estimates. In this paper, this is only performed at the initial pilot based stage, where the gain is observed to be the largest. In later stages, multiple internal iterations are not producing any significant gain, thus mainly adding to the computational complexity.

# 4 Soft-Input Soft-Output Multi-user detectors

With estimates of the transmission channel having been made available by the channel estimator, the next stage of the iterative receiver structure is to produce

likelihood-ratios of the coded data symbols. This operation is performed by the MUD, which apart from the received signal and channel estimate, uses a-priori information of the transmitted symbols. This information is provided, from the previous iteration, by the channel decoder. The optimal SISO detector is the symbol-wise MAP detector, implemented through the BCJR algorithm [27]. Unfortunately, the complexity of the MAP detector in the MIMO case is prohibitive in most situations, except for the cases when the number of users $K$ is small. Therefore, reduced complexity techniques have to be considered for most practical applications. Furthermore, although optimal detection is not generally feasible in practice, it remains important as a benchmark reference, and will therefore be considered in this paper. The principles behind the MAP algorithm are outlined in Section 4.1.

Many reduced complexity detection algorithms have been proposed in the literature [2]. To restrict the investigations, two such algorithms have been selected and are presented in Section 4.2. Both algorithms are based on parallel interference cancellation (PIC). The first algorithm applies a matched filter after the cancellation, while the other applies an MMSE filter, in an attempt to further suppress the inter-user interference. While the latter approach yields better performance it is also more complex. In later sections we shall investigate whether the performance gain motivates the increased complexity.

## 4.1 MAP

As stated previously, the optimal MUD is the symbol-wise MAP detector. While the PIC-based algorithms, being introduced in Section 4.2, only make use of the mean values $\tilde{x}_k[m,s]$, the symbol-wise MAP detector works with the probability mass function of $\boldsymbol{x}[m,s]$, denoted $P_{\mathrm{a}}(\boldsymbol{x}[m,s])$.

In the case of QPSK transmission, the data vector $\boldsymbol{x}[m,s]$ contains $2K$ code bits, $c_1,\ldots,c_{2K}$. The MAP detector computes the marginal mass functions, represented by LLR values, for these $2K$ bits:

$$\Lambda(c_q) = \log\left(\frac{\sum_{\boldsymbol{x}:c_q=1}\exp\left(-\frac{|\boldsymbol{r}[m,s]-\boldsymbol{H}[m]\,\boldsymbol{x}|^2}{\sigma_w^2}\right)P_{\mathrm{a}}(\boldsymbol{x})}{\sum_{\boldsymbol{x}:c_q=0}\exp\left(-\frac{|\boldsymbol{r}[m,s]-\boldsymbol{H}[m]\,\boldsymbol{x}|^2}{\sigma_w^2}\right)P_{\mathrm{a}}(\boldsymbol{x})}\right), \qquad q=1\ldots 2K. \quad (15)$$

As was discussed above, the complexity of the symbol-wise MAP detector (15) may in many cases be prohibitively large, showing the demand for low complexity schemes.

## 4.2 PIC based detectors

A popular low-complexity approach is to make use of interference cancellation. Though simple in their implementation, PIC based detectors have shown good performance [8,10,28]. The interference cancellation is operating separately on each subcarrier and OFDM symbol, and makes use of the most recent channel estimate $\hat{\boldsymbol{H}}[m]$, and soft symbol estimates $\tilde{\boldsymbol{x}}[m,s]$ from the SISO decoders. Following the notation in (1), the interference cancelled output for user $k$ is given by

$$\tilde{\boldsymbol{r}}_k[m,s] = \boldsymbol{r}[m,s] - \hat{\boldsymbol{H}}[m]\,\tilde{\boldsymbol{x}}_{\neq k}[m,s]\,, \tag{16}$$

where $\tilde{\boldsymbol{x}}_{\neq k}[m,s]$ is equal to $\tilde{\boldsymbol{x}}[m,s]$, except for element $k$, which is set to zero. A filtering of the signal $\tilde{\boldsymbol{r}}_k[m,s]$ is then applied to produce an estimate of the transmitted symbol $x_k[m,s]$. A mapping to LLR values then follows.

The first algorithm, which will be referred to as PIC-MF, applies a matched filter (MF) to the interference canceled output, *i.e.*

$$\hat{\boldsymbol{x}}_k[m,s] = \frac{\hat{\boldsymbol{h}}^{\mathrm{H}}_{k,:}[m]}{\left\|\hat{\boldsymbol{h}}_{k,:}[m]\right\|^2}\tilde{\boldsymbol{r}}_k[m,s]\,, \tag{17}$$

where $\hat{\boldsymbol{h}}_{k,:}[m]$ is an estimate of the channel between user $k$ and the base-station. In case of QPSK, the complex valued LLRs (with one symbol per complex dimension) are produced as

$$\Lambda_k[m,s] = \frac{2\left\|\hat{\boldsymbol{h}}_{k,:}[m]\right\|^2}{\sigma_k^2}\hat{\boldsymbol{x}}_k[m,s]\,. \tag{18}$$

where

$$\sigma_k^2 = \sigma_w^2 + \sum_{j\neq k}\left|\hat{\boldsymbol{h}}^{\mathrm{H}}_{k,:}[m]\hat{\boldsymbol{h}}_{j,:}[m]\right|^2\left(1-|\tilde{x}_j[m,s]|^2\right). \tag{19}$$

is the variance of the residual interference plus noise for user $k$.

The drawback of PIC-MF is that the noise and residual interference is not taken into account when performing user separation. To alleviate this problem, an MMSE filter can be applied instead of the MF. The resulting algorithm will be referred to as PIC-MMSE. An appropriate MMSE filter can be shown to yield [8]

$$\hat{\boldsymbol{x}}_k[m,s] = \frac{\boldsymbol{i}_K^{(k)\mathrm{T}}\left(\hat{\boldsymbol{H}}^{\mathrm{H}}[m]\hat{\boldsymbol{H}}[m] + \sigma_w^2\boldsymbol{V}^{-1}_{(k)}[m,s]\right)^{-1}\hat{\boldsymbol{H}}^{\mathrm{H}}[m]}{\boldsymbol{i}_K^{(k)\mathrm{T}}\left(\hat{\boldsymbol{H}}^{\mathrm{H}}[m]\hat{\boldsymbol{H}}[m] + \sigma_w^2\boldsymbol{V}^{-1}_{(k)}[m,s]\right)^{-1}\hat{\boldsymbol{H}}^{\mathrm{H}}[m]\hat{\boldsymbol{h}}_{k,:}[m]}\tilde{\boldsymbol{r}}_k[m,s]\,,$$

where $\boldsymbol{i}_K^{(k)}$ is the $k$th column of $\boldsymbol{I}_K$, and $\boldsymbol{V}_{(k)}[m,s] = \mathrm{diag}(d_{k,1}[m,s],\ldots,d_{k,K}[m,s])$ is a diagonal matrix with elements

$$d_{k,k'}[m,s] = \begin{cases} 1-|\tilde{x}_{k'}[m,s]|^2 & ,k' \neq k \\ 1 & ,k' = k. \end{cases}$$

The output of the MMSE filter can be modeled as $\hat{x}_k[m,s] = x_k[m,s] + v_k[m,s]$, with $v_k[m,s] \sim \mathcal{CN}(0,\eta_k^2)$, where

$$\eta_k^2[m,s] = \left( \boldsymbol{i}_K^{(k)\mathrm{T}} \left( \boldsymbol{H}^{\mathrm{H}}[m]\boldsymbol{H}[m] + \sigma_w^2 \boldsymbol{V}_{(k)}^{-1}[m,s] \right)^{-1} \boldsymbol{H}^{\mathrm{H}}[m]\boldsymbol{h}_{k,:}[m] \right)^{-1} - 1. \quad (20)$$

The complex LLR output is then produced as

$$\Lambda_k[m,s] = \frac{2}{\eta_k^2[m,s]} \hat{\boldsymbol{x}}_k[m,s]\,. \quad (21)$$

# 5 Complexity analysis

When it comes to practical implementations of iterative multi-user receivers, complexity considerations are of great importance. Since several receiver iterations are generally needed to reach a desired performance, the total computational effort can grow very large. To get an estimate of this cost, we have chosen to present and compare the complexity of the addressed algorithms in terms of the required number of complex-valued multiplications. This measure is chosen since it provides a reasonable estimate of the complexity, while being analytically tractable. Obviously, the final computational and hardware complexity depends on a large number of parameters, such as memory requirements, parallelization, hardware reuse, word lengths, etc.

In the following sections, the complexities of the algorithms for both MUD and channel estimation are presented. The expressions for the complexity of the SISO decoder, not being treated in a separate section, is given as derived in [29]. The expressions for the complexity per user of the various algorithms are given in Table 2, where the required number of complex multiplications per user is shown. Furthermore, in Table 3, an example of the required number of multiplications per information bit is given, assuming QPSK modulation and rate 1/2 convolutional code, for the following system settings; $N = 4$ receive antennas, $K = 4$ users, $S = 20$ OFDM symbols, $S_p = 1$ OFDM pilot symbol, $M = 256$ subcarriers and $I = 36$ DPS sequences. Note that the DPS sequences, which are used for channel estimation, are assumed to be precalculated and read from memory, thus their construction does not contribute to the computational complexity.

**Table 2:** Expresions for the complexity per user for the different receiver components.

| *Algorithm* | *Total no. of complex mult.* * |
|---|---|
| | Channel estimators |
| SAGE ML | $2MNS + 2MNL + IN$ |
| Joint MMSE | $MS(3+K) + KMI(1+I) + K^2I^3 + N(MS + 2MI + KI^2)$ |
| Krylov MMSE | $3MS + MSN + 2IMN + C_{Ax}(S_k + 1) + IN(5S_k + 2) + 3NS_k/K$ |
| with | $C_{Ax} = 3MSN + IN(M + 1)$ |
| | MUD |
| PIC-MF | $2MSN + 4MS + MNK$ |
| PIC-MMSE | $4SM + 3SMN + SMNK + SMK^3 + MNK$ |
| MAP | $SMN\,2^{2K}/K$ |
| | SISO decoder |
| MAP ** | $(42\,M(S - Sp))/3$ |

* The expressions are given per user and per transmitted data block.
** Expression valid for QPSK and a code rate of $R = 1/2$, and a factor of 3 is included for conversion between real and complex multiplications.

## 5.1 Channel estimator complexity

Three different channel estimation algorithms were presented in Section 3, joint MMSE, Krylov MMSE and SAGE ML. As seen in Table 3, the difference in complexity is significant. For the discussions below, we will assume that the number of OFDM symbols in each block is smaller than the number of subcarriers, *i.e.*, $S < M$.

Looking at the first algorithm, the optimal joint MMSE algorithm, the complexity is large, as previously discussed. Since all user channels are estimated jointly, using all available frequency and time samples, the dimensionality of the problem to solve becomes very large. Looking at (6), a straightforward implementation would be very costly due to the dimensionality of the involved data structures. Fortunately, considerable reductions can be achieved. Firstly, under the assumption of independent receive antenna channels, the same estimator can be used independently on each antenna. Secondly, under the block fading assumption, the matrix $\boldsymbol{\Xi} = \bar{\boldsymbol{X}}_N \bar{\boldsymbol{U}}_N$ is the product of a block diagonal matrix and a block matrix with diagonal sub-matrices. Thus, the operations involving this structure can be computed efficiently. It should be noted that

**Table 3:** Numbers for the required number of complex multiplications per information bit. The numbers are obtaind by evaluating Table 2, and are given for the case of $N = 4$ receive antennas, $K = 4$ users, $M = 256$ subcarriers, $S = 20$ and $S_p = 1$ OFDM symbol, and $I = 36$ DPS sequences. Further, QPSK and a code rate of 1/2 is assumed. The subspace order in Krylov MMSE is set to $S_K = 5$.

| *Algorithm* | *Complex mult. per info. bit* |
|---|---|
| Channel estimators | |
| SAGE ML | 24 |
| Joint MMSE | 465 |
| Krylov MMSE | 145 |
| MUD | |
| PIC-MF | 13 |
| PIC-MMSE | 97 |
| MAP | 256 |
| SISO decoder | |
| MAP | 56 |

under the assumption of independent receive antennas, $\boldsymbol{\Xi}$ is block diagonal with identical sub-matrices. The estimator only involve one of these $SM \times KI$ submatrices. In the end, the main part of the complexity is related to two operations; the product of $\hat{\boldsymbol{\Xi}}^{\mathrm{H}}\boldsymbol{\Delta}^{-1}\hat{\boldsymbol{\Xi}}$ and the inverse operation of a $KI \times KI$ matrix. The computational complexity of the former is approximately $M(IK)^2$, while approximately $(KI)^3$ for the latter. For the system settings considered in this paper the two are of comparable size. Also note that the hermitian properties of the data structures can be exploited to further reduce complexity.

The second algorithm make use of a Krylov subspace method to avoid the explicit matrix inversion in (6). At the same time the explicit computation of $\hat{\boldsymbol{\Xi}}^{\mathrm{H}}\boldsymbol{\Delta}^{-1}\hat{\boldsymbol{\Xi}}$ can be avoided. This will be beneficial as long as $S < M$. Referring back to Section 3.2 and Table 1, the main part of the complexity lies in calculating $\boldsymbol{A}\boldsymbol{v}_s$, which is performed once for every subspace dimension $S_K$. From a complexity point of view, its preferable to keep $S_K$ low. On the other hand, a too small value will provide a poor approximation of the matrix inverse, and thus poor performance. The value thus needs to be chosen with care, trading complexity for performance. An upper limit on the number of dimensions may be set by timing constraints in the receiver.

The last algorithm, based on SAGE, has the lowest complexity and performs a separate channel estimate for each user channel. SAGE ML has less then half the complexity of Krylov MMSE with $S_K = 1$. This suboptimal approach has an attractively low complexity and, as will be seen in Section 6, also delivers good performance. The complexity is linear in the number of user, *i.e.* the complexity per user is constant. The main part of the complexity is shared between the per symbol estimate, the interference cancellation, and the subspace filtering, *i.e.*, the utilization of the frequency correlation. The former two is proportional to the number of OFDM symbols $S$, while the latter to the subspace order $I$, all with the same proportionality constant. The complexity can thus be reduced by lowering the number of OFDM symbols taken into account when performing the estimation, or by reducing $I$. Both actions would come at the price of a performance loss.

## 5.2 MUD complexity

As for the different channel estimation algorithms, the complexity of the considered MUDs differ significantly, as seen from Table 3. The one with the lowest complexity is the PIC-MF, which due to its simplicity requires relatively few arithmetic operations. The complexity is shared between the interference cancellation plus matched filter, and generating the LLRs. The former requiring a bit more computational effort. Despite its low complexity, as will be seen in Section 6, the performance is still competitive at low user loads.

Using a soft information based MMSE filter instead of the matched filter, the performance will be shown to improve. This comes at a cost of an increased complexity due to the MMSE filter in (20) which needs to be calculated for each user and for each data symbol. The filter includes an inverse of a $K \times K$ matrix. At high user loads, computing the inverse will dominate the complexity. If the number of users grow very large, subspace methods as the one used in the Krylov MMSE estimator could be used to reduce the complexity.

If the optimal MAP receiver is considered, the complexity is significantly increased. The complexity, as derived in [30], grows exponentially in the number of users. For few users, the complexity is manageable but, as the number of users grows, it rapidly becomes prohibitive. It should be noted that there exist a number of reduced complexity MAP-like detectors which are based upon searching trees [31, 32], which are not included in our comparison.

# 6 Simulation results

In order to investigate the receiver performance under the use of the different algorithms, computer simulations were performed. In the simulations, each user transmits $S = 20$ OFDM symbols, each with $M = 256$ subcarriers. If nothing else is stated, a single OFDM symbol is dedicated for training information, *i.e.* $S_p = 1$, which is generated randomly for each user. Non-orthogonal transmission of the pilot symbols are assumed, *i.e.* all users transmit their pilot symbols simultaneously in time and frequency. This may incur a loss in performance, but is motivated by the flexibility it brings to the system configuration if varying number of users is to be supported. A rate 1/2 convolutional code with generator polynomial $(7, 5)_8$ is used to generate the code bits, which after random interleaving are mapped to QPSK symbols. For the receiver, we are restricting the investigation to $N = 4$ antennas, while different number of transmitting users are considered.

A fading multi-path IID channel is assumed, mimicking a rich scattering environment. The channel impulse response between user $k$ and receive antenna $n$ is given by [33]

$$g_{k,n}(\tau) = \sum_{p=0}^{P-1} \alpha_{p,k,n} \delta(\tau - \tau_{p,k,n}),$$

where $\alpha_{p,k,n}$ are zero-mean complex Gaussian random variables with an exponential power delay profile, $\theta(\tau_{p,k,n}) = Ce^{-\tau_{p,k,n}/\tau_{\text{rms}}}$, where $C$ is a constant, and the delays $\tau_{p,k,n}$ are uniformly distributed within the cyclic prefix (CP). In this paper, the length of the channel, normalized to the symbol duration, is $\tau_{\max} = 0.1$, the root mean square delay spread set to $\tau_{\text{rms}} = 0.03$, and the number of multi-path components $P = 100$. The channel delay is assumed to be no longer than the cyclic prefix, and the block fading channel is generated independently for each user and receive antenna link. The number of DPS sequences used in the channel estimation process is chosen as $I = 36$, guided by the discussion in Section 2.2, and adding a few for improved performance at high SNR. The subspace order in Krylov MMSE estimator is set to $S_K = 5$, if nothing else is stated.

In the following, the motive behind performing the complex operation of channel estimation in the loop of an iterative receiver is first illustrated with an example. In the example, the average bit error rate (BER) performance at different $E_b/N_0$ is compared for receivers using the channel estimator inside or outside of the iterative loop. It will be seen that the gains by performing the estimation inside the loop can provide significant performance gains. Here, $E_b$ is the average bit energy at the receiver. Furthermore, the impact of the array

gain has been removed by scaling the noise variance by $N$.

We then study the evolution of the BER and mean squared error (MSE) of the channel estimate, over the receiver iterations. This is done for different user loads. The results illustrate the difference in convergence speed of the different receiver configurations, which is important when assessing the total computational complexity needed to reach a certain level of performance. Finally, the convergence analysis is extended with the use of EXIT charts; providing additional insight on the receiver.

## 6.1 Illustration of the gains of using channel estimation inside the detection loop

As was seen in Section 5, performing channel estimation adds significantly to the total receiver complexity. Furthermore, having the estimation inside the loop of an iterative receiver, this costly operation needs to be performed multiple times. It would therefore, from a complexity point of view, be attractive to move the estimation outside the loop, only performing it once for each code block based on the transmitted pilot symbols.

To illustrate the motive behind using the channel estimation inside the iterative receiver, simulations were performed for a system with $N = 4$ receive antennas and $K = 4$ users. Two different receiver configurations were considered. The first is performing pilot based channel estimation only, while the other is performing channel estimation inside the iterative loop. For both receivers, the MAP MUD was used in combination with the joint MMSE channel estimator. In Fig. 2, the BER performance is shown for different number of pilot symbols transmitted. For the purely iterative receiver, only one pilot OFDM symbol is used, while for the other receiver $S_p = 1, 2$ and 10 pilot symbols are transmitted. For comparison, single user performance when perfect channel state information (PCSI) is available at the receiver is also shown. Also, an example with orthogonal pilots is provided, where the users consecutively transmit one pilot symbol each during the first four symbol intervals. Each pilot have been boosted, containing the equivalent energy of four regular symbols.

As seen from the figure, if only pilot based estimates are used, there is a significant performance loss, as compared to when using channel estimation in the iterative loop. For few pilot symbols, a loss in performance of $1 - 3$ dB is observed, while if the number of pilot symbols is increased to $S_p = 10$, the loss is small. Remember that the total number of OFDM symbols in a block is $S = 20$, thus transmitting 10 symbols yields a 50% pilot overhead, which is unacceptable for most applications. Transmitting orthogonal boosted pilots also result in a loss of up to 1 dB. The performance achieved with orthogonal pilots is only slightly better than when transmitting $S_p = 4$ non-orthogonal

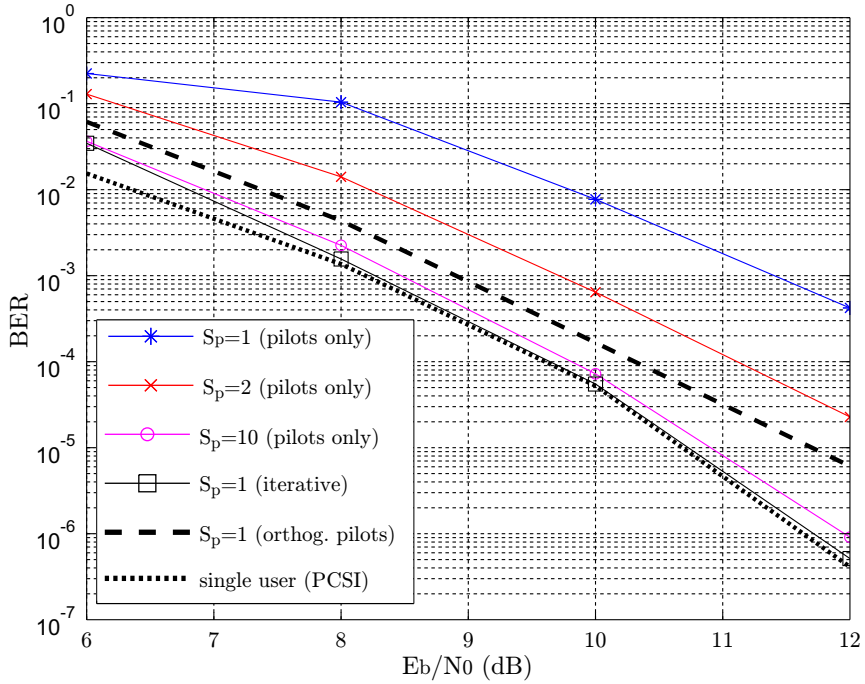


**Figure 2:** The BER at different $E_b/N_0$ for $N = 4$ receive antennas and $K = 4$ users. Different number of pilot OFDM symbols are used, $S_p = 1, 2$ and 10, where the total number of symbols is $S = 20$. Also shown is the performance obtained when using the channel estimator in the loop of the iterative receiver, as well as single user performance with PCSI, and the case of orthogonal boosted pilots. The MAP MUD and joint MMSE estimator is used.

pilots, since joint channel estimation is performed. Furthermore, if iteratively updating the channel estimates, close to single user performance with PCSI is achieved. It can therefore be concluded that the use of channel estimation inside an iterative receiver can give significant performance gains, as compared to pure pilot based approaches. This means that pilot density can be kept low, without sacrificing performance, thus improving the system throughput.

## 6.2 Convergence performance: BER and MSE

In the previous section we illustrated how iterative channel estimation can provide a significant performance gain. At the same time, the complexity can be significant, as seen in Section 5. Since the computational cost increases linearly with iterations, the convergence properties of the different receiver configurations are therefore important. To illustrate their properties, the BER as well as the MSE is shown, as a function of the number of iterations, in Fig. 3 and Fig. 4, respectively. The results are shown for the cases of $K = 4$ and 7 users, at an $E_b/N_0 = 10$dB.

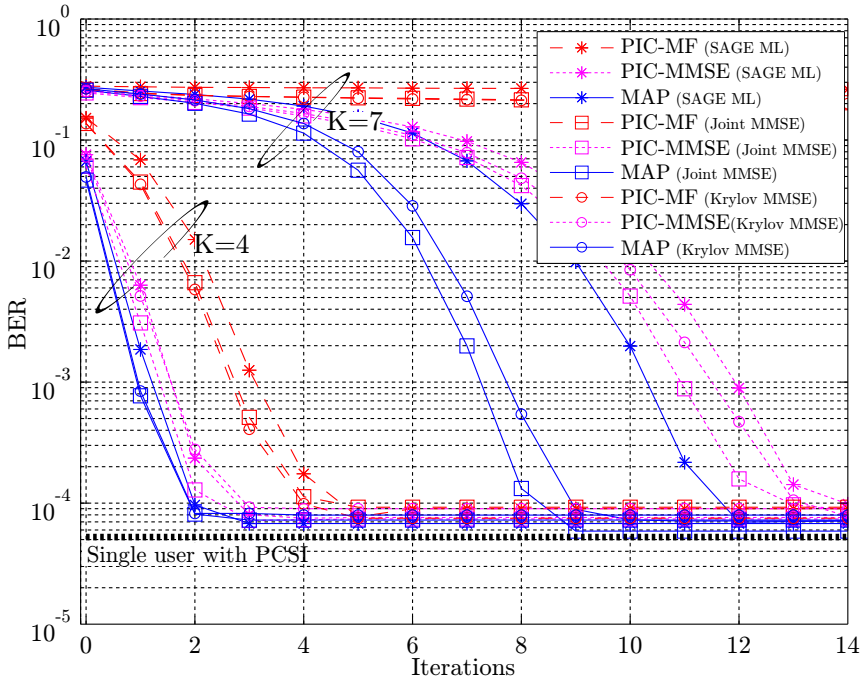


**Figure 3:** The BER convergence for the different algorithms for $N = 4$ receive antennas, $K = 4$ and 7 users, at an $E_b/N_0 = 10$dB.

Starting with the BER in Fig. 3, it is clear that convergence properties differ between algorithm combinations. At the smaller user load, *i.e.* $K = 4$, the difference in convergence is relatively small, with all algorithms reaching roughly the same BER within $3 - 8$ iterations. The fastest convergence is achieved using the MAP based MUD with joint MMSE channel estimation, while the slowest is obtained if using the PIC-MF detector with SAGE ML

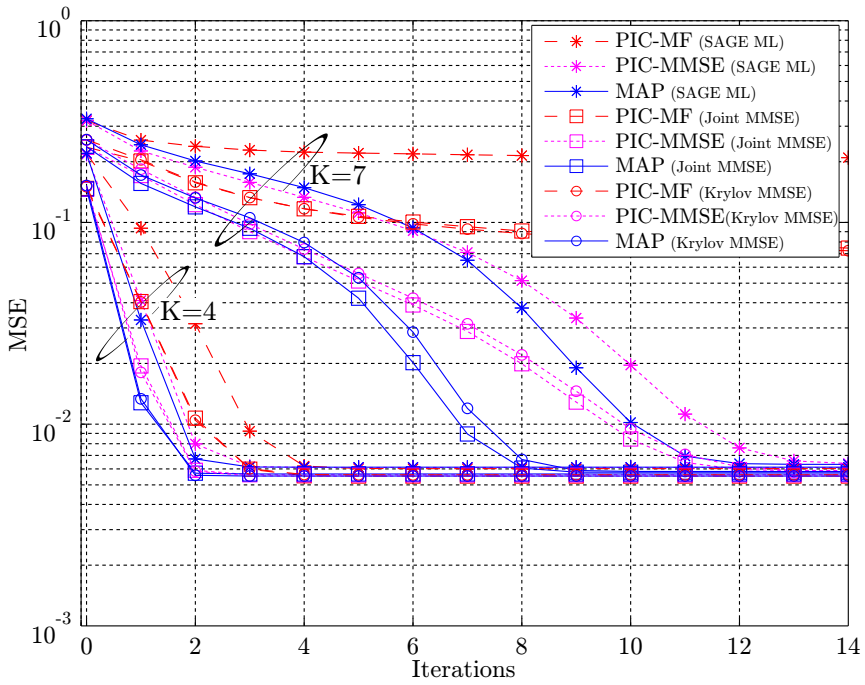


**Figure 4:** The MSE convergence for the different algorithms for $N = 4$ receive antennas, $K = 4$ and 7 users, at an $E_b/N_0 = 10$dB.

estimation. By using the MMSE Krylov estimator with $S_K = 5$, a small performance loss as compared to joint MMSE is observed. Increasing this value to $S_K = 10$, close to joint MMSE performance has been observed. Looking at a system load of $K = 7$ users, a similar behavior as with $K = 4$ is seen. Comparing the performance achieved when using the different MUDs, the best performance is given by the MAP. A gain of $1-5$ iterations over the PIC-MMSE detector is observed. There is a large difference in convergence depending on which estimator is used, and additional insight on this will be given when looking at the EXIT charts in the next section. Furthermore, at this high user load, the PIC-MF can not provide sufficient detection performance for receiver convergence. It is also interesting to note that performance close to that of a single user with PCSI at the receiver is achieved for all receiver configurations, except for PIC-MF at $K = 7$ users. This illustrate the good performance obtained by the iterative receiver.

Looking at the average MSE, as shown in Fig. 4, similar trends as for the

BER are seen. The convergence speed of the joint MMSE estimator is better than that of SAGE ML, and the difference increases with the user load. Furthermore, in the first iteration, only pilot symbols are used for channel estimation, and a large MSE is obtained due to the relatively small number of available pilots. In the iterative process, as the reliability of the symbol estimates increases with iterations, so does the accuracy of the channel estimate.

## 6.3 Convergence performance: EXIT charts

Even though the BER and MSE convergence provide some insight on the behavior of the different algorithms, they have some limitations. One significant drawback is that the performance of the channel estimation and detection algorithms cannot be separated from that of the code. Other means are therefore of interest for the receiver evaluation.

One popular technique for visualizing the convergence behavior of iterative decoders is the extrinsic information transfer (EXIT) charts [15]. The charts are used to visualize the exchange of extrinsic information between the SISO units making up an iterative decoder. In [34], it was shown that the MUD could be seen as SISO unit being serially concatenated with the outer channel decoder. In our case, we have three units, the MUD, the channel estimator and the decoder. Even though it is possible to visualize the exchange between all three SISO units [35, 36], it is more convenient to combine the estimator and the MUD into a single SISO unit [37], referred to as MUD/CE.

In order to produce an EXIT chart, information transfer functions of the SISO units have to be produced. Each unit can be seen a LLR transformer ($\Lambda_\mathrm{a} \rightarrow \Lambda_\mathrm{ext}$), where the transfer function measures the improvement of the LLR-transformation in terms of mutual information between the LLRs and the underlying variables $\boldsymbol{x}$. The transfer function is given as [38]

$$I_\mathrm{ext} = T\left(I_\mathrm{a}\right) , \tag{22}$$

where $I_\mathrm{a} = I\left(X; \Lambda_\mathrm{a}\right)$ is the *a priori* input mutual information and $I_\mathrm{ext} = I\left(x; \Lambda_\mathrm{ext}\right)$ is the output extrinsic information.

When producing the transfer functions, all elements of $\Lambda_\mathrm{ext}$ (becoming $\Lambda_\mathrm{a}$ for the next component decoder) are assumed independent and to follow a Gaussian distribution, $\mathbb{N}\left(x\mu_\mathrm{ext}, \sigma^2_\mathrm{ext}\right)$, with consistency condition $\mu_\mathrm{ext} = \sigma^2_\mathrm{ext}/2$ and where $x = \pm 1$. With this distribution of the LLRs, there is a one-to-one mapping between the mutual information $I_\mathrm{ext}$ and the variance $\sigma^2_\mathrm{ext}$ given by

$$I_\mathrm{ext} = J\left(\sigma_\mathrm{ext}\right) , \tag{23}$$

with the J-function defined in [15]. When generating the transfer functions, the J-function is used for generating input sequences with different *a priori*

information content. More specifically, given an input symbol $x$, and a value for the *a priori* information $I_{\mathrm{a}}$, the input LLRs are given by

$$\Lambda_{\mathrm{ext}}(I_{\mathrm{a}}) = \frac{\sigma_{\mathrm{ext}}^2}{2} x + w\sigma_{\mathrm{ext}}\,, \tag{24}$$

where $w \sim \mathcal{N}(0,1)$, and $\sigma_{\mathrm{ext}}^2 = J^{-1}(I_{\mathrm{a}})$.

For the MUD/CE, as shown in Fig. 1, the transfer function is now derived for a number of $I_{\mathrm{ext}} \in [0,1]$. We first generate the soft input symbols $\tilde{x}_k = \tanh(\Lambda_{\mathrm{ext}}(I_{\mathrm{a}})/2)$ and the known pilot symbols for all users. After QPSK mapping, channel estimation and MUD is performed. The LLR output generated by the MUD is then feed to a sink, where the mutual information is computed through [38]

$$I_{\mathrm{ext}} = \frac{1}{2} \sum_{x=\pm 1} \int_{-\infty}^{\infty} p(\hat{x}|x) \log_2 \left( \frac{2p(\hat{x}|x)}{p(\hat{x}|-1) + p(\hat{x}|1)} \right) d\hat{x}, \tag{25}$$

where the probability density function, $p(\hat{d}|d)$, is approximated using histogram calculations. The transfer functions are then averaged over 20 channel realizations. The transfer function for the SISO decodercan is obtained in a similar way.

When generating the transfer function for the MUD/CE, the initial guess for the Krylov MMSE and SAGE ML has to be provided. In the receiver this value is given by the estimate obtained in the previous iteration. Since this value is unknown, we solve it by running the channel estimator twice, first initialized with the all one channel then reinitialized with the new output. This potentially leads to an over estimated performance at high $I_{\mathrm{ext}}$. For SAGE ML this also leads to an under estimated performance at low values.

In Fig. 5 the EXIT chart is shown for the different receiver combinations for the case of $N = 4$ receive antennas and $K = 4$ users at $E_b/N_0 = 10$dB. The transfer functions in the case of PCSI is also shown. Furthermore, the convergence path for PIC-MF with SAGE ML estimation is shown as a dashed line, and the receiver is estimated to converge in 5 iterations. This coincide with the observation for the BER in Fig. 3. For the receivers where SAGE ML is used, a dip is seen in the transfer function at low $I_{\mathrm{a}}$. This occurs since the algorithm is not taking the quality of the soft symbols into account, thus producing estimates based on very unreliable hard estimates of the transmitted symbols. This dip could be partly removed if only pilots are considered ($I_{\mathrm{a}} = 0$) in the estimator if the reliability of the produced soft symbols are low.

Comparing the channel estimation algorithms, Krylov MMSE, used with $S_K = 5$, delivers performance identical to Joint MMSE. For SAGE ML, the

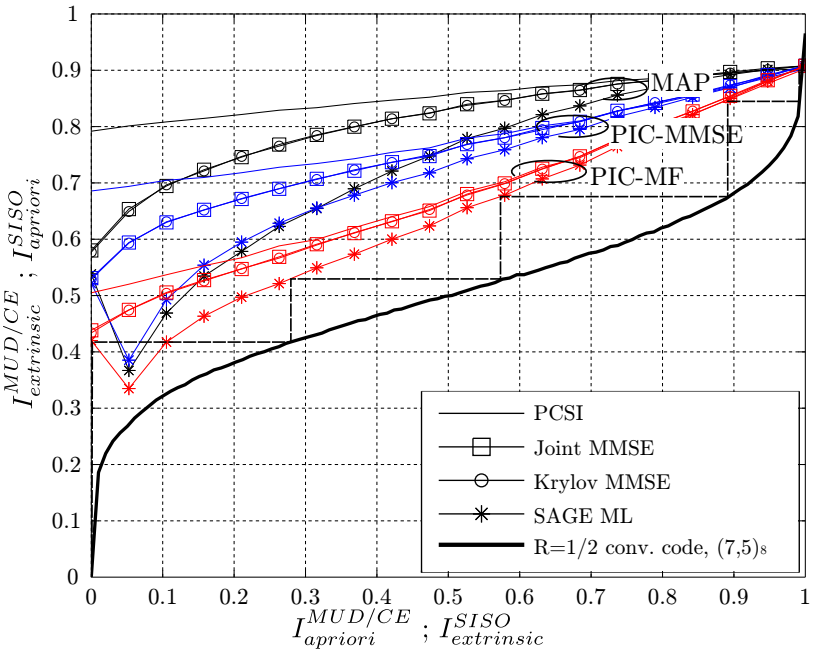


**Figure 5:** EXIT chart for the case of $N = 4$ receive antennas, $K = 4$ users, $S_p = 1$ and $S = 20$ OFDM symbols, $M = 256$ subcarriers and $I = 36$ DPS sequences.

performance is much worse, but the performance at low $I_{\mathrm{a}}$ is somewhat underestimated as discussed above. Looking at the MUDs, the MAP obviously has the best performance, followed by PIC-MMSE and PIC-MF. We also see the impact of inaccurate channel state information. When the SNR reduced, essentially leading to downward shift of the transfer functions of the MUD/CE, of when increasing the user load, essentially changing the slope of the transfer functions, the PIC-MF will be the first MUD closing the gap to the SISO decoder transfer function, and thus failing to converge.

Overall, we see that the insight given by the EXIT chart matches fairly well with what was observed for the BER. Furthermore, observing the MAP detector for $K = 7$ users in Fig. 3, large difference in convergence performance between using the MMSE estimators or SAGE ML was observed. This could be explained by the fact that the gap in the EXIT chart is smaller for the latter estimator. From a algorithm design point of view, it is also interesting to observe that for the case presented in Fig. 5 there is still room for further

simplifications of the receiver structure. Additionally, by replacing the transfer function for the chosen convolutional code in Fig. 5, the performance when using other codes can be estimated.

# 7 Complexity versus performance trade-off

From a receiver design point of view, the trade-off between performance and complexity is an important aspect. In an attempt to shed some light on this aspect, the total receiver complexity, in terms of the number of complex multiplications, needed to reach a specific target BER is investigated. The total complexity depends both on the choice of channel estimator and MUD, as well as on the number of iterations needed to reach the target. For the evaluation, a target BER of $10^{-3}$ is chosen. The system settings are the same as described in Section 6, *i.e.* $N = 4$ receive antennas, $S_p = 1$ and $S = 20$ OFDM symbols, $M = 256$ subcarriers and $I = 36$ DPS sequences. The subspace order in Krylov MMSE is set to $S_K = 5$.

To start with, the case of $K = 4$ users, signaling at an $E_b/N_0 = 10$ dB, is considered. In Fig. 6, the BER is plotted versus the number of complex multiplications, for the different combinations of the MUD and channel estimation algorithms.

As was previously seen in Fig. 3, under these system settings, all receivers reach the same BER performance of $\sim 10^{-4}$. On the other hand, looking at the number of multiplications needed to reach this value, there is more than an order of magnitude difference between the receiver configurations. The receiver configurations using the MAP detector is found on the right, requiring the largest number of multiplications to reach convergence. To the left, we find the PIC based MUDs using SAGE ML, providing the cheapest alternative. Looking at the target BER of $10^{-3}$, the algorithms with the lowest total complexity is PIC-MF followed by PIC-MMSE. Reaching the target in about 70 and 100 complex multiplications per information bit, respectively. When using the MMSE Krylov estimator, we see that PIC-MF and PIC-MMSE reach the target using approximately the same number of multiplications, though PIC-MF require one more iteration.

Finally, an overview of which algorithm combinations to choose in different scenarios is given. In Fig. 7, the receiver configuration with the lowest total complexity, at different user loads and $E_b/N_0$, is shown for a target BER of $10^{-3}$. The shape indicates which MUD that is used, while the color indicates the choice of channel estimation algorithm. Due to their large complexity, neither the MAP detector, nor the joint MMSE estimator are competitive in any of the evaluated scenarios – not even at high system loads. Note that 8 users

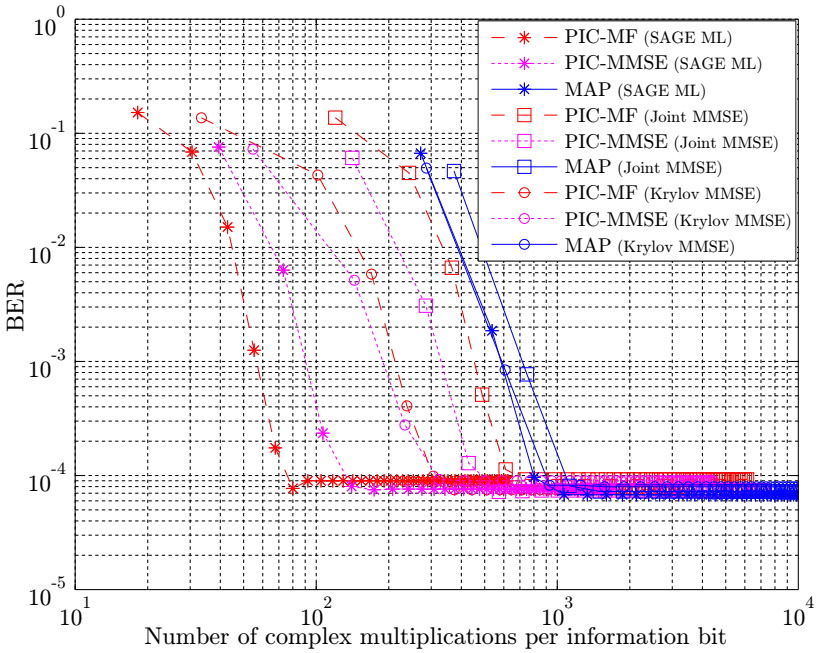


**Figure 6:** The complexity in terms of the number of complex multiplications per information bit plotted versus the BER. The results are shown for $N = 4$ receive antennas, $K = 4$ users, $S_p = 1$ and $S = 20$ OFDM symbols, $M = 256$ subcarriers and $I = 36$ DPS sequences.

is at the border of what the system can handle, still, even with sub-optimal algorithms, low BER can be achieved. Overall, the most favorable receiver configuration to use, from a complexity point of view, is the PIC-MF MUD combined with the SAGE ML estimator. At higher user loads though, the PIC-MMSE detector gives the best trade-off between complexity and performance. For channel estimation, using anything but SAGE ML is in general not required for the considered system.

The results shown in Fig. 7 take overall computational complexity into account and may therefore fail to show other interesting trade-offs. An example of this is seen in Fig. 3, where the difference in convergence speed between the algorithms is large. Depending on the hardware architechture used, this may affect the latency of the system, and for time critical systems, the choice of algorithm combinations may therefore be another. We believe, however, that our evaluation shows that combinations of algorithms with low computational

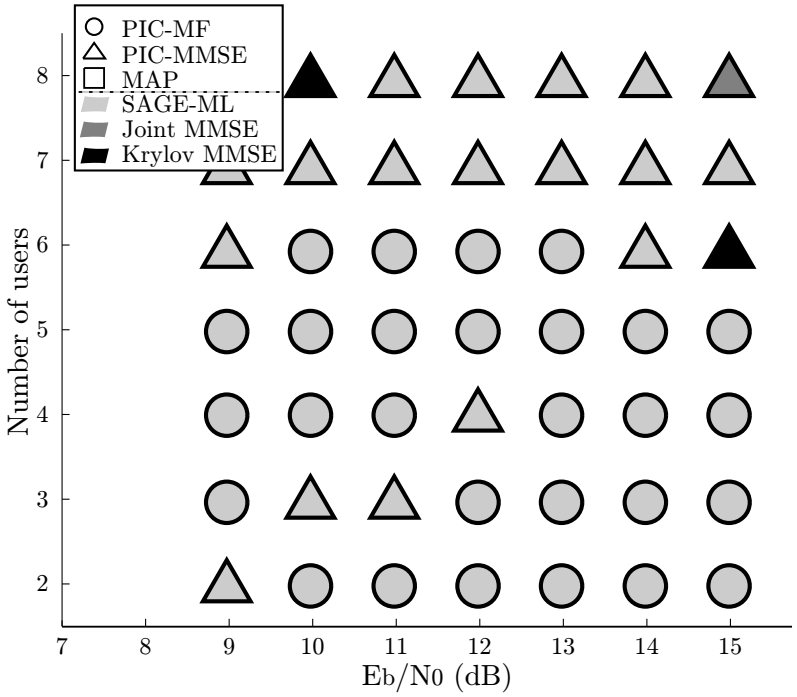


**Figure 7:** Complexity-performance trade-off for the different algorithms, when $N = 4$ receive antennas, at different $E_b/N_0$ and user loads. The figure show the algorithm combination reaching a BER threshold of $10^{-3}$ in the fewest number of complex multiplications. The shape indicates the MUD algorithm, while color indicates channel estimation algorithm.

complexity, in an iterative receiver, can deliver very competitive performance for a large range of scenarios.

# 8 Conclusion

In this paper, we have studied the trade-off between complexity and performance for uplink receivers in a packet based multi-user MIMO-OFDM system. The considered iterative receivers contained three main components; a MUD, a channel estimator and a convolutional decoder. Three different MUD algorithms were considered, two suboptimal approaches based on PIC and one op-

timal based on MAP. For channel estimation, three algorithms were evaluated, one optimal joint MMSE based estimator, a low complexity Krylov subspace based version of the same, and one sub-optimal based on SAGE. The difference in complexity between the algorithms were shown to be large.

When only considering performance, the high complexity algorithms naturally showed the fastest convergence. The low-complexity algorithms showed similar BER performance as the more complex ones, when converging, but at a generally slower convergence speed. More insight on the convergence was also provided through EXIT charts. When also taking complexity into account, we demonstrate that the sub-optimal low-complexity algorithms often are the most attractive choice. Even though a larger number of receiver iterations were needed, the total number of complex multiplications was still lower, due to a significantly lower computational cost per-iteration. At the same time, it should be noted that the most simple receiver failed earlier than the others at high user loads, which indicates that an appropriate balance between complexity reduction and performance needs to be achieved. Furthermore, for time critical systems where convergence speed is at focus, high complexity algorithms may be a better choice.

## References

[1] E. Dahlman, S. Parkvall, J. Sköld, and P. Beming, *3G Evolution HSPA and LTE for Mobile Broadband*. Academic Press, 2nd ed., 2008.

[2] E. Larsson, "MIMO detection methods: How they work," *IEEE Signal Processing Magazine*, vol. 26, no. 3, pp. 91–95, 2009.

[3] H. Vikalo, B. Hassibi, and P. Stoica, "Efficient joint maximum-likelihood channel estimation and signal detection," *IEEE Transactions on Wireless Communications*, vol. 5, pp. 1838–1845, June 2006.

[4] W. Xu, M. Stojnic, and B. Hassibi, "On exact maximum-likelihood detection for non-coherent MIMO wireless systems: a branch-estimate-bound optimization framework," *Proc. IEEE International Symposium on Information Theory*, pp. 2017–2021, June 2008.

[5] D. Ryan, I. Collings, and I. Clarkson, "GLRT-optimal noncoherent lattice decoding," *IEEE Transactions on Signal Processing*, vol. 55, pp. 3773–3786, July 2007.

[6] C. Berrou and A. Glavieux, "Near optimum error correcting coding and decoding: turbo-codes," *IEEE Transactions on Communications*, vol. 44, no. 10, pp. 1261–1271, 1996.

[7] X. Wautelet, A. Dejonghe, and L. Vandendorpe, "MMSE-based fractional turbo receiver for space-time BICM over frequency-selective MIMO fading channels," *IEEE Transactions on Signal Processing*, vol. 52, no. 6, pp. 1804–1809, 2004.

[8] T. Zemen, C. Mecklenbrauker, J. Wehinger, and R. Muller, "Iterative joint time-variant channel estimation and multi-user detection for MC-CDMA," *IEEE Transactions on Wireless Communications*, vol. 5, pp. 1469–1478, Jun. 2006.

[9] P. Salvo Rossi and R. Müller, "Slepian-based two-dimensional estimation of time-frequency variant MIMO-OFDM channels," *IEEE Signal Processing Letters*, vol. 15, pp. 21–24, 2008.

[10] B. Hu, I. Land, L. Rasmussen, R. Piton, and B. Fleury, "A divergence minimization approach to joint multiuser decoding for coded cdma," *IEEE Journal on Selected Areas in Communications*, vol. 26, pp. 432–445, Apr. 2008.

[11] M. E. Honig, *Advances in Multiuser Detection*. John Wiley & Sons, Inc., 2009.

[12] C. Dumard and T. Zemen, "Low-complexity MIMO multiuser receiver: A joint antenna detection scheme for time-varying channels," *IEEE Transactions on Signal Processing*, vol. 56, pp. 2931 –2940, Jul. 2008.

[13] J. Ketonen, M. Juntti, and J. Cavallaro, "Performance - complexity comparison of receivers for a LTE MIMO-OFDM system," *IEEE Transactions on Signal Processing*, vol. 58, pp. 3360–3372, Jun. 2010.

[14] J. Gao and H. Liu, "Low-complexity MAP channel estimation for mobile MIMO-OFDM systems," *IEEE Transactions on Wireless Communications*, vol. 7, no. 3, pp. 774–780, 2008.

[15] S. ten Brink, "Convergence of iterative decoding," *IEEE Electronics Letters*, vol. 35, pp. 806–808, May 1999.

[16] J. Ylioinas, M. Raghavendra, and M. Juntti, "Avoiding matrix inversion in DD SAGE channel estimation in MIMO-OFDM with M-QAM," in *Proc. IEEE Vehicular Technology Conference 2009 fall*, pp. 1–5, Sept. 2009.

[17] D. Slepian, "Prolate spheroidal wave functions, Fourier analysis, and uncertainty - V: The discrete case," *Bell System Technical Journal*, vol. 57, pp. 1371–1430, May/Jun. 1978.

[18] T. Zemen and C. Mecklenbrauker, "Time-variant channel estimation using discrete prolate spheroidal sequences," *IEEE Transactions on Signal Processing*, vol. 53, pp. 3597–3607, Sept. 2005.

[19] O. Edfors, S. Wilson, and P. Börjesson, "OFDM channel estimation by singular value decomposition," *IEEE Transactions on Communications*, vol. 46, no. 7, pp. 931–939, 1998.

[20] S. M. Kay, *Fundamentals of Statistical Signal Processing, Volume I: Estimation Theory*. Prentice Hall, 1993.

[21] P. Salvo Rossi and R. Müller, "Joint iterative time-variant channel estimation and multi-user detection for MIMO-OFDM systems," in *Proc. IEEE Global Communications Conference*, pp. 4263–4268, Nov. 2007.

[22] Y. Li, N. Seshadri, and S. Ariyavisitakul, "Channel estimation for OFDM systems with transmitter diversity in mobile wireless channels," *IEEE Journal on Selected Areas in Communications*, vol. 17, pp. 461–471, Mar. 1999.

[23] M. Münster and L. Hanzo, "Parallel-interference-cancellation-assisted decision-directed channel estimation for OFDM systems using multiple transmit antennas," *IEEE Transactions on Wireless Communications*, vol. 4, no. 5, pp. 2148–2162, 2005.

[24] T. Zemen, M. Loncar, J. Wehinger, C. Mecklenbrauker, and R. Muller, "Improved channel estimation for iterative receivers," in *Proc. IEEE Global Communications Conference*, vol. 1, pp. 257–261, Dec. 2003.

[25] J. Fessler and A. Hero, "Space-alternating generalized expectation-maximization algorithm," *IEEE Transactions on Signal Processing*, vol. 42, pp. 2664 –2677, Oct. 1994.

[26] R. Barrett, M. Berry, T. F. Chan, J. Demmel, J. Donato, J. Dongarra, V. Eijkhout, R. Pozo, C. Romine, and H. Van der Vorst, *Templates for the Solution of Linear Systems: Building Blocks for Iterative Methods*. Philadelphia, PA: SIAM, 2nd ed., 1994.

[27] L. Bahl, J. Cocke, F. Jelinek, and J. Raviv, "Optimal decoding of linear codes for minimizing symbol error rate," *IEEE Transactions on Information Theory*, vol. 20, pp. 284–287, Mar. 1974.

[28] H. Lee and I. Lee, B.; Lee, "Iterative detection and decoding with an improved V-BLAST for MIMO-OFDM systems," *IEEE Journal on Selected Areas in Communications*, vol. 24, no. 3, pp. 504–513, 2006.

[29] D. Costello, A. Banerjee, C. He, and P. Massey, "A comparison of low complexity turbo-like codes," in *Signals, Systems and Computers. Conference Record of the Thirty-Sixth Asilomar Conference on*, vol. 1, pp. 16–20, 2002.

[30] S. Roy and T. Duman, "Soft input soft output Kalman equalizer for MIMO frequency selective fading channels," *IEEE Transactions on Wireless Communications*, vol. 6, no. 2, pp. 506–514, 2007.

[31] J. Boutros, N. Gressety, L. Brunel, and M. Fossorier, "Soft-input soft-output lattice sphere decoder for linear channels," in *Proc. IEEE Global Communications Conference*, Dec. 2003.

[32] K. K. V. Wong, *The soft-output M-algorithm and its applications.* Dept. Electrical and Computer Eng., Queens University, Canada: Ph.D. thesis, 2006.

[33] P. Hoeher, "A statistical discrete-time model for the WSSUS multipath channel," *IEEE Transactions on Vehicular Technology*, vol. 41, pp. 461–468, Nov. 1992.

[34] P. Alexander, A. Grant, and M. Reed, "Iterative detection in code-division multiple-access with error control coding," *European Transactions on Telecommunications*, vol. 9, p. 419425, Sept. 1998.

[35] F. Brannstrom, L. Rasmussen, and A. Grant, "Convergence analysis and optimal scheduling for multiple concatenated codes," *IEEE Transactions on Information Theory*, vol. 51, no. 9, pp. 3354–3364, 2005.

[36] D. Shepherd, Z. Shi, M. Anderson, and M. Reed, "EXIT chart analysis of an iterative receiver with channel estimation," *Proc. IEEE Global Communications Conference*, pp. 4010–4014, Nov. 2007.

[37] R. Otnes and M. Tchler, "EXIT chart analysis applied to adaptive turbo equalization," *Proc. 5th Nordic Signal Processing Symp.*, 2002.

[38] S. ten Brink, "Convergence behavior of iteratively decoded parallel concatenated codes," *IEEE Transactions on Communications*, vol. 49, pp. 1727–1737, Oct. 2001.

# *Paper II*

# EXIT Chart Evaluation of a Receiver Structure for Multi-User Multi-Antenna OFDM Systems

**Abstract**

In this paper we evaluate, by means of Extrinsic Information Transfer (EXIT) charts, an iterative receiver that has emerged as a promising candidate for non-coherent multi-user multi-antenna OFDM systems. The receiver performs parallel interference cancellation (followed by linear filtering) and channel estimation, using soft symbols obtained from a bank of single-user decoders. For the sake of conceptual clarity we study a system with two single antenna users and a receiver with two antennas, and we demonstrate how the convergence behavior of the receiver can be visualized using paired three dimensional EXIT surfaces. Our results show that the actual decoder trajectories obtained through simulations are well predicted from the EXIT charts.

For the iterative receiver under investigation we identify a very specific problem with EXIT chart generation; the EXIT curve for the inner component decoder depends on the outer encoder. To handle this problem we propose a modification to the iterative receiver which solves the aforementioned problem; the performance degradation is demonstrated to be small.

---


P. Hammarberg, F. Rusek, P. Salvo Rossi, and O. Edfors,
"EXIT Chart Evaluation of a Receiver Structure for Multi-User Multi-Antenna OFDM Systems,"
in *Proc. IEEE Global Communications Conference (GLOBECOM)*, Dec. 2009.

# 1 Introduction

In the last few years we have seen a large growth in data traffic over wireless networks. With increasing traffic, capacity of wireless networks must scale proportionally. Future systems thus need to make better use of the available, limited, spectrum and/or search for available resources elsewhere. A number of technologies that provide increased spectral efficiency have been proposed; in particular, multi-antenna systems have received much attention lately. With the use of multi-antenna systems large gains can be harvested due to multiplexing in the spatial domain alongside the frequency and time domains. Multiple antennas at the receiver can also be used to perform multi-user detection (MUD) or interference cancellation, allowing improved resource utilization.

In order to harvest the promised gains, some form of advanced coding method must be used in conjunction with the multi-antenna system. The invention of turbo codes made it possible to implement capacity achieving codes with a reasonable decoding complexity. The convergence behavior of turbo codes can be visualized by the use of EXtrinsic Information Transfer (EXIT) charts, as proposed in [1]. These charts visualize the exchange of mutual information between concatenated code blocks and have become a valuable tool for designing turbo codes.

Since the invention of turbo codes, the turbo principle has successfully been applied to channel equalization [2] and estimation [3] [4], further improving performance of wireless receivers. Also for these applications, EXIT charts have shown to be a helpful tool for visualizing convergence behavior and aid performance evaluation. In, e.g., [5] the convergence behavior of an iterative MIMO receiver is evaluated using EXIT charts, assuming perfect channel state information (PCSI) and a single code stream multiplexed over the antennas. Kansanen [6] treats the case with multiple code streams and shows paired three dimensional (3D) EXIT surfaces for a turbo equalizer, again assuming PCSI. Sand et al. [7] evaluate a receiver with iterative channel estimation and equalization, analyzing the convergence behavior. In [8] a 3D EXIT chart is used to show the information flow between the code, equalizer and channel estimator for a single antenna link.

In this paper we evaluate an iterative receiver, as proposed in [9], by means of EXIT charts. The receiver is intended for multi-user multi-antenna OFDM systems performing parallel interference cancellation and channel estimation, using soft symbols obtained from a block of single user decoders. That is, unlike in above cited work, we look at a system with imperfect channel state information, and multiple code streams. We show how the convergence behavior of the receiver can be visualized using EXIT surfaces. The case of two single antenna users, and a receiver with two antennas, is treated. For this system we show

that the corresponding EXIT chart can be visualized using paired 3D charts, one for each user code stream. We also propose changes to the receiver simplifying EXIT chart generation, and look at the convergence region, represented as projections onto a plane. Our results show that the convergence trajectory obtained through simulations are close to the one obtained by the EXIT chart.

The outline of the paper is as follows; in section 2 the system model and the receiver structure is briefly introduced, followed by a presentation of the EXIT chart representation in section 3. Our results are presented in section 4 before we conclude our findings in section 5.

## 2 System Model

A multi-user OFDM system with $K$ users equipped with a single antenna each, and a receiver with $N$ antennas is considered. The users are assumed non-cooperative, i.e. they transmit independent data, but for simplicity we assume them to be synchronous. For the sake of clarity we restrict the presentation to the case $K = N = 2$ with the remark that the extension to arbitrary $N$ and $K$ is straightforward.

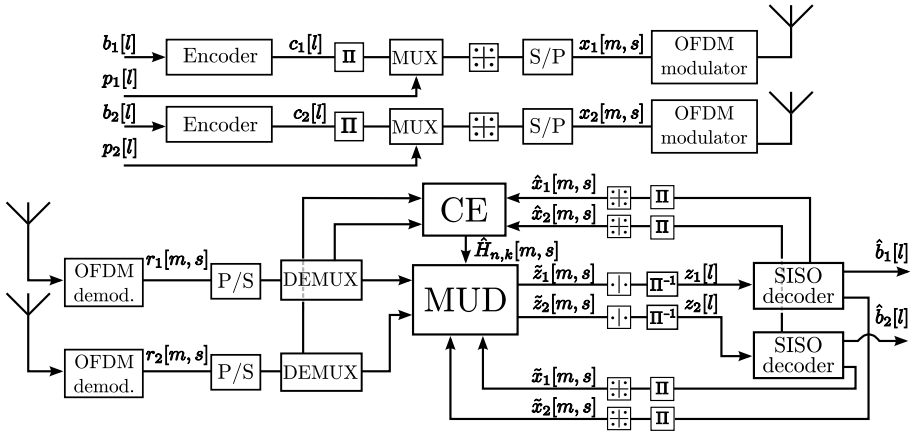


**Figure 1:** The structure of the iterative receiver.

The transmit/receive chain is depicted in Fig. 1 for the case considered. Each stream is encoded via convolutional coding and interleaved using an s-random interleaver [10]. QPSK mapping, serial to parallel conversion, and OFDM modulation follows. To provide the iterative receiver with an initial

channel estimate, $S_p$ pilot OFDM symbols are inserted. We assume (small) finite packet transmission, with $S$ denoting the total number of OFDM symbols sent from the transmitter within a frame (not to confuse with the interleaver s-parameter); the number of information carrying symbols is thus $S - S_p$. Consequently, each user transmits $2(S - S_p)MR_c$ information bits, where $M$ is the number of subcarriers, $R_c$ is the rate of the encoder and the factor 2 stems from the QPSK modulation. The frame structure is shown in Fig. 2.

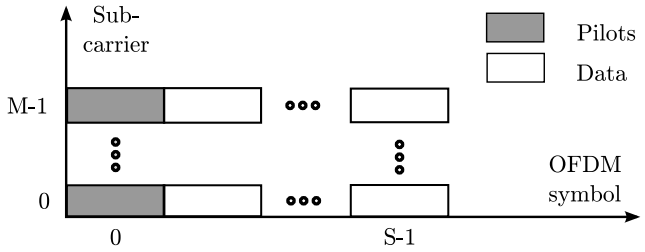


**Figure 2:** $M$ subcarrier OFDM frame structure with, in this case, one pilot symbols followed by S-1 data symbols.

Referring to the $m$th subcarrier during transmission of the $s$th OFDM symbol, we denote the transmitted vector, the channel matrix, the AWGN vector ($\sim \boldsymbol{C}\mathcal{N}(\boldsymbol{0}, \sigma_w^2 \boldsymbol{I}$)), and the received vector as

$$\begin{aligned}
\boldsymbol{x}[m,s] &= (x_1[m,s], \ldots, x_K[m,s])^{\mathrm{T}} \ , \\
\boldsymbol{H}[m,s] &= \begin{pmatrix} H_{1,1}[m,s] & \ldots & H_{1,K}[m,s] \\ \vdots & \ddots & \vdots \\ H_{N,1}[m,s] & \ldots & H_{N,K}[m,s] \end{pmatrix} \ , \\
\boldsymbol{w}[m,s] &= (w_1[m,s], \ldots, w_N[m,s])^{\mathrm{T}} \ , \text{and} \\
\boldsymbol{r}[m,s] &= (r_1[m,s], \ldots, r_N[m,s])^{\mathrm{T}} \ .
\end{aligned}$$

The discrete-time model for the received signal can then be written as

$$\boldsymbol{r}[m,s] = \boldsymbol{H}[m,s]\boldsymbol{x}[m,s] + \boldsymbol{w}[m,s] \ . \tag{1}$$

Note that $\boldsymbol{H}$ is the multi-user channel, containing the coefficients for all users.

At the receiver, as illustrated in Fig. 1, OFDM symbols are demodulated and sent to the iterative decoder, performing MUD, Soft-Input Soft-Output (SISO) decoding and channel estimation (CE). The multi-user detector and SISO decoders exchange extrinsic information on symbols $x_k$, denoted $\tilde{x}_k$ (resp. $\tilde{z}_k$) when going to the multi-user detector (resp. the SISO decoders). The SISO

decoders also provide *a posteriori* information of the transmitted symbols $x_k$, denoted $\hat{x}_k$, to the channel estimator, and *a posteriori* information on source bits. The channel estimator provides channel coefficient estimates ($\hat{H}_{n,k}$).

## 2.1 MUD

Multi-user detection is a demanding task and a number of strategies can be applied. When there is a large number of users $K$ and/or the modulation order grows beyond QPSK, optimum MUD (BCJR-type) is not a viable approach due to its enormous complexity. Therefore, reduced complexity MUDs should be looked into; these can roughly be categorized into linear and non-linear methods. In this paper we adopt a linear approach: Soft interference cancellation + linear MMSE filtering. The associated computational complexity scales linearly with $K$ and is independent of the modulation order. The MUD under investigation was first proposed in [3] for CDMA systems, and adapted to MIMO-OFDM systems in [11].

The received signals (1) are processed separately for each subcarrier and OFDM symbol. Parallel interference cancellation is performed using $\tilde{\boldsymbol{x}}$ from the SISO decoders and $\hat{\boldsymbol{H}}$ from the channel estimators. The residual term from the interference cancellation for the $k$th transmit antennas, $\tilde{\boldsymbol{r}}^{(k)} = \boldsymbol{r} - \hat{\boldsymbol{H}}(\tilde{\boldsymbol{x}} - \tilde{x}_k \boldsymbol{i}_K^{(k)})$, with $\boldsymbol{i}_K^{(k)}$ being the $k$:th column of the $K \times K$ identity matrix $\boldsymbol{I}_K$, is then MMSE filtered to reduce multi-user interference, giving the soft output symbols

$$\tilde{z}_k = \frac{\boldsymbol{i}_K^{(k)\mathrm{T}} \left( \hat{\boldsymbol{H}}^{\mathrm{H}} \hat{\boldsymbol{H}} + \sigma_w^2 (\boldsymbol{V}^{(k)})^{-1} \right)^{-1} \hat{\boldsymbol{H}}^{\mathrm{H}} \tilde{\boldsymbol{r}}^{(k)}}{\boldsymbol{i}_K^{(k)\mathrm{T}} \left( \hat{\boldsymbol{H}}^{\mathrm{H}} \hat{\boldsymbol{H}} + \sigma_w^2 (\boldsymbol{V}^{(k)})^{-1} \right)^{-1} \hat{\boldsymbol{H}}^{\mathrm{H}} \hat{\boldsymbol{h}}_k^{(\mathrm{tx})}} \,, \tag{2}$$

with $\boldsymbol{V}^{(k)} = \mathrm{diag}\left( (1 - |\tilde{x}_1|^2, \ldots, 1 - |\tilde{x}_{k-1}|^2, 1, 1 - |\tilde{x}_{k+1}|^2, \ldots, 1 - |\tilde{x}_K|^2) \right)$ and $\boldsymbol{h}_k^{(\mathrm{tx})}[m, s]$ denoting the channel vector from the $k$th user. For the derivation we refer to [3].

## 2.2 SISO Decoding

The demapped and deinterleaved output of the MUD is *assumed* to be described by the equation

$$z_k[l] = x_k[l] + v_k[l], \quad k = 1..K, \tag{3}$$

where $v_k[l] \sim \mathcal{N}(0, \eta_k^2)$ with the variance estimated as

$$\eta_k^2 = \frac{1}{\boldsymbol{i}_K^{(k)\mathrm{T}} \left( \boldsymbol{H}^{\mathrm{H}} \boldsymbol{H} + \sigma_w^2 (\boldsymbol{V}^{(k)})^{-1} \right)^{-1} \boldsymbol{H}^{\mathrm{H}} \boldsymbol{h}_k^{(\mathrm{tx})}} - 1. \tag{4}$$

The interpretation of (3)-(4) is that the multi-user interference at the output of the MUD is approximated as a Gaussian variate, which validity has been shown in [12]. We now face a classical decoding problem, namely *a posteriori* probability (APP) decoding of a convolutional code in additive white Gaussian noise. Since low-memory convolutional codes will be used subsequently, optimum decoding is feasible and we have deployed the log-domain BCJR algorithm [13].

### 2.3 Channel Estimation

Assuming that the maximum normalized delay spread ($\eta_{\max}^{(\mathrm{d})}$) is within the cyclic prefix, and the channel to be static over a code block, the receiver implements a low-complexity estimator using a discrete prolate spheroidal basis representation [14] of the channel. Using the proposed model, an MMSE channel estimator is derived that uses both known pilot symbols, as well as soft data symbols based on *a posteriori* information from the SISO decoders. We omit a detailed presentation of the estimator here, and instead refer to [11] replacing Doppler domain with delay domain.

## 3 EXIT Chart Representation

In order to produce an EXIT chart, information transfer functions of the different decoding blocks have to be produced. Each component decoder is viewed as a statistical Log-Likelihood-Ratio (LLR) transformer; it takes an LLR-sequence as input and outputs another (hopefully improved) version. The transfer function measures the improvement of the LLR-transformation in terms of mutual information between the LLR's and the variables that the LLR's represent. To be more specific, assume that a component decoder produces extrinsic LLR's $\Lambda_{\mathrm{ext}}$ on variables $X$ given *a priori* information $\Lambda_{\mathrm{a}}$ and possibly a set of observations. The quality of the *a priori* information is, in terms of mutual information, measured by $I_{\mathrm{a}} = I(X;\Lambda_{\mathrm{a}})$ while the quality of the output is $I_{\mathrm{ext}} = I(X;\Lambda_{\mathrm{ext}})$. The transfer function can now be statistically established as [15]

$$I_{\mathrm{ext}} = T(I_{\mathrm{a}}). \tag{5}$$

When producing the transfer functions, all elements of $\Lambda_{\mathrm{ext}}$ (becoming $\Lambda_{\mathrm{a}}$ for the next component decoder) for both users are assumed independent and to follow a Gaussian distribution, $\mathcal{N}\left(x\mu_{\mathrm{ext}}, \sigma_{\mathrm{ext}}^2\right)$, with consistency condition $\mu_{\mathrm{ext}} = \sigma_{\mathrm{ext}}^2/2$ and where $x = \pm 1$ is the transmitted symbol. With the above given distribution of the LLR's, there is a one-to-one mapping between the

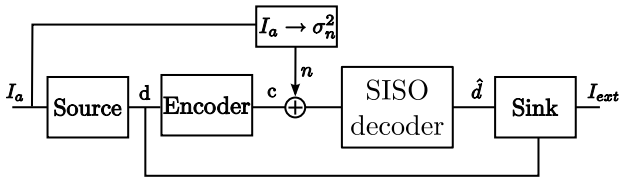


**Figure 3:** System setup for producing EXIT chart for the SISO decoder.

mutual information $I_{\text{ext}}$ and the variance $\sigma_{\text{ext}}^2$ which is given by the J-function defined in [1]

$$I_{\text{ext}} = J\left(\sigma_{\text{ext}}\right). \tag{6}$$

The J-function is useful when generating sequences with different *a priori* information content, which is needed when generating transfer functions. In the following sections, we describe the procedure for generating transfer functions for the SISO decoder and the MUD/CE.

## 3.1 SISO Decoder

The framework for computing the SISO EXIT curve in this paper differs from the standard approach due to the assumed channel model at the front-end of the SISO decoder ((3)-(4)), though the principles and outcome are the same. We provide a brief summary in section.

The system setup used for generating the SISO decoder transfer function is given in Fig. 3. First a number of data symbols $d$ are generated, coded with the convolutional encoder and mapped to binary symbols $c \in \{-1, 1\}$. Zero-mean Gaussian noise with variance $\sigma_{\text{n}}^2$ is added to the symbols to produce the signal, $y = c + n$, feed into the SISO decoder. The variance $\sigma_{\text{n}}^2$ is chosen to match a given input mutual information value $I_{\text{a}}$, and some manipulations give that

$$\sigma_{\text{n}}^2 = \left(\frac{2}{J^{-1}(I_{\text{a}})}\right)^2.$$

After the SISO decoder the soft extrinsic output symbols are feed to the sink where the mutual information is computed through [15]

$$I_{\text{ext}} = \frac{1}{2}\sum_{d=\pm 1}\int_{-\infty}^{\infty} p(\hat{d}|d)\log_2\left(\frac{2p(\hat{d}|d)}{p(\hat{d}|-1)+p(\hat{d}|1)}\right)\partial\hat{d}, \tag{7}$$

where the probability density function, $p(\hat{d}|d)$, is approximated using histogram calculations, and the integral thus becoming a summation.

The procedure is repeated for a number of evenly spaced values of $I_{\text{a}} \in ]0, 1]$.

## 3.2 MUD/CE

For the MUD/CE, the system model used for obtaining the information transfer function is shown in Fig. 4. Since the system under investigation has multiple inputs and outputs, a generalized multi-dimensional transfer function must be used. The transfer function is dependent on the channel realizations and the noise variance of the system, apart from the input a priori mutual information, and is for $K = 2$ given by

$$\left[I_{\text{ext}}^{(1)}, I_{\text{ext}}^{(2)}\right] = T_e\left(I_a^{(1)}, I_a^{(2)}, \boldsymbol{H}, \sigma_w^2\right) \tag{8}$$

assuming equal noise variance at both antennas.

We will shortly show that the EXIT chart depends on the specific code being used, since the input to the channel estimator is the *a posteriori* output symbols of the SISO decoder. This is a major difference compared to conventional EXIT charts. Consequently, the problem of finding suitable codes to a certain modulation scheme is no longer a "curve-matching" problem since the outer code impacts *both* EXIT curves. Note that this problem is solely a consequence of the considered MUD/CE design and not of the multi-dimensional EXIT chart technique itself. To overcome this problem we propose a modification to the MUD/CE and evaluate the impact on performance.

The transfer function is obtained in the following way. First two sets of code and pilot symbols are generated, one per user. These are then mapped to QPSK symbols, OFDM modulated, and sent through the channel. Then, given the pair of input information values, $(I_{\text{a}}^{(1)}, I_{\text{a}}^{(2)})$, *extrinsic* and *a posteriori* based LLR's are generated for each of the code symbols, mapped to soft QPSK symbols ($\tanh(\Lambda_x/2)$ followed by a QPSK mapper) before being sent to the MUD and CE, respectively. The LLR's are obtained as described above making use of the J-function.

Let $\Lambda_{\text{ext,c}}$ and $\Lambda_{\text{app,c}}$ in Fig. 4 and in the text below refer to the LLR's at the output of the decoder. To generate a sequence of input *extrinsic* based LLR's, given the input information values, is straightforward. However, the same does not hold for the corresponding *a posteriori* based LLR's $\Lambda_{\text{app,c}}$ (fed to the CE). Instead, the EXIT function calculated for the SISO decoder has to be used. Assuming some *a priori* information $I_{\text{a}}$, $\Lambda_{\text{app,c}}$ are related to $\Lambda_{\text{ext,c}}$ through

$$\Lambda_{\text{app,c}} = \Lambda_{\text{ext,c}} + \Lambda_{\text{a,c}}, \tag{9}$$

where $\Lambda_{\text{ext,c}}$ and $\Lambda_{\text{a,c}}$ are independent by the definition of extrinsic information (under the assumption of large interleaver length) and $\Lambda_{\text{a,c}}$ is the input LLR's to the SISO decoder. Since we are assuming an information content $I_{\text{a}}$ in $\Lambda_{\text{ext,c}}$, we know that $\Lambda_{\text{ext,c}}$ must have been produced from $\Lambda_{\text{a,c}}$ with an

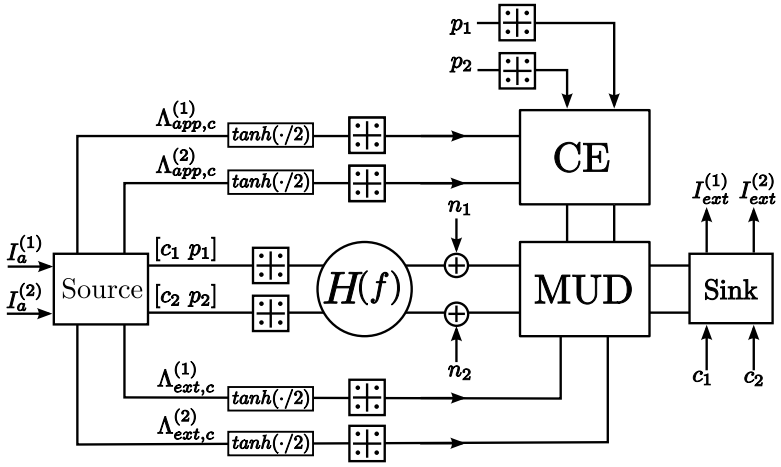


**Figure 4:** System setup for producing EXIT charts for the receiver structure.

information content $T_c^{-1}(I_\mathrm{a})$. Thus, again making use of the J-function, $\Lambda_\mathrm{a,c}$ can be generated independently from $\Lambda_\mathrm{ext,c}$.

In order to simplify the evaluation of the receiver, we propose a modification that decouples the SISO decoder from the MUD/CE. By simply replacing $\Lambda_\mathrm{app,c}$ by $\Lambda_\mathrm{ext,c}$ in the feedback loop to the CE, the generated *a priori* information input, used for obtaining the EXIT surfaces, may be generated independently from the code/decoder being used. We will demonstrate that this has a minimal impact on the EXIT surface of the MUD/CE.

# 4 Results

The system under consideration consists of two users with one antenna each transmitting independent codewords, interleaved over time and frequency, over a frequency fading channel to a receiver having two antennas. The codewords span $S$ OFDM symbols including $S_p$ OFDM pilot symbols, where each OFDM symbol contains $M = 64$ subcarriers (see Fig. 2). Code bits are generated using a rate 1/2 recursive systematic convolutional encoder [16] with generators $(7, 5)_8$ and with two tail bits forcing the encoder to terminate in the all-zero state. A tapped delay line model with an exponential power delay profile is used to generate the channel coefficients [17], where the different transmit-receive links are generated independently of each other. Each impulse response consist of $N_{MPC} = 100$ randomly arriving multi-path components, and the normalized

delay spread of the channel is set to $\eta_{\max}^{(\mathrm{d})} = 0.15$. The coherence time of the channel is assumed to be much larger than the duration of a code block; thus no variations in time are considered. Noise is added at the receiver to obtain $E_\mathrm{b}/N_0 = 7dB$, where $E_\mathrm{b}$ denotes the average total available energy per bit at the receiver and $N_0 = \sigma_w^2$.

EXIT surfaces are generated, using the above settings, for both the SISO decoder and the MUD/CE for a particular channel realization. In Fig. 6 and Fig. 7 the EXIT charts are shown, corresponding to the two different user streams, with $S = 100$ and $S_p = 1$. The upper surfaces of the figures correspond to the MUD/CE, and the lower s-shaped surfaces correspond to the SISO decoder.

When generating the EXIT surfaces for the CE/MUD shown in Fig. 6 and Fig. 7, extrinsic, instead of a posteriori, information are used as input to the CE. In Fig. 5 the diagonal of an EXIT surface for one user is shown for both the case of *extrinsic* (dashed line), and *a posteriori* (solid line), input. Clearly the discrepancy between the two is insignificant, motivating the use of *extrinsic* information in the CE when creating EXIT surfaces for the considered receiver.

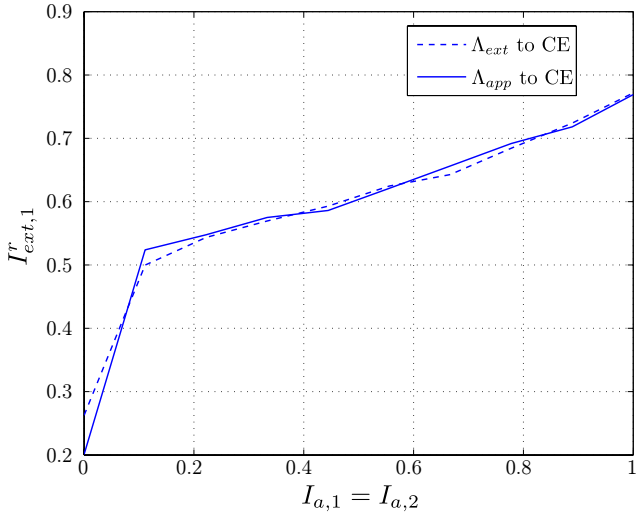


**Figure 5:** Diagonal values of an EXIT surface for the CE/MUD for when extrinsic and a posteriori information is used in CE.

Moreover, since the SISO decoders are working in parallel independent of each other, the performance of one user is independent of the information

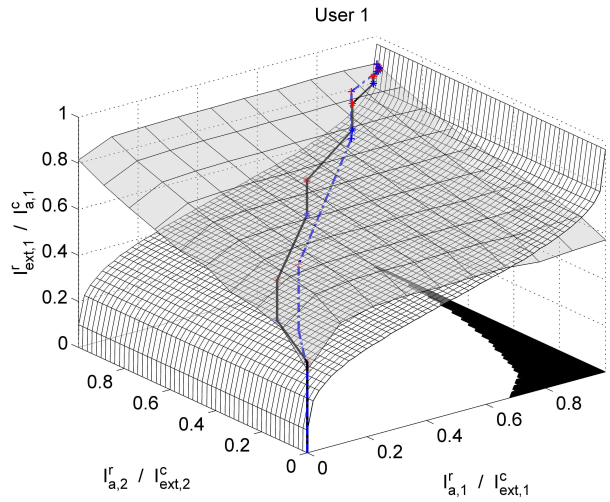


**Figure 6:** EXIT chart for user 1. The solid line show an actual decoding trajectory and the dashed line the EXIT chart prediction.

content of the other, as clearly seen in Fig. 6 and Fig. 7. Looking at the surfaces corresponding to the MUD/CE; when the mutual information is zero, meaning that there is no soft information available, the output is produced without interference cancellation and only based on the initial channel estimates obtained from the pilot symbols. The starting point of the convergence path is thus dependent of the quality of the initial estimate, closely dependent on the amount of available pilot symbols. As the input information grows, Fig. 6 show that the performance of user 1 is mainly a function of the information content of the other user, with the reversed valid for user 2. This is because the accuracy of the interference cancellation is only dependent on the amount of knowledge about the interfering user. If varying the SNR, the EXIT surfaces of the MUD/CE are shifted up or down, essentially with a preserved shape. These results are not shown here.

The two paths included in the two figures show an actual decoding trajectory (solid line) and the EXIT chart prediction (dashed). The two trajectories show some differences, but they converge to the same point. For the first few iterations, there is a gap between the trajectory obtained by simulations and the surface of the MUD/CE. This discrepancy is most likely due to the mismatch between the statistics used for the LLR's, when deriving the the chart and the ones obtained from the simulations. The true LLR's show a non-Gaussian

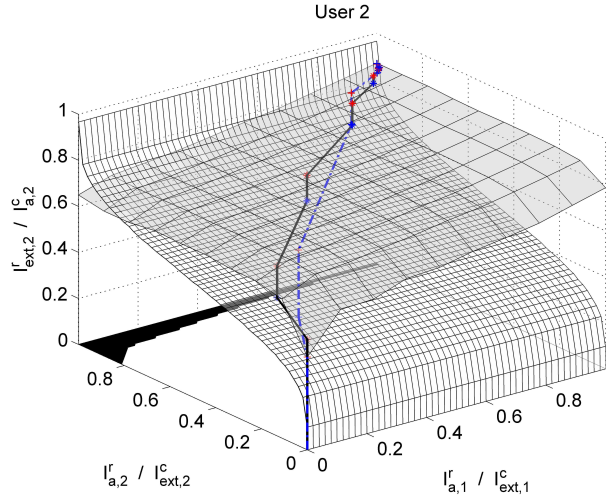


**Figure 7:** EXIT chart for user 2. The solid line show an actual decoding trajectory and the dashed line the EXIT chart prediction.

behavior, with a large variance, the first few iterations. With iterations the output LLR's become more and more Gaussian, and the gap between the chart and the decoding trajectory decrease.

In Fig. 8 the convergence area of the receiver is plotted as obtained from the EXIT charts. The area is given by

$$\begin{aligned}&\left(T_{c,1}^{-1}(I_a^{(1)}, I_a^{(2)}) < T_{e,1}(I_a^{(1)}, I_a^{(2)})\right)\\ \cup &\left(T_{c,2}^{-1}(I_a^{(1)}, I_a^{(2)}) < T_{e,2}(I_a^{(1)}, I_a^{(2)})\right)\end{aligned}$$

where the numbers in $T_{\cdot,1}$ and $T_{\cdot,2}$ refer to the separated per user transfer functions. The figure also shows the decoding trajectory and the EXIT chart prediction (with the paths of the two users superimposed on each other). As seen, the two paths follow roughly the same track, though the one obtained from simulations is lagging behind in terms of iterations. It is also worth pointing out that the point of convergence is the intersection of the four 3D surfaces. The similarities between the two trajectories changes depending on the channel realization, the block length and SNR. Our experience is that larger block lengths and higher SNR improve the fit.

As a final result, we present an analysis of the impact of the multi-user channel on the performance of the receiver algorithm. We look at the EXIT

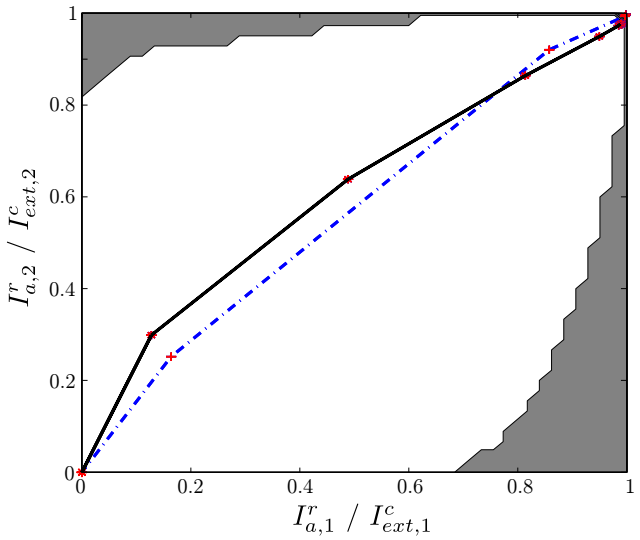


**Figure 8:** Convergence area for the receiver. The figure also show the decoding trajectory and the EXIT chart prediction (with the paths of the two users superimposed on each other).

curve of the MUD/CE in two points; in the initial stage when no soft information is available from the SISO decoders ($T_e(0,0)$) and when perfect knowledge about the transmitted symbols are available ($T_e(1,1)$). Fig. 9 shows the cumulative distribution functions (CDFs) of the extrinsic information output of the MUD for one of the users at an SNR ($E_b/N_0$) of 0 and 5dB, for the two cases considered. The CDFs are computed over 200 channel realizations, for the case of $S = 40$ and $S_p = 1$. The total multi-user channel power is constant over the different channel realizations. As is seen the information output show large variation depending on the quality of the channel. Though the total channel gain is constant, it will be distributed unevenly between the two users, depending on the outcome of the channel realization. Unless this is combated using an appropriate power control, the outage probability of the system will be large. If looking at the curves corresponding to the starting point ($T_e(0,0)$) we see that with an increasing SNR the quality of the initial channel estimate improve, at the same time as the number of noise induced errors decreases; thus providing a better starting point for the iterative process.

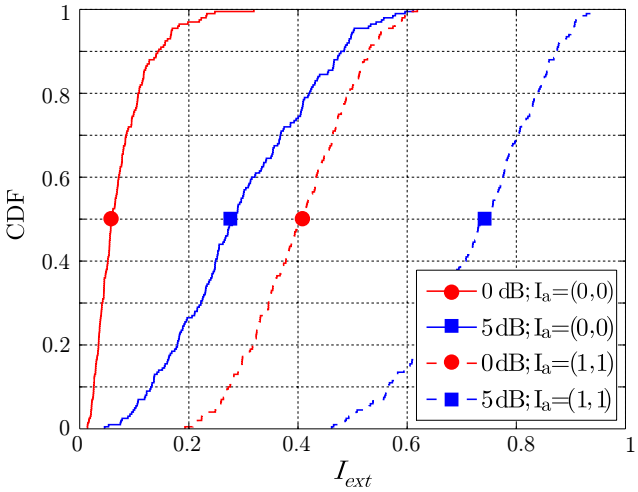


**Figure 9:** The CDF of the extrinsic information output from the MUD/CE for two points, $T_e(0,0$ and $T_e(1,1)$. Results are shown for SNR values of 0 and 5dB.

## 5 Conclusions

In this paper we have studied a promising receiver candidate for non-coherent multi-antenna OFDM systems. For the considered multi-user receiver we have seen that the convergence path, and the point of convergence, can be estimated using multi-dimensional EXIT charts. We have proposed a modification of the receiver structure, simplifying the generation of the transfer function of the MUD/CE; making it possible to generate the transfer function independent of the code/decoder. This greatly simplifies the work of finding a suitable outer code for the receiver; making it into a curve fitting problem. The modifications are seen to have an insignificant impact on the transfer function.

## References

[1] S. ten Brink, "Convergence of iterative decoding," *IEEE Electronics Letters*, vol. 35, pp. 806–808, May 1999.

[2] R. Koetter, A. Singer, and M. Tuchler, "Turbo equalization," *IEEE Signal Processing Magazine*, vol. 21, pp. 67–80, Jan. 2004.

[3] T. Zemen, C. Mecklenbrauker, J. Wehinger, and R. Muller, "Iterative joint time-variant channel estimation and multi-user detection for MC-CDMA," *IEEE Transactions on Wireless Communications*, vol. 5, pp. 1469–1478, Jun. 2006.

[4] X. Wautelet, C. Herzet, A. Dejonghe, J. Louveaux, and L. Vandendorpe, "Comparison of EM-based algorithms for MIMO channel estimation," *IEEE Transactions on Communications*, vol. 55, pp. 216–226, Jan. 2007.

[5] S. Ahmed, T. Ratnarajah, M. Sellathurai, and C. Cowan, "Iterative receivers for MIMO-OFDM and their convergence behavior," *IEEE Transactions on Vehicular Technology*, vol. 58, pp. 461–468, Jan. 2009.

[6] K. Kansanen, *Wireless broadband single-carrier systems with MMSE turbo equalization receivers*. PhD thesis, Oulu University, Oulu, Finland, Dec. 2005.

[7] S. Sand, "Iterative OFDM receiver with channel estimation," in *Proc. International Symposium on Wireless Personal Multimedia Communications*, (San Diego, USA), Sept. 2006.

[8] D. Shepherd, Z. Shi, M. Anderson, and M. Reed, "EXIT chart analysis of an iterative receiver with channel estimation," *Proc. IEEE Global Communications Conference*, pp. 4010–4014, Nov. 2007.

[9] P. Salvo Rossi, P. Hammarberg, F. Tufvesson, O. Edfors, P. Almers, V.-M. Kolmonen, J. Koivunen, K. Haneda, and R. Muller, "Performance of an iterative multi-user receiver for MIMO-OFDM systems in a real indoor scenario," *Proc. IEEE Global Communications Conference*, pp. 1–5, Nov. 2008.

[10] C. Heegard and S. B. Wicker, *Turbo Coding*. Kluwer Academic Publishers, 1999.

[11] P. Salvo Rossi and R. Müller, "Joint iterative time-variant channel estimation and multi-user detection for MIMO-OFDM systems," *Proc. IEEE Global Communications Conference*, pp. 4263–4268, Nov. 2007.

[12] X. Wang and H. Poor, "Iterative (turbo) soft interference cancellation and decoding for coded CDMA," *IEEE Transactions on Communications*, vol. 47, no. 7, pp. 1046–1061, 1999.

[13] P. Robertson, E. Villebrun, and P. Hoeher, "A comparison of optimal and sub-optimal map decoding algorithms operating in the log domain," *Proc.*

*IEEE International Conference on Communications*, vol. 2, pp. 1009–1013 vol.2, Jun. 1995.

[14] D. Slepian, "Prolate spheroidal wave functions, Fourier analysis, and uncertainty - V: The discrete case," *Bell System Technical Journal*, vol. 57, pp. 1371–1430, May/Jun. 1978.

[15] S. ten Brink, "Convergence behavior of iteratively decoded parallel concatenated codes," *IEEE Transactions on Communications*, vol. 49, pp. 1727–1737, Oct. 2001.

[16] J. G. Proakis, *Digital Communication*. McGraw-Hill Publishing Company, UK, 4th ed., 2000.

[17] P. Hoeher, "A statistical discrete-time model for the WSSUS multipath channel," *IEEE Transactions on Vehicular Technology*, vol. 41, pp. 461–468, Nov. 1992.

# *Paper III*

# Using Measured Channels in Performance Evaluations of Multi-User OFDM Systems

**Abstract**

In this paper we provide a tutorial overview of the use of channel measurement data in wireless communication system evaluations. Channel measurements are mainly used as a basis for generating channel models, but can also be used directly in system simulations to provide a close to reality channel scenario. This paper describes a number of measurement specific issues, and provide suggestions on how these problems can be alleviated. The main focus is on wideband multi-user multiple antenna (MU-MIMO) systems, but most observations are applicable to other scenarios and systems. At the end of the paper, we provide illustrations of some of the discussed issues through performance evaluations of an iterative receiver structure. For the evaluation, the performance with the true channel is compared with that of the measurement impaired channel. The true channel is given as the output of the COST 2100 multi-link MIMO channel model.

---


P. Hammarberg, F. Tufvesson and O. Edfors,
"Using Measured Channels in Performance Evaluations of Multi-User OFDM Systems".

# 1 Introduction

When developing algorithms for wireless receivers, appropriate system evaluations need to be performed. The ideal procedure would be to implement the algorithms in an actual wireless receiver, and perform field tests in various environments. Such operations are in general both costly and time consuming, and are therefore in most cases not an alternative in the early development phase. Furthermore, since the properties of the wireless channel differ significantly from location to location, or from one time to another, fair comparisons between different algorithms and parameter settings may become difficult. Furthermore, it is not possible, in general, to reproduce specific channel realizations for deeper analysis of algorithm behavior.

For practical reasons, as the ones stated above, system level computer simulations are usually performed for algorithm evaluations. In order to catch the behavior of the wireless channel, and to investigate its effect on system performance, an accurate channel model is needed. The models are designed to mimic the properties of the wireless channel, often with a specific system in mind. Based on measurements of the wireless channel, the statistical (and possibly geometrical) properties of the channel are modeled and parameterized. Typical channels can then be generated based on this underlying statistical model. Apart from enabling accurate and realistic computer based system simulations, the output of the models are reproducible, which helps when comparing different systems or receiver structures.

An alternative to the use of channel models, or real life field trials, is the use of measured channels. Commonly, channel measurements are performed with the purpose of being used for channel modeling and characterization. Such measurements could, as well as being used for these purposes, be used directly for system evaluation. The idea is that the measurements provide an accurate description of the environment, catching all properties of the wireless channel. Properties that might be overlooked in the design of a channel model. Furthermore, for novel system designs channel models may not be available, or the available models have not been properly verified. In such situations measurements could be an attractive option to speed up the design and evaluation process.

Despite the potential benefits of using measurements in system evaluations, there are a number of issues to keep in mind. The main contribution of this paper is to provide a tutorial overview of the issues encountered when using channel measurement data in wireless communication system evaluations. The paper summarize our experiences when working with measurements within the WILATI+ project, which focuses on channel modeling and modem design for wireless LAN applications, primarily for wideband dual-link multiple trans-

mit/receive antenna (MIMO) systems. Therefore, the issues described here are related to the dual-link MIMO measurements performed within the project, even though most observations are applicable to other types of measurements. We believe that the information provided in this tutorial will be helpful both for someone using measurements for simulations, as well as for people performing measurements.

The paper is organized as follows. First the basics of channel sounding is presented. We then go through a number of issues that relates to channel measurements when used for system evaluations. The cause and consequences are described, as well as potential solutions. We then provide system simulation examples in order to further illustrate some of these issues. The evaluated system is an uplink multi-user orthogonal frequency division multiplexing (OFDM) MIMO system, with cooperative base stations using an iterative receiver structure. Finally, we provide a summary with concluding remarks.

## 2 The basics of channel sounding

Channel sounding is the term used for measurements performed with the aim of understanding and estimating the properties of the wireless channel, and is the basis of channel modeling. A channel sounding system may be seen as an ordinary communication system, with the difference that only known signals, usually with good statistical properties, are transmitted. Furthermore, the receiver is generally synchronized to a common clock, which is, e.g., required for estimation of the propagation delay. Positioning systems may also be used if the (absolute) location of the transmitter/receiver is of interest.

The sounder may be designed either to estimate the channel impulse response or frequency response. The estimate in the delay domain can be achieved by the transmission of an impulse like signal, where the received signal is the actual impulse response of the channel, or a pseudo-random sequence could be transmitted, with the impulse response being obtained through a correlating matched filter. A frequency domain estimate can be obtained by transmitting a chirp signal, i.e., sweeping the frequency domain, or by performing "one shot" estimation by using an OFDM type of signal. In many cases the multiple antenna or angular properties are also of interest, requiring antenna array measurements to produce an estimate of the directional channel. For more information on channel sounding, please refer [1], and references therein.

# 3 Issues when using measurements in receiver evaluations

As mentioned above, using channel measurement data for evaluating wireless receivers is not always straightforward. There are a number of aspects that need to be kept in mind. In this section we go through a few of these, and also discuss their implications and possible counter measures.

## 3.1 Additive measurement noise

One of the largest problems when it comes to measurements is the presence of measurement noise. Like in any wireless receiver, the channel sounding equipment will add noise to the received signal. This noise will contaminate the estimated channel, which has consequences when using the channel for system evaluations. In most cases, the additive measurement noise is uncorrelated and follows a Gaussian distribution.

The presence of noise will inevitably affect the properties of the channel. For example, the noise may hide correlation properties of the channel, e.g., spatial correlation (rank deficiency) in MIMO channels [2], time domain correlation (limited Doppler spread), and frequency correlation (limited delay spread) of wideband channels. The latter is illustrated in Figure 1, where an impulse response is shown with and without the presence of additive measurement noise. As can be seen the impulse response has energy in all delay positions, which is generally not the case for wireless channels.

The delay and Doppler limited nature of wireless channels are often exploited when designing low-complexity channel estimation algorithms [3–5]. Evaluating such algorithms using measured channels will inevitably lead to the presence of an irreducible error floor, since the measurement noise does not show this behavior and thus can not be completely estimated. Such effect would not be seen when using the estimator in a real channel. We will illustrate this phenomena through system simulations in Section 4.3.

Though measurement noise can never be removed, a number of counter measures can be taken to minimize its effect. The simplest solution is of course to increase the transmit power during measurements, which would improve the measurement signal-to-noise ratio (SNR). Due to regulatory restrictions, the transmit power is generally restricted, which sets a limit on the achievable SNR. Furthermore, power limitations also set a limit on the distance over which the channel can be accurately measured.

An alternative strategy to improve the SNR is to increase the length of the transmitted measurement signal, leading to an increase in the total received energy. For a perfectly static channel an arbitrarily high SNR could be achieved,

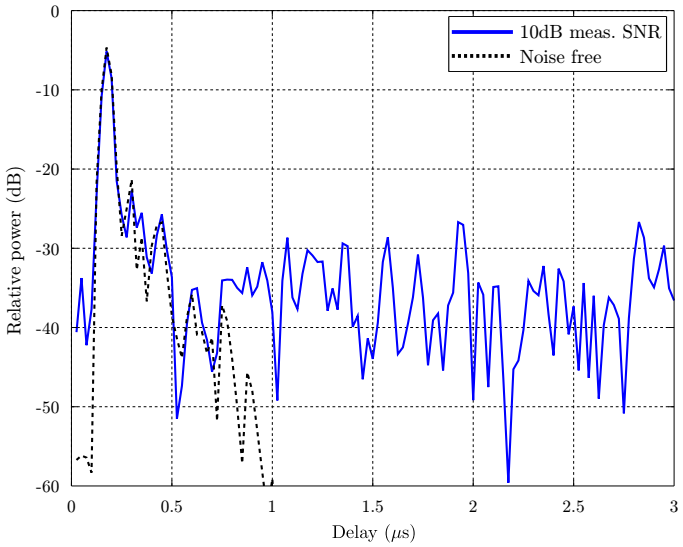


**Figure 1:** Illustration of an impulse response, with and without measurement noise. The measurement SNR is 10 dB.

but for most wireless scenarios the coherence time of the channel sets a limit on the length of the measurement signal. This is especially evident when performing mobile measurements, in which the coherence time, depending on the speed, can be very short. More specifically, to meet the Nyquist sampling criteria the following restriction is placed on the duration between two consecutive samples, i.e., between two transmitted measurement signals, $T_s \leq 1/(2\nu_{\max})$, where $\nu_{\max}$ is the maximum Doppler shift.

Direct actions for improving the measurement SNR are not always sufficient. In addition, post-processing of the estimated channel can be used to further improve the situation. Several approaches can be used. Most common is to utilize assumed correlation properties in time/frequency of the (over-sampled) channel, applying some form of low-pass filter, e.g., Wiener filters [6]. Similarly, by estimating the maximum channel delay, all energy above this value can be nulled in the impulse response, i.e., applying an ideal low-pass filter in the frequency domain. Alternatively, if the noise power level can be estimated, all values in the impulse response below this level can be set to zero [7]. An alternative sub-space based method, based on singular value decomposition of the multi-dimensional channel matrix, has also shown good performance [8].

## 3.2 Phase noise

One other type of noise that is added in wireless transceivers is phase noise [9]. Due to oscillator instabilities at transmitter and receiver, the received signal will show unwanted phase variations. These variations are unknown, and can therefore in general not be separated from a channel induced phase shift[2]. For a communication system, such phase variation can be handled by a channel estimator in combination with an equalizer. But, for the case of channel measurements and characterization, phase noise is a more severe problem.

When measuring the behavior of the wireless channel, presence of phase noise will unavoidably cause measurement errors, since the transceiver and channel induced phase variations can not be separated. The presence of phase noise is generally a smaller problem when measuring time varying channels, where short sounding signals are used. On the other hand, when measuring static channels with long sounding signals (or averaging over many short signals), the phase noise has a larger impact.

Phase noise is also an issue in MIMO channel measurements, if time domain switching over the antenna elements is performed. For large antenna arrays, the switching time can be relatively long, thus catering for large noise induced phase variations over the measurement interval. The resulting phase errors has the largest impact if the MIMO channel is of low rank, leading to an over estimation of the channel capacity [9, 10].

In general, the only way to reduce phase noise is to use more stable oscillators, adding to the cost of the measurement equipment. From the above discussion we can deduce that from a system evaluation point of view, extra caution is needed when using MIMO measurements from scenarios where low rank channels can be expected, and where low quality measurement equipment has been used.

## 3.3 Sampling and interpolation

As when sampling any signal, the channel has to be sampled sufficiently often in both time/space and frequency/delay, to allow for perfect reconstruction. As stated previously, the maximum Doppler frequency in the channel sets an upper limit on the duration between samples. Similarly, the maximum channel length $\tau_{\max}$ sets a lower limit, i.e., $\tau_{\max} \leq T_s$. Below this limit, inter-symbol interference becomes present, and consecutively measured impulse responses can not be separated.

If care is not taken when performing the measurements, the sampling criteria is not met, and the measurements may become useless. This is for example

[2] If the two have significantly different statistical properties, separation may be possible.

important when evaluating algorithms making use of time variations of the channel, e.g., channel tracking algorithms. Evaluation of such systems may also require that interpolation is performed to achieve sufficient resolution in time, which is not possible if the channel is under-sampled.

## 3.4 Antenna configurations

One other important aspect to consider is the choice of antennas used during measurements. For direct use of measurement data, the properties of the antenna is not possible to separate from those of the channel. The measured channel will therefore inevitably depend on the antennas and their radiation pattern. For example, if the antenna is directive, the measured channel output in a specific location may differ significantly depending on the orientation of the antenna. Directive antennas are often used in array measurements, where the end goal is to model the directive properties of the channel [1].

In Figure 2 the problem with directive antennas is exemplified with data from real array measurements. The measurements are performed in a scenario where a 16 element circular antenna array is placed on a roof top, and a single-antenna transmitter is located on a parking lot in a north-east direction. The illustration in the center of Figure 2 shows the relative received power at the different patch antenna elements of the circular antenna array. As can be seen, for this line of sight scenario, the received power differs up to 20dB depending on which antenna element is considered. Due to the directivity of the patch antenna elements, who's radiation pattern is shown at the center of Figure 2 for a northbound antenna (without exact scale), the strongest channel is seen in the direction of the transmitter. Furthermore, the channel impulse response at four different antenna positions is shown in the sub-figures of Figure 2. The direction, and receive power, of the four elements are indicated by red circles. As can be seen the impulse responses for the antenna elements are quite different; the one pointing towards the transmitter have a dominant line-of-sight component, while the one facing the opposite direction lacks such dominant component.

As the example of Figure 2 shows, the choice of antennas used during the measurements are an important aspect when planing the measurements. Measurements which are used for system simulations should preferably be obtained using the same type of antennas as intended for the final system. In Section 4.3, we will exemplify how the choice of measurement antennas can effect the system performance.

A solution to the problem of directive antennas can be found through the use of antenna array measurements, followed by directional analysis [1]. By using an appropriately designed antenna array at the receiver, the spatial properties

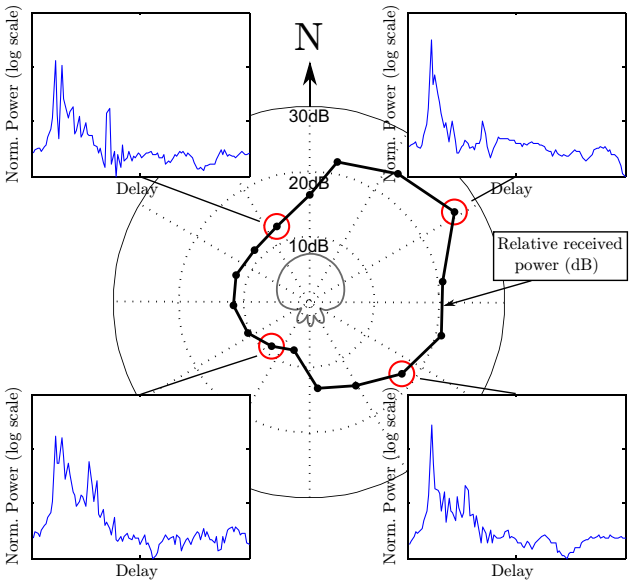


**Figure 2:** In the center of the figure, the received power at the different patch antenna elements of a circular array is shown. The impulse responses corresponding to the antenna elements circled in red is shown in the sub-figures.

of the channel can be estimated based on the resulting vector valued observation. Based on the directional analysis, the channel may be described as a sum of incoming plane waves with certain delays and directions (possibly together with a dense tail of multipath components). Based on this description, the resulting channel for an arbitrary antenna geometry, and radiation pattern, can be generated. Unfortunately, the directional analysis require significant computational effort, and the method also contains model assumptions, which may possibly hide properties of the channel.

## 3.5 Delay synchronization

Depending on how the channel measurement equipment is designed, the measured impulse response can be shifted in the delay domain. A natural delay shift occurs due to the propagation delay between the transmitter and receiver. This shift is of importance for channel characterization and modeling, and may also be useful if evaluating receiver algorithms dealing with synchronization.

Unwanted delay shift can also occur due to synchronization errors caused by, e.g., clocks drift if a common reference not used for transmitter and receiver.

In Figure 3, an illustration of a measured impulse response is shown, as evolved over time. As time progresses, a shift of the channel power is seen in the delay domain. The source of the delay could, as mentioned, be distance related, or caused by synchronization related errors.

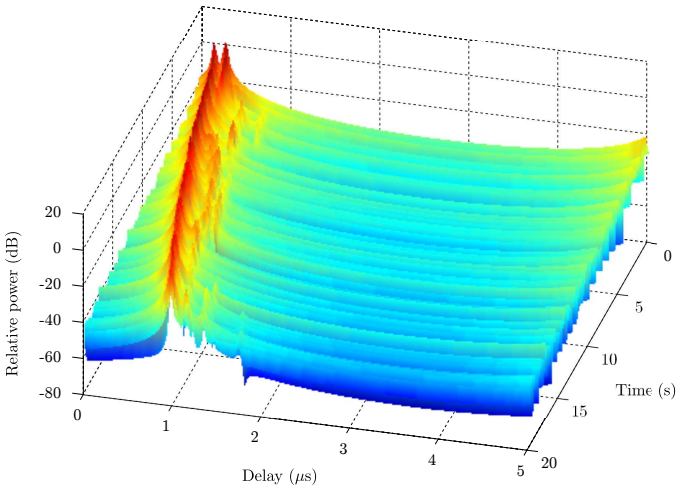


**Figure 3:** Illustration of an impulse response measured over time as the transmitter moves away from the receiver. The impulse response is obtained from the inverse discrete Fourier transform of a computer generated frequency response.

Such shift in the delay can cause problems in system evaluations, since a common assumption in algorithm design is that the system is perfectly synchronized. Using such measurements may in those cases cause problems. For example, as will be illustrated in Section 4.3, for low-complexity channel estimation algorithms which make use of the delay limited, low-pass nature of the channel, significant errors can occur.

The propagation delay can easily be removed through post-processing. That is, by performing an appropriate shift in the delay domain so that the energy of the impulse response becomes located at, e.g., zero delay. Note that for noisy measurements, finding the start of the impulse response may not be possible, since early week components may be hidden in the noise.

### 3.6 Creating "virtual" multi-user channels

Multi-user channel measurements require that a number of receiving, or transmitting, units are used [11]. Since high quality receiving units can be quite expensive, such measurements can become costly. Furthermore, if multi-point measurements are to be considered, e.g., a system with multiple base stations and users, the technical challenges are huge.

A more simple way to create multi-user channels is to combine a number of single-user measurements [12]. In that way a "virtual" multi-user channel is created where users can be added and removed dynamically. When doing so, it is important that the measurement environment stays the same between measurements, otherwise, the different user channels can not be approximated as co-located in time. This is also important when representing joint shadowing effects or other correlation effects. Therefore, creating virtual multi-user channels in highly dynamic environments should be avoided, since the channel may change significantly between the different single-user measurements.

## 4 System simulation examples

In this section we will exemplify three of the discussed issues with using channel measurements in system evaluations, i.e., measurement noise, directive antennas and delay synchronization. To visualize the effects, system simulations are performed, where an iterative receiver structure for multi-user MIMO-OFDM systems is used. The considered uplink system, consisting of two users and two collaborating base stations, is briefly described in Section 4.1.

The channels used for the demonstration are obtained using the COST2100 multi-link channel model [13]. Modifications are then performed on the output of the model to obtain channels which contain the given measurement artifacts. The reasoning behind using the output of a channel model, rather than using actual measurements, is that we by doing so have the true channel to compare with. In this way the effect of the artifacts can be clearly visualized. The considered channel scenario is introduced in Section 4.2.

### 4.1 System description

The considered multi-user multi-link MIMO-OFDM system is shown in Figure 4. Two mobile users (MU) are transmitting independent, synchronized, coded signals to two cooperating base stations (BS). Both users and base stations are equipped with two antennas each. The channel is assumed to be block-fading, i.e., the channel is considered constant in time over a transmitted block consisting of $S = 20$ OFDM symbols, including $S_p = 2$ pilot symbols.

The system bandwith of 20 MHz, at 5.3 GHz, is divided into 128 subcarriers. Before transmission, the data bits are encoded using a rate 1/2 convolutional code, and mapped to QPSK symbols.

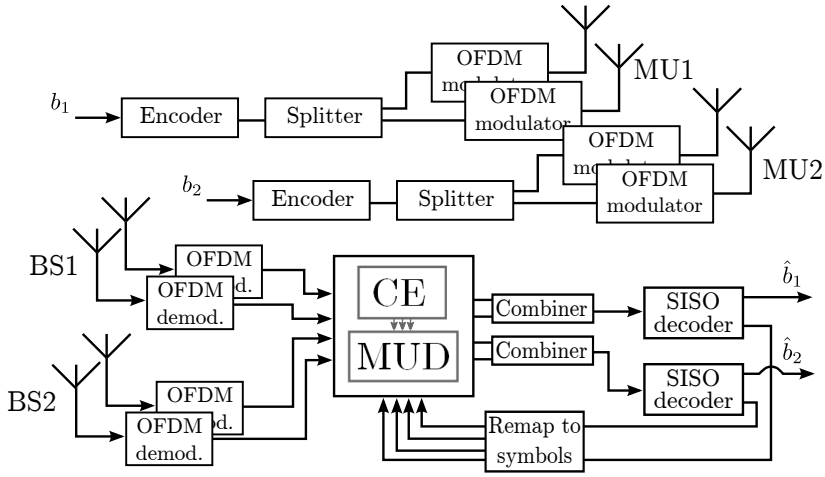


**Figure 4:** Schematic view of the system under consideration, consisting of two users and two cooperating basestations.

At the receiver side, the two base stations are cooperating, using an iterative multi-user receiver with soft interference cancellation and channel estimation, described in detail in [14]. The receiver consists of three parts; a channel estimator, a parallel interference canceling multi-user detector (PIC-MUD), and soft-input-soft-output (SISO) decoders for the convolutional code. The three parts exchange information iteratively, and jointly converge towards an estimate on the transmitted information bits.

The channel estimation algorithm, which has a central part in the following illustrations, produces an estimate based on a low-rank approximation of the channel. In the channel estimator, the channel is assumed to be accurately described by a limited number of delay-limited base functions, more precisely discrete prolate spheroidal (DPS) sequences. Based on this model for the multi-user MIMO channel, a minimum mean square error (MMSE) estimate is produced, making use of the pilot symbols transmitted from all users and antennas, as well as soft estimates of the transmitted code symbols. As we will demonstrate, this type of low-rank channel estimators, with their assumption on the frequency correlation of the channel, show a reduced performance when evaluated using noisy channel measurement data.

## 4.2 Channel scenario

The COST 2100 model, which is used for generating the channel, is a geometry based stochastic channel model, where the environment is stochastically generated based on a number of parameters. The environment consists of a number of clusters, which scatter the transmitted signal, creating a group of impulses in the impulse response. Each cluster has certain spatial/angular properties, and is visible within a specific region. For a more detailed description of the model, please refer [13]. For the implementation we have used the parameters corresponding to case *RS-BS1* in [15], and dense multipath components have been added as described in [16].

In the considered model scenario, two BSs located 20 meters apart, and two MUs are moving along a route according to Figure 5. The two MUs are seen to change place with each other, traveling about 20 m. The wideband MIMO channel is sampled 400 times along the route (making the samples essentially uncorrelated in time). Both the BSs and MUs are equipped with two antennas, spaced half a wave length apart. Furthermore, the channels are generated with both omnidirectional antennas, as well as directional patch antennas, at the MUs. The directive antennas are pointing in the direction of travel of the two users. For both antenna types, the underlaying channel before applying the antenna pattern is identical, thus allowing for a fair comparison between the two cases.

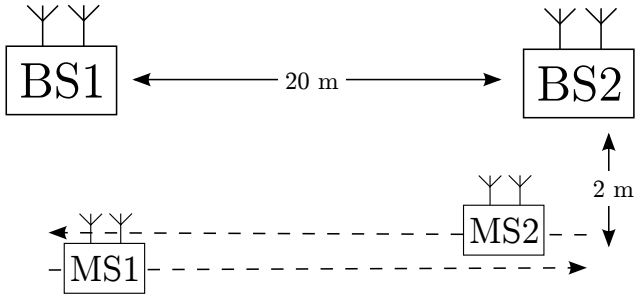


**Figure 5:** The considered scenario for the model, consisting of two base stations 20 m apart and two mobile users moving in opposite direction along the route.

The power of the resulting channel will show large variations depending on the position of the MUs. In Figure 6 the average receive power, for each of the 400 time snapshots, of the links between the MUs and BSs are shown. Averaging is performed over the subcarriers and antennas. The power levels are shown for both omnidirectional (top) and directional MU antennas (bot-

tom). The figure also shows the 10 and 20 dB power levels of the noise signals which are added in order to simulate measurement noise. These will be further discussed in 4.3. As Figure 6 shows, the receive power will change when using directive antennas, as compared to the omnidirectional case. This occurs since the reflected power from some objects in the environment will be significantly attenuated by the directive antenna array. This phenomena can, e.g., be observed by comparing the received power of the link between MU1 and BS1 during the first 50 samples, in the two cases.

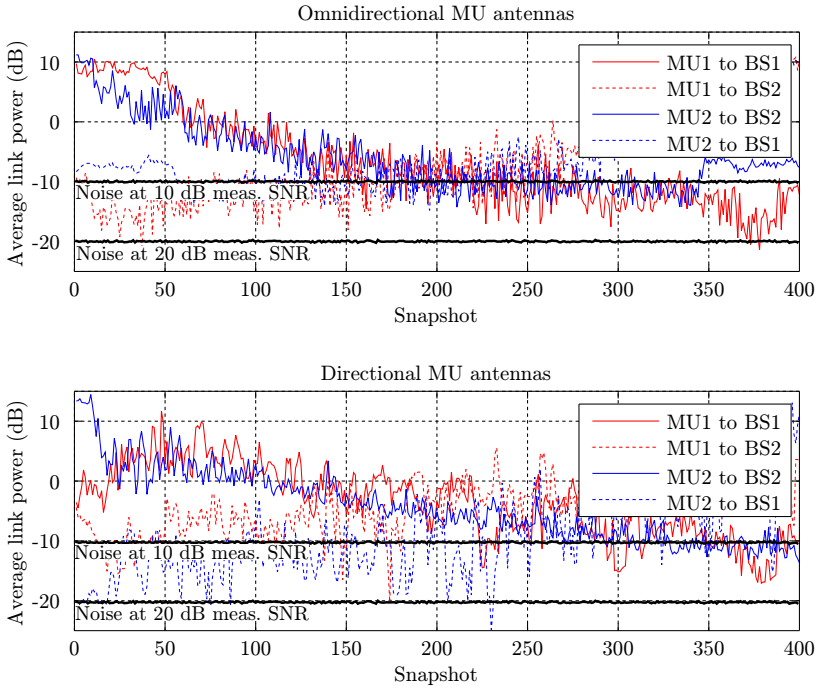


**Figure 6:** The sub-channel powers between the different users and base stations for the case of omnidirectional antennas (top), and directional patch antennas pointing in the direction of travel (bottom).

When using the channel in the coming examples, the power variations between the different MU-to-BS links are preserved. At the same time, for each snapshot the average channel power is normalized to unity. That is, power control is used in each snapshot so that the total receive power is constant over the snapshots. It should be noted that the powers levels of the individual users could, alternatively, be scaled according to some appropriate power

control scheme.

## 4.3 Results

In this section we will illustrate the impact on system performance caused by three of the measurement related issues discussed in Section 3. We first look at the presence of measurement noise, before the impact of directional antennas is exemplified. Finally the performance degradation due to the presence of propagation delay is illustrated.

### Measurement Noise

As discussed in Section 3.1, the presence of measurement noise is one of the main problems encountered when using channel measurements. It may distort the correlation properties of the channel, which are often exploited when designing wireless receiver algorithms.

To begin with, the impact of measurement noise on the spatial correlation of the channel is considered, where we restrict the investigation to omnidirectional antennas. Two noisy measurements are produced based on the original computer generated channel. This is achieved by adding complex white noise, obtaining an overall average measurement SNR of 10 and 20 dB. The noise is added as illustrated in Figure 6, where the power of both the channels and the noise is plotted. Due to the chosen normalization, the instantaneous measurement SNR will change over the snapshots, as would be expected in most channel measurement systems. As seen in Figure 6, at the center of the routes the measurement SNR is significantly lower than the average.

Before looking at the bit error rate (BER) performance of the iterative receiver in the different channels, we take a look at the information theoretic channel capacity. In Figure 7 the empirical cumulative distribution functions (CDF) of the average channel capacities at the different snapshots are shown. For each snapshot, the averaging is performed over all OFDM subcarriers. The capacity is given for the case of no channel state information at the transmitter [1], and is evaluated at an average receiver SNR of 10 dB. The cases of no measurement noise, along with 10 and 20 dB measurement SNR are shown. Furthermore, the capacities of the directional antenna case, further discussed in Section 4.3, and of a channel with independent identically distributed channel (IID) coefficients is shown for comparison.

As can be seen in Figure 7, the presence of measurement noise will change the capacity distribution of the channel. The impact is most visible for the 10 dB measurement SNR, where the noise is strong enough to falsely increase the richness of the measured channel, leading to an increased channel capacity.

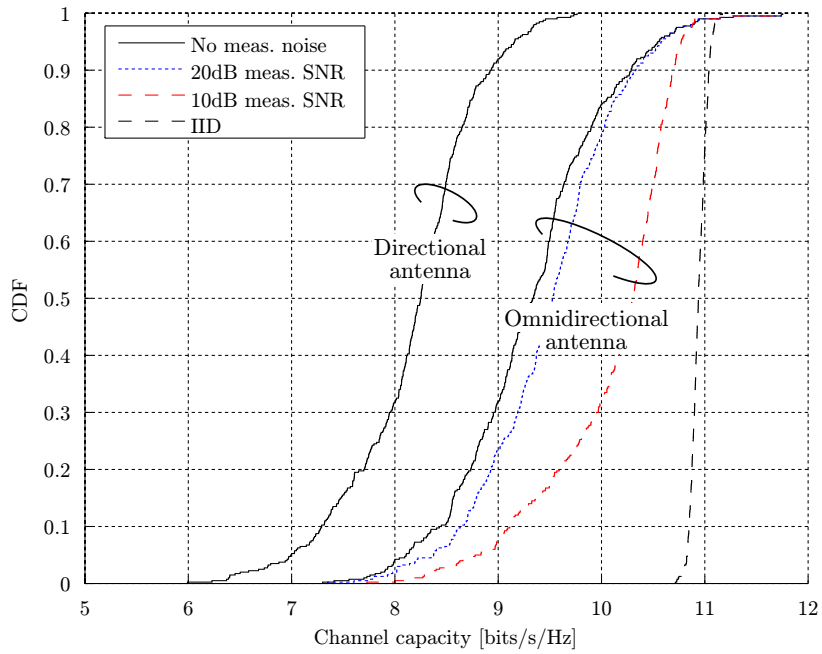


**Figure 7:** The CDF of the frequency averaged channel capacity, in case of omnidirectional and directional antennas, is shown for the multi-user MIMO link over the different snapshots. The for the omnidirectional antenna, capacity is shown for different measurement noise levels. The capacity for an IID channel also is shown for comparison, and the capacity is evaluated at a receiver SNR of 10 dB.

If the measurement noise is increased even more, the capacity will converge towards that of the IID channel. Furthermore, due to the large variations in received power over snapshots, as seen in Figure 6, the capacity increase due to measurement noise is largest at the center of the route. At the beginning and end of the routes, the MIMO channel matrix is dominated by two of the sub-channels. A low measurement SNR on the weak sub-channels will therefore not significantly effect the channel capacity.

Having looked at the capacity expressions, the BER performance at the output of the iterative receiver is considered next. In Figure 8, the CDFs of the instantaneous BER obtained at each snapshot is shown for the omnidirectional antenna case. The BER is shown after 15 receiver iterations, and at an average $E_b/N_0 = 10$ dB, where $E_b$ and $N_0$ are the received bit energy and

noise power spectral density, respectively. Furthermore, the performance when using channel estimation, and when assuming perfect channel state information (PCSI) at the receiver, is evaluated.

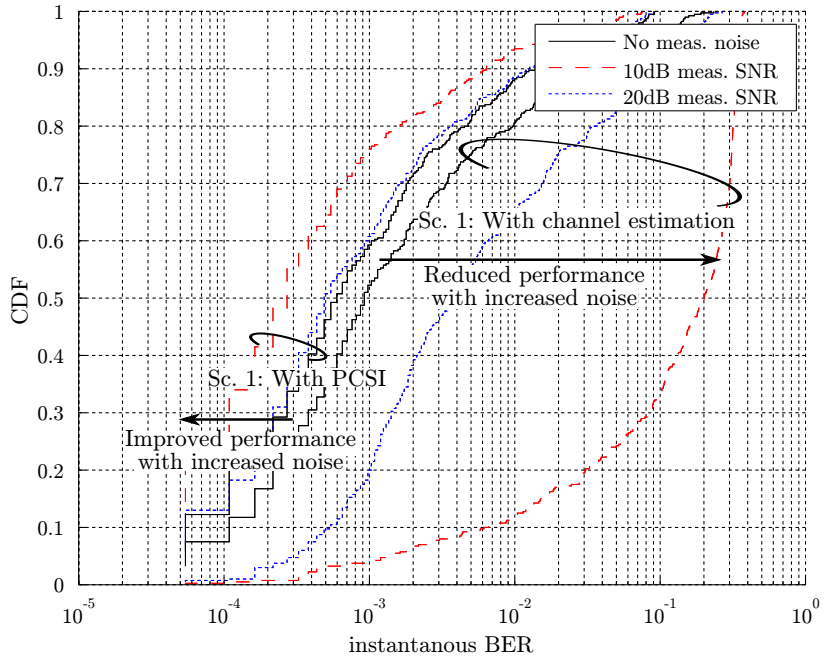


**Figure 8:** CDF of the BER as taken over 400 channel snapshots. The BER is shown for the case of PCSI and when the channel estimator is used, both after 15 receiver iterations, and at an average system $E_b/N_0 =$ 10 dB. Furthermore, the performance at different levels of measurement SNR is shown.

Starting with the case of PCSI, as seen in Figure 8, the BER is improved when the measurement noise is present. In this case, the same conclusions as for the capacity can be made; increasing the measurement SNR will improve system performance. The noise reduce the spatial correlation of the channel, thus making it easier for the MUD to separate the different user streams.

If we instead consider the use of the channel estimator, which is exploiting the delay limited nature of the wireless channel, the situation changes. Due to the presence of measurement noise, the frequency correlation of the channel is altered, i.e., the channel is no longer delay limited as discussed in Section 3.1. Therefore, the estimator will fail to obtain an accurate estimate, since a large

portion of the channel energy is outside the assumed maximum delay. In Figure 8 this can be clearly observed. Already at 20 dB measurement SNR, a performance loss is seen as compared to the noise free channel. Increasing the measurement noise power even more, achieving a 10 dB average measurement SNR, the performance almost collapses due to the inaccurate channel estimates.

It is interesting to note that the noise will have a different impact depending on which system we are investigating. For the case of PCSI, the measurement noise will cause an overestimate of the system performance, while the opposite is true when using the low-rank estimator.

### Directional antennas

As mentioned in Section 3.4, the choice of measurement antennas will inevitably change the properties of the measured channel. In this section we exemplify this by looking at the system performance when using either directional, or omnidirectional, antennas at the MUs. As previously seen in Figure 7, the use of directional antennas, in the chosen configuration, significantly reduced the channel capacity. This occurs since the directive antennas mainly receive energy coming from one direction, leading to a reduced spatial diversity in the measured channel.

We now take a look at how the BER performance is affected. In Figure 9 the CDFs of the instantaneous BER obtained at each snapshot is shown for both omnidirectional, and directional, antennas. As before, the BER is shown after 15 receiver iterations, and at an average $E_b/N_0 = 10$ dB. As seen from the figure, the performance is significantly lower for the case of directional antennas. The performance is also significantly worse when channel estimation is performed, as previously discussed.

### Delay synchronization

We now proceed by exemplifying how the presence of a delay shift in the measurements can affect system performance. As mentioned in Section 3.5, a shift of the impulse response due to propagation delay, or synchronization errors, can affect the performance of algorithms exploiting the delay limited nature of the wireless channel. This is, e.g., the case for the channel estimator in our iterative receiver. To achieve a channel with suitable properties, we generate a channel for the presented scenario, and then added an artificial delay, which is increasing for each snapshot. It should be noted that the obtained channel is not entirely realistic, but it has properties which allow us to clearly visualize the effect of a delay shift.

In the lower part of Figure 10, the impulse response of one of the multiple

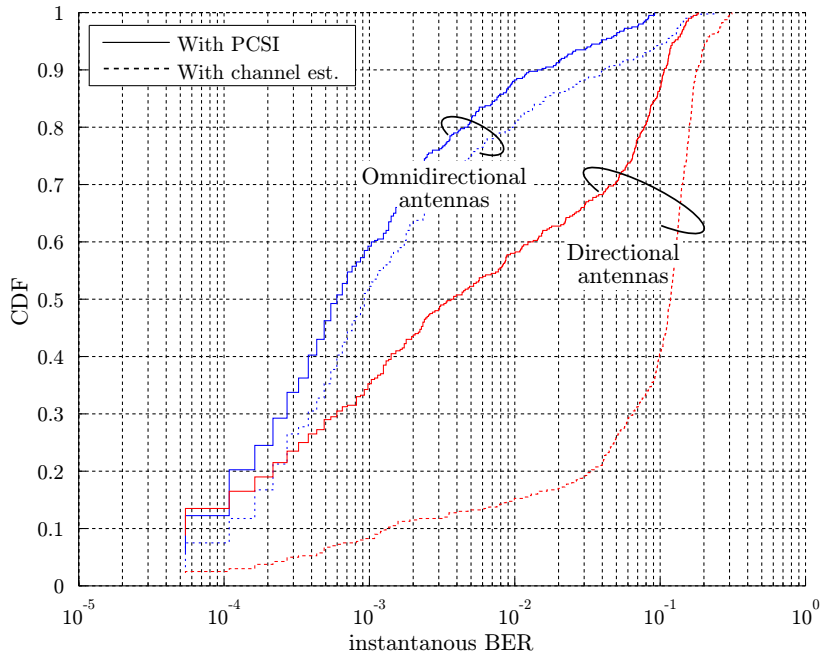


**Figure 9:** CDF of the BER, obtained with directional and omnidirectional antennas, taken over the 400 channel snapshots. The BER is shown for the case of PCSI and when the channel estimator is used, both after 15 receiver iterations, and at an average system $E_b/N_0 = 10$ dB.

antenna links is shown. The maximum delay, assumed by the channel estimator, is shown with the solid black line. As seen from the figure, as the snapshot number increases, so does the delay. At the same time, more and more of the channel power end up outside the maximum delay supported by the channel estimator. The effect this has on the estimator performance is shown in upper part of Figure 10, where the mean square estimation error (MSE) is shown. The figure shows the MSE when signaling at an $E_b/N_0 = 10$ and 20 dB.

As seen in Figure 10, as the impulse response slides outside the supported delay the MSE increases. The effect is becoming visible around snapshot number 150 when signaling at $E_b/N_0 = 20$ dB, but not until snapshot number 230 at 10 dB. As long as the errors due to the delay shift is small enough, the errors due to noise will dominate. Therefore, the delay shift induced errors become visible later in the 10 dB case, as compared to the 20 dB case. A similar behavior can be seen when using this type of estimator over noisy measured

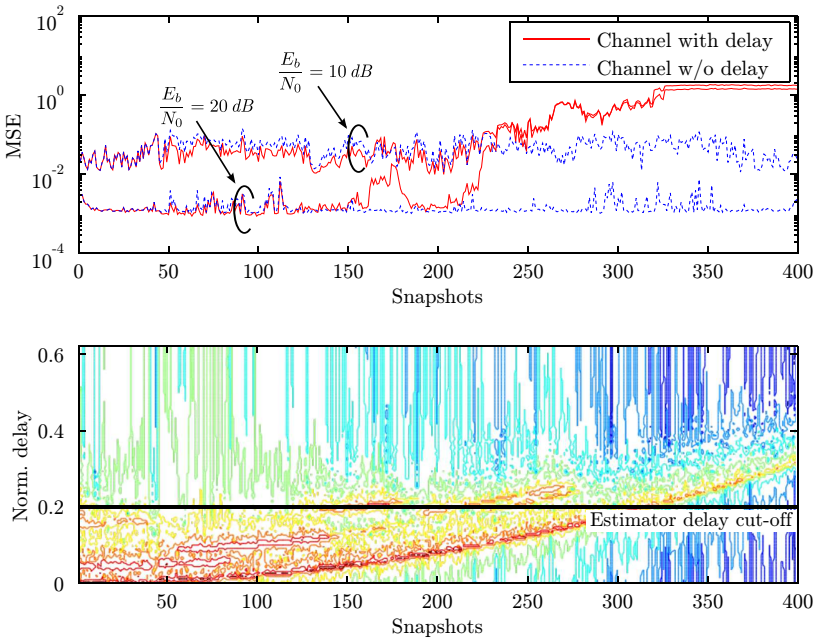


**Figure 10:** Impact of the propagation delay on MSE performance. The upper part of the figure is showing the MSE, while the lower is showing the shift of the impulse response over time/distance.

channels, as in section 4.3. In that case, the measurement SNR needs to be well below the signaling SNR in order to hide the estimation errors caused by noisy measurements.

# 5 Summary and Conclusion

In this paper we have discussed the use of channel measurements in wireless communication system evaluations. A number of issues related to measurements is presented, and potential solutions are pointed out. We have also demonstrated three of the issues by looking at the performance of an iterative multi-user MIMO-OFDM receiver. One of the most important problem is the presence of additive measurement noise, which can hide correlation properties of the channel. Though appropriately designed measurements can keep the noise levels low, filter based post-processing of the measurements may be needed. Other aspects that needs to be kept in mind is the presence of phase

noise, propagation delay, and the use of directive antennas during measurements.

As we have discussed and illustrated, the use of channel measurements for system evaluation is not necessarily straightforward. In general, it is important to design the measurements well, and take into account the requirements of the specific system in mind. Specifically when evaluating algorithms exploiting the correlation properties of the wireless channel. A critical eye is also important when looking at potential measurement data. Plotting the data in various ways and domains (delay/frequency, Doppler/time, power, phase) is important to make sure that no obvious measurement errors exist. If something looks strange, it is important to find out why.

Finally, if handled with care, measurement data can be a good alternative for system evaluations since it provides a direct snapshot of a real life scenario. For novel wireless systems, measurements can help to speed up the design process, by providing a good test environment at an early stage, before appropriate models are available.

## References

[1] A. Molisch, *Wireless Communications*. John Wiley & Sons ltd., 2nd ed., 2011.

[2] P. Almers, F. Tufvesson, and A. Molisch, "Keyhole effect in MIMO wireless channels: Measurements and theory," *IEEE Transactions on Wireless Communications*, vol. 5, pp. 3596–3604, Dec. 2006.

[3] O. Edfors, S. Wilson, and P. Börjesson, "OFDM channel estimation by singular value decomposition," *IEEE Transactions on Communications*, vol. 46, no. 7, pp. 931–939, 1998.

[4] Y. Li, N. Seshadri, and S. Ariyavisitakul, "Channel estimation for OFDM systems with transmitter diversity in mobile wireless channels," *IEEE Journal on Selected Areas in Communications*, vol. 17, pp. 461–471, Mar. 1999.

[5] T. Zemen, C. Mecklenbrauker, J. Wehinger, and R. Muller, "Iterative joint time-variant channel estimation and multi-user detection for MC-CDMA," *IEEE Transactions on Wireless Communications*, vol. 5, pp. 1469–1478, Jun. 2006.

[6] T. Ekman, *Prediction of mobile radio channels. Modeling and Design*. PhD thesis, Uppsala University, Uppsala, Sweden, Dec. 2002.

[7] K. Haneda, V.-M. Kolmonen, T. Riihonen, R. Wichman, P. Vainikainen, and J. Takada, "Evaluation of relay transmission in outdoor-to-indoor propagation channels," in *1st COST2100 Workshop, Trondheim, Norway*, 2008.

[8] J. Salmi, A. Richter, and V. Koivunen, "Sequential unfolding SVD for tensors with applications in array signal processing," *IEEE Transactions on Signal Processing*, vol. 57, pp. 4719–4733, Dec. 2009.

[9] D. Baum and H. Bolcskei, "Impact of phase noise on MIMO channel measurement accuracy," in *Proc. IEEE Vehicular Technology Conference*, vol. 3, pp. 1614–1618, Sept. 2004.

[10] P. Almers, S. Wyne, F. Tufvesson, and A. Molisch, "Effect of random walk phase noise on MIMO measurements," in *Proc. IEEE Vehicular Technology Conference*, vol. 1, pp. 141–145, May 2005.

[11] V.-M. Kolmonen, P. Almers, J. Salmi, J. Koivunen, K. Haneda, A. Richter, F. Tufvesson, A. Molisch, and P. Vainikainen, "A dynamic dual-link wideband MIMO channel sounder for 5.3 GHz," *IEEE Transactions on Instrumentation and Measurement*, vol. 59, pp. 873–883, Apr. 2010.

[12] N. Czink, B. Bandemer, G. Vazquez-Vilar, L. Jalloul, and A. Paulraj, "Can multi-user MIMO measurements be done using a single channel sounder?," in *COST 2100, TD(08)621, Lille, France, Tech. Rep.*, Oct. 2008.

[13] *The COST2100 book*. to appear.

[14] P. Salvo Rossi and R. Müller, "Joint iterative time-variant channel estimation and multi-user detection for MIMO-OFDM systems," in *Proc. IEEE Global Communications Conference*, pp. 4263–4268, Nov. 2007.

[15] J. Poutanen, K. Haneda, L. Liu, C. Oestges, F. Tufvesson, and P. Vainikainen, "Parameterization of the COST 2100 MIMO channel model in indoor scenarios," in *Proc. European Conference on Antennas and Propagation*, pp. 3606–3610, Apr. 2011.

[16] J. Poutanen, F. Tufvesson, K. Haneda, L. Liu, C. Oestges, and P. Vainikainen, "Adding dense multipath components to geometry-based MIMO channel models," in *Proc. IEEE International Symposium on Signal Processing and Information Technology*, pp. 54–57, Nov. 2010.

# *Paper IV*

# On the performance of iterative receivers for interfering MIMO-OFDM systems in measured channels

**Abstract**

This paper investigates the gains harvested through base station cooperation in the up-link for a multi-user (MU) Multiple-Input Multiple-Output Orthogonal Frequency Division Multiplexing (MIMO-OFDM) system, operating in a real indoor environment. The base stations perform joint detection using an iterative receiver that carries out multi-user detection and channel estimation via soft information from the single-user decoders. Performance evaluation is carried out using real channels from an indoor dynamic dual MIMO link measurement campaign. The measured scenario represent a real life situation where two users communicate with two base stations, each with two antennas, in an environment resembling a shopping mall or an airport terminal. System performance is evaluated in terms of both Bit-Error Rate (BER) vs. Signal-to-Interference Ratio (SIR) and Cumulative Distribution Functions (CDF) for the instantaneous BER. Also, the impact of using soft information in the channel estimation is analyzed.

---


P. Hammarberg, P. Salvo Rossi, F. Tufvesson, O. Edfors, V.-M. Kolmonen, P. Almers, R.R. Muller, A.F. Molisch,
"On the Performance of Iterative Receivers for Interfering MIMO-OFDM Systems in Measured Channels,"
in *Proc. Asilomar Conference on Signals, Systems, and Computers*, Oct. 2008.

# 1 Introduction

Multiple-Input Multiple-Output (MIMO) systems in combination with Orthogonal Frequency Division Multiplexing (OFDM) and iterative receivers have gained interest in current wireless communication research. MIMO-OFDM [1] systems can simultaneously mitigate inter-symbol interference and enhance system capacity through increased diversity, spatial multiplexing or interference suppression. At the same time iterative receivers, implementing Multi-User Detection (MUD) and channel estimation, achieve near-optimum performance with reasonable complexity [2].

In this paper we evaluate an iterative receiver for MIMO-OFDM systems using real channel measurements from an indoor dynamic dual-link scenario assuming a "quasi-static", i.e. block-fading, channel. The receiver performance has earlier been evaluated in [3], were focus was on analyzing Bit-Error Rate (BER) performance at different Signal-to-Interference Ratios (SIR). This paper focus on how the receiver can be used for interference mitigations through base station cooperation. By combining the received signals from two base stations a virtual antenna array is created that allow for joint detection of the two users. In this paper a system with two users and two base stations, each with two antennas, is considered. The system is shown in Fig. 1. Evaluation of the BER performance at different SIR levels is performed both with and without cooperating base stations. Additionally, an analysis of the impact of using soft information, obtained by decoding the received symbols, in the channel estimator is performed.

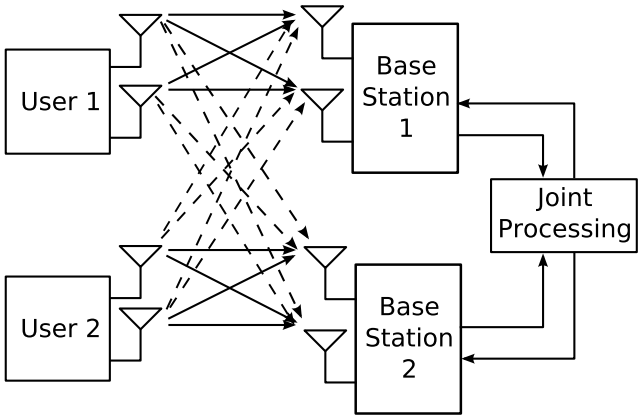


**Figure 1:** The considered multi-user system with cooperative detection.

## 2 System Model

A MIMO-OFDM system with $K$ transmit and $N$ receive antennas is considered, where each transmit antenna sends an independent data stream. The transmit/receive antennas may belong to different users/base stations. Each stream is encoded via convolutional coding and random interleaving, with codewords spanning both time and frequency dimensions. OFDM symbols with pilot data are inserted for channel estimation at the receiver. QPSK modulation is considered, and each frame (codeword + pilots) consists of $L$ bits grouped in $S$ OFDM symbols of $M$ subcarriers each. The frame structure is shown in Fig. 2.

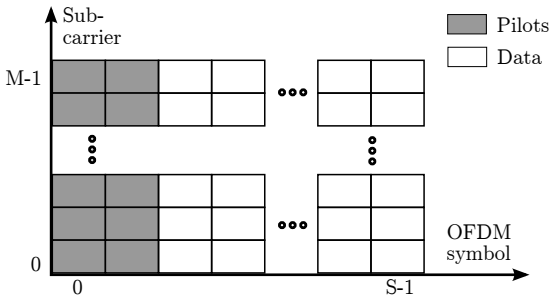


**Figure 2:** $M$ subcarrier OFDM frame structure with, in this case, two pilot symbols followed by S-2 data symbols.

Referring to the $m$th subcarrier during transmission of the $s$th OFDM symbol, we denote the transmitted vector, the channel matrix, the AWGN vector, and the received vector as

$$\boldsymbol{x}[m,s] = (x_1[m,s],\ldots,x_K[m,s])^{\mathrm{T}} ,$$

$$\boldsymbol{H}[m,s] = \begin{pmatrix} H_{1,1}[m,s] & \ldots & H_{1,K}[m,s] \\ \vdots & \ddots & \vdots \\ H_{N,1}[m,s] & \ldots & H_{N,K}[m,s] \end{pmatrix} ,$$

$$\boldsymbol{w}[m,s] = (w_1[m,s],\ldots,w_N[m,s])^{\mathrm{T}} , \text{and}$$

$$\boldsymbol{r}[m,s] = (r_1[m,s],\ldots,r_N[m,s])^{\mathrm{T}} .$$

The discrete-time model for the received signal can then be written as

$$\boldsymbol{r}[m,s] = \boldsymbol{H}[m,s]\boldsymbol{x}[m,s] + \boldsymbol{w}[m,s] . \tag{1}$$

Note that $\boldsymbol{H}$ contains the coefficients for both useful and interfering channels and that synchronous transmissions are assumed. The channel vector from the $k$th transmit antenna is denoted $\boldsymbol{h}_k^{(\mathrm{tx})}[m,s]$.

At the receiver, as illustrated in Fig. 3, OFDM symbols are demodulated and sent to the iterative decoder, performing MUD, Soft-Input Soft-Output (SISO) decoding and channel estimation. The multi-user detector and SISO decoders exchange extrinsic information on symbols $x_k$, denoted $\tilde{x}_k$ (resp. $\tilde{z}_k$) when going to the multi-user detector (resp. the SISO decoders). SISO decoders also provide *a posteriori* information on symbol $x_k$, denoted $\hat{x}_k$, to the channel estimator, and *a posteriori* information on source bits. The channel estimator provides channel coefficient estimates ($\hat{H}_{n,k}$).

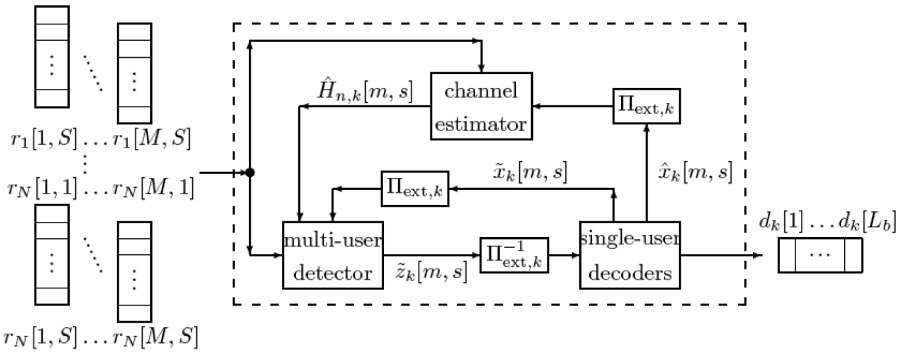


**Figure 3:** The structure of the iterative receiver.

## 2.1 MUD

The received signals (1) are processed separately for each subcarrier and OFDM symbol. Parallel interference cancellation is performed using $\tilde{\boldsymbol{x}}$ from the SISO decoders and $\hat{\boldsymbol{H}}$ from the channel estimators. The residual term from the interference cancellation for the $k$th transmit antennas, $\tilde{\boldsymbol{r}}^{(k)} = \boldsymbol{r} - \hat{\boldsymbol{H}}(\tilde{\boldsymbol{x}} - \tilde{x}_k \boldsymbol{i}_K^{(k)})$, is then MMSE filtered, to reduce noise and multi-user interference, giving the extrinsic information

$$\tilde{z}_k = \frac{\boldsymbol{i}_K^{(k)\mathrm{T}} \left( \hat{\boldsymbol{H}}^{\mathrm{H}} \hat{\boldsymbol{H}} + \sigma_w^2 (\boldsymbol{V}^{(k)})^{-1} \right)^{-1} \hat{\boldsymbol{H}}^{\mathrm{H}} \tilde{\boldsymbol{r}}^{(k)}}{\boldsymbol{i}_K^{(k)\mathrm{T}} \left( \hat{\boldsymbol{H}}^{\mathrm{H}} \hat{\boldsymbol{H}} + \sigma_w^2 (\boldsymbol{V}^{(k)})^{-1} \right)^{-1} \hat{\boldsymbol{H}}^{\mathrm{H}} \hat{\boldsymbol{h}}_k^{(\mathrm{tx})}} , \tag{2}$$

with $\boldsymbol{V}^{(k)} = \mathrm{diag}\left((1-|\tilde{x}_1|^2, \ldots, 1-|\tilde{x}_{k-1}|^2, 1, 1-|\tilde{x}_{k+1}|^2, \ldots, 1-|\tilde{x}_K|^2)\right)$. For the derivation we refer to [2].

## 2.2 SISO Decoding

After collecting $\{z_k[\ell]\}_{\ell=1}^{L}$, each transmit antenna can be decoded independently using the log-domain BCJR algorithm. The SISO decoder for the $k$th transmit antenna uses the model $z_k = x_k + v_k$, with $v_k \sim \mathcal{N}_{\mathbb{C}}(0, \eta_k^2)$ and $\eta_k^2 = \frac{1}{\boldsymbol{i}_K^{(k)\mathrm{T}}(\boldsymbol{H}^{\mathrm{H}}\boldsymbol{H}+\sigma_w^2\boldsymbol{I}_N)^{-1}\boldsymbol{H}^{\mathrm{H}}\boldsymbol{h}_k^{(\mathrm{tx})}}$.

## 2.3 Channel Estimation

Assuming that the maximum normalized delay spread ($\eta_{\max}^{(\mathrm{d})}$) is known, the receiver implements a low-complexity estimator based on the Slepian expansion

$$H_{n,k}[m] \approx \sum_{i=1}^{I} \psi_{n,k}[i] v_i[m] \ ,$$

where $\psi_{n,k}[i]$ is the $i$th Slepian coefficient for the link between the $k$th transmit antenna and the $n$th receive antenna; $v_i[m]$ is the $m$th sample of the $i$th time-shifted Discrete Prolate Spheroidal (DPS) sequence associated to the interval $m = 1, \ldots, M$ with time support $[0, \eta_{\max}^{(\mathrm{d})}]$ with corresponding eigenvalue $\lambda_i^{(\mathrm{d})}$; the approximate signal space extension is $\left\lceil \eta_{\max}^{(\mathrm{d})} M \right\rceil + 1 \leq I \leq M$. See [4] for more details. Also, we denote $\boldsymbol{v}[m] = (v_1[m], \ldots, v_I[m])^{\mathrm{T}}$, $\boldsymbol{\lambda}^{(\mathrm{d})} = \left(\lambda_1^{(\mathrm{d})}, \ldots, \lambda_I^{(\mathrm{d})}\right)^{\mathrm{T}}$, $\boldsymbol{\Xi}[m,s] = \boldsymbol{I}_N \otimes (\boldsymbol{x}[m,s] \otimes \boldsymbol{v}[m])^{\mathrm{T}}$, $\boldsymbol{\psi}_{n,k} = (\psi_{n,k}[1], \ldots, \psi_{n,k}[I])^{\mathrm{T}}$, where $\otimes$ denotes the Kronecker product. The signal model for channel estimation is

$$\boldsymbol{r} = \boldsymbol{\Xi}\boldsymbol{\psi} + \boldsymbol{w} \ ,$$

with $\boldsymbol{r}$, $\boldsymbol{\Xi}$, $\boldsymbol{\psi}$ and $\boldsymbol{w}$ appropriately collecting received signals, transmitted signals, Slepian coefficients and noise.

A linear MMSE estimate is performed

$$\hat{\boldsymbol{\psi}} = \left(\hat{\boldsymbol{\Xi}}^{\mathrm{H}}\boldsymbol{\Delta}^{-1}\hat{\boldsymbol{\Xi}} + \boldsymbol{C}_{\psi}^{-1}\right)^{-1} \hat{\boldsymbol{\Xi}}^{\mathrm{H}}\boldsymbol{\Delta}^{-1}\boldsymbol{r} \ ,$$

where $\boldsymbol{C}_{\psi}$ is the diagonal correlation matrix of the Slepian coefficients depending on the eigenvalues; $\hat{\boldsymbol{\Xi}}$ contains the expected transmitted symbols computed via *a posteriori* information from SISO decoders; $\boldsymbol{\Delta}$ is a diagonal matrix depending on the *a posteriori* information from the SISO decoders and the SNR.

# 3 Dynamic Multi-link MIMO Channel Measurements

## 3.1 Dynamic Multi-link MIMO Channel Measurements

The channel measurements [5] used in this evaluation were carried out in September 2007 in the CS-building at *Helsinki University of Technology*, Finland. The building is a modern four story building with corridors and offices surrounding a large atrium in the middle, resembling an airport terminal or a shopping mall. A mobile transmitter and two stationary receivers were used to measure the behavior of the dynamic multi-link channel. Fig. 4 shows a photograph of the building with both the receiver locations and the two transmitter routes marked.

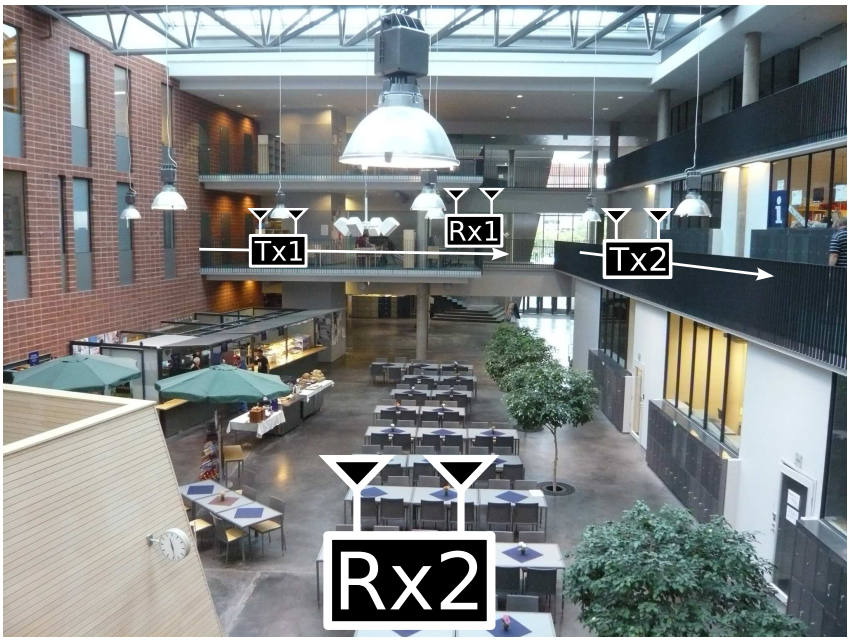


**Figure 4:** Photograph of the measurement location. The receivers (Rx1 and Rx2) are static, while the transmitters (Tx1 and Tx2) move along the paths indicated by arrows.

The measurement setup is summarized here, and the basic measurement

parameters are found in Table 1. In order to capture the behavior of the multi-link MIMO scenario, a single signal was transmitted from the transmitter to both receiving channel sounders. The transmitter was moved along several routes with a speed of about 1 m/s, and the MIMO channel transfer function was sampled each 39 ms. Sixteen dual-polarized antennas were used at each link end and local rubidium clocks in the channel sounders were used for synchronization.

**Table 1:** Measurement parameters.

| | |
|---|---|
| Center frequency | 5.3 GHz |
| Bandwidth | 120 MHz |
| TX power | 0.5 W (27 dBm) |
| Gap between MIMO blocks | 39.3216 ms |

In order to create a scenario with multiple users and base stations, measurements from two different routes of the mobile transmitter were combined. Even though these measurements were performed at different time instances, the environment is considered static between the measurements; thus the measurements are treated as co-located in time. The resulting channel data files from the measurements include two $32 \times 32$ MIMO channels per receiver. From these, four $2 \times 2$ MIMO channels were extracted, two for each receive and transmit combination. The combined channel represent the links between two mobile users and two base stations, with two antennas each.

The upper part of Fig. 5 displays a map of the considered scenario, showing the location of the static transmitters and moving receivers. The light gray area is the atrium area and the white area indicate the second floor where the measurements took place.

## 3.2 Processing of Channel Measurements

Post processing of the data has been performed in order to reduce the measurement noise present in the channel data. Further, interpolation has been performed in order to change the original frequency spacing in the measurements (0.6250 MHz) to a subcarrier spacing of 0.3125 MHz, in accordance with the recent IEEE 802.11n WLAN proposal [6]. The processing was performed using an interpolating Wiener filter [7] in the frequency domain, assuming a rectangular power delay profile. In essence, the filter removes all energy beyond a certain delay. The maximum delay was chosen in such way that a reasonable noise reduction was obtained, while still preserving the channel energy.

A simple power control scheme was used in the simulation. The principles

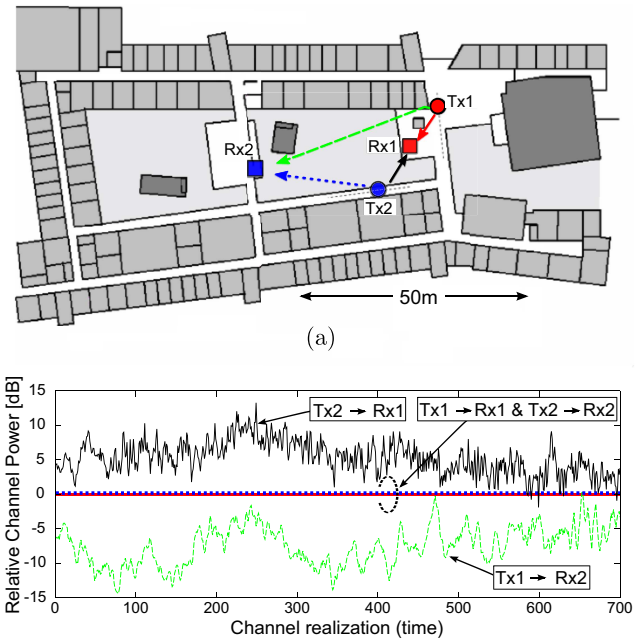


**Figure 5:** Part (a) displays a map of the measurement location showing the position of the receivers (Rx) and the routes of the transmitters (Tx). The arrows represent the signal paths from the transmitters to the receivers. In part (b) the average power in the different links, for the different channel realizations, after power control.

of the schemes were as follows; the average powers in the links between the users and their intended base station were normalized to unity for each channel realization. That is, the receive power from the primary user was held constant at the base stations. At the same time the interfering links were scaled by the same amount, preserving the relative power levels of the measured channel. Fig. 5 shows the average power in each link, as indicated on the map, after the power control scheme has been applied.

# 4 Results

As mentioned above, the system under consideration consists of two mobile users and two base stations, each with two antennas. The two users send independent codewords from each antenna spanning $S = 10$ OFDM symbols, including $S_p = 2$ OFDM pilot symbols, where each OFDM symbol contains $M = 64$ subcarriers (see Fig. 2). The channel is considered to be static over several frames, and each frame covers one code word. Code bits are generated by a rate 1/2 recursive systematic convolutional encoder [8] with generators $(7, 5)_8$ and with two tail bits forcing the final state into 1, giving 1020 information bits per frame and user. Assuming an OFDM symbol duration of $4\mu s$ [6], each user in the considered system transmits at a rate of 25.6 $Mbps$.

System simulations have been conducted in order to investigate the gains harvested through base station cooperation. Both the case of no cooperation, meaning that the inter-user interference is ignored at the receiver, and the case of full cooperation are treated. Results are presented in terms of the BER as a function of SIR, as well as in terms of the Cumulative Distribution Function (CDF) of the instantaneous BER at each channel realization. In the simulations a fixed receiver noise variance is set to give an $E_b/N_0$ of $5dB$ per receiver branch.

It is worth noting that for the case of base station cooperation, it is in this case somewhat misleading to talk about SIR, since the interference actually becomes useful signals power that can be used for detecting the transmitted signals. This additional power will also cause the effective $E_b/N_0$ to vary depending on the received power in the interfering link.

In Fig. 6 the performance for the user with the most favorable interference situation (Rx2 in Fig. 5) is shown for both with and without base station cooperation, after the $0th$ (when performing spatial filtering only) and $2nd$ iteration. As a comparison, the performance with Perfect Channel State Information (PCSI) at the receiver is shown. A sliding window mean taken over the different instantaneous SIR values has been performed to obtain the presented results.

Additional insight of the behavior of the system can be found by looking at the CDF of the instantaneous BER. Fig. 7 shows the CDF calculated from 230 individual channel realizations, corresponding to different positions of the users. The figure shows the performance after the $0th$, $1st$ and $2nd$ iteration, both with and without cooperation. Again the case of PCSI is shown for comparison.

Considering the performance with no cooperation, the interference and noise levels are so severe that the performance of the system is very poor. From Fig. 6 it is seen that the BER only reach values in the order of $10^{-1}$. Looking at Fig. 7,

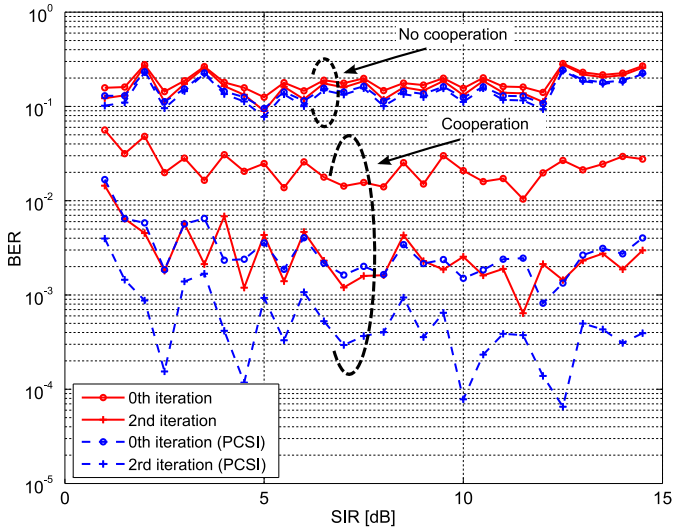


**Figure 6:** BER versus SIR with and without base station cooperation. The results shows the performance after the $0th$ and $2nd$ iteration. The case of PCSI is shown with dashed lines.

it is seen that the variance of the BER values is small; thus the performance is relatively independent of the individual channel realizations in the evaluated scenario. It is also seen that with PCSI the performance is still poor, though slightly better than when estimating the channel. Further, the gain obtained by performing iterations in the receiver is small. One iteration gives a small gain, but performing yet another iteration has an insignificant impact.

If instead the two base stations are allowed to cooperate, joint detection of the two users greatly improve performance. As can be seen in Fig. 6 the performance after two iterations are almost two orders of magnitude better than for the case of no cooperation. From Fig. 7 it can be seen that there is a significant performance difference between different channel realizations. Depending on the structure of the channel, and the total available power in the link, the instantaneous BER performance is seen to differ more than one order of magnitude between different measured channel realizations. This difference is growing considerably with iterations, while the average BER decreases.

It can also be seen that the difference in BER performance between PCSI and an estimated channel decreases with iterations. This is explained by the

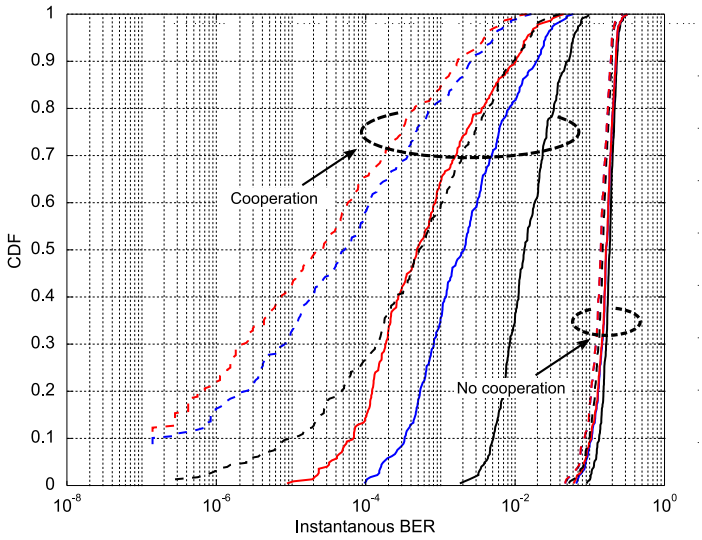


**Figure 7:** CDF of instantaneous BERs, with and without base station cooperation. The performance after the $0th$, $1st$ and $2nd$ iteration is shown. The case of PCSI is shown with dashed lines.

reduction of the channel estimation error due to improvements of the soft information with iterations.

In order to show the impact of using soft information in the channel estimation, performance simulations have been performed using only the known pilots in the estimator. Fig. 8 shows the CDF of the BER when using, and not using, soft information. The results are for the case of base station cooperation, after the $0th$, $1st$ and $2nd$ iteration. The performance is, as expected, identical before starting iterations, differing only due to independent noise realizations. When using only known pilots, the gain of performing more than one iteration is insignificant. If instead soft information is used to update the channel estimate, performance improve with every iteration. When designing MIMO-OFDM systems, this property can be used to decrease the amount of pilots transmitted, thereby decrease pilot overhead and increase spectral efficiency.

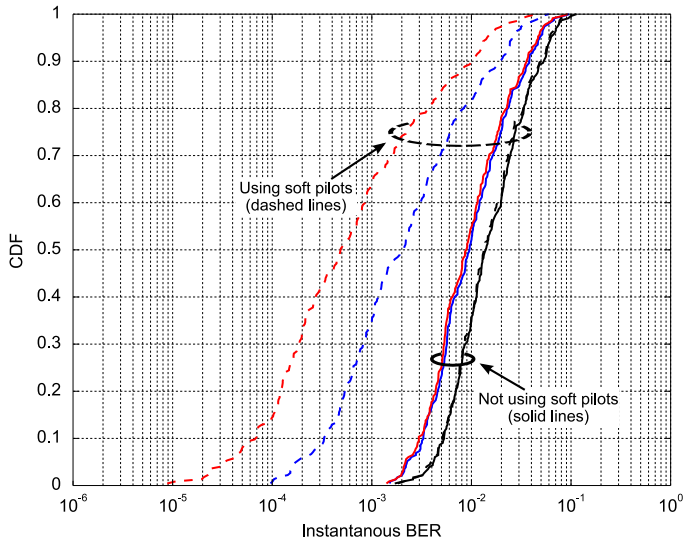


**Figure 8:** CDF of the BER when using (dashed lines), and not using (solid lines), soft information in the channel estimator. The results are for the case of base station cooperation, and shows performance after the $0th$, $1st$ and $2nd$ iteration. As expected, the performance is identical for the two cases after the $0th$ iterations.

# 5 Conclusion

A performance evaluation of an iterative receiver for MU-MIMO-OFDM has been performed, focusing on how the algorithm can be used for base station cooperation in the up-link. Computer simulations have been performed using real channels from an indoor dynamic dual-link MIMO measurement campaign. The considered system has two users and two base stations, all with two antennas.

It has been seen that by allowing the two base stations to cooperate in the detection of the two users, large gains are achieved. When there is no cooperation, the interference and noise severely limits performance and iterations in the receiver do not give any significant performance gains. On the other hand, if base stations are allowed to cooperate a significant performance increase is achieved. Especially if iterations are performed, making use of soft information for channel estimation and interference cancellation. The performance gain in terms of BER is orders of magnitude. Using soft information in the estimator

also open up the possibility of reducing the overhead in terms of transmitted pilot symbols, yielding increased spectral efficiency.

## References

[1] G. Stüber, J. Barry, S. McLaughlin, Y. Li, M. Ingram, and T. Pratt, "Broadband MIMO-OFDM wireless communications," *Proceedings of the IEEE*, vol. 92, pp. 271–294, Feb. 2004.

[2] T. Zemen, C. Mecklenbrauker, J. Wehinger, and R. Muller, "Iterative joint time-variant channel estimation and multi-user detection for MC-CDMA," *IEEE Transactions on Wireless Communications*, vol. 5, pp. 1469–1478, Jun. 2006.

[3] P. Salvo Rossi, P. Hammarberg, F. Tufvesson, O. Edfors, P. Almers, V.-M. Kolmonen, J. Koivunen, K. Haneda, and R. Muller, "Performance of an iterative multi-user receiver for MIMO-OFDM systems in a real indoor scenario," *Proc. IEEE Global Communications Conference*, pp. 1–5, Nov. 2008.

[4] D. Slepian, "Prolate spheroidal wave functions, Fourier analysis, and uncertainty - V: The discrete case," *Bell System Technical Journal*, vol. 57, pp. 1371–1430, May/Jun. 1978.

[5] J. Koivunen, P. Almers, V.-M. Kolmonen, J. Salmi, A. Richter, F. Tufvesson, P. Suvikunnas, A. Molisch, and P. Vainikainen, "Dynamic multi-link indoor MIMO measurements at 5.3 GHz," in *Proc. European Conference on Antennas and Propagation*, pp. 1 –6, Nov. 2007.

[6] S. Coffey, A. Kasher, and A. Stephens, "Joint proposal: High throughput extension to the 802.11 standard: PHY," in *IEEE 802.11-05/1102r2*, Jan. 2006.

[7] S. M. Kay, *Fundamentals of Statistical Signal Processing, Volume I: Estimation Theory*. Prentice Hall, 1993.

[8] J. G. Proakis, *Digital Communication*. McGraw-Hill Publishing Company, UK, 4th ed., 2000.

# *Paper V*

# Channel estimation algorithms for OFDM-IDMA: Complexity and performance

**Abstract**

In this paper, a number of channel estimation algorithms for iterative receivers are compared for an up-link orthogonal frequency division multiplexing interleave division multiple access (OFDM-IDMA) system. Both pilot based algorithms, used to obtain an initial estimate, as well as semi-blind decision-directed algorithms working as a component of the iterative receiver are considered. Algorithms performing either joint minimum mean square error (MMSE) channel estimation, or iterative estimation using space-alternating expectation maximization (SAGE), are evaluated. The considered algorithms differ in terms of complexity, as well as performance. The main contribution of this paper is to give an overview of different channel estimation approaches for OFDM-IDMA, where the complexity versus performance tradeoff is at the focal point. There is no single channel estimator providing the best tradeoff and our analysis shows how the number of users and the SNR influence the estimator choice.

---


P. Hammarberg, F. Rusek and O. Edfors,
"Channel Estimation Algorithms for OFDM-IDMA: Complexity and Performance,"
to appear in *IEEE Transactions on Wireless Communications*.

# 1 Introduction

In recent years a new multiple access technique, where the users are separated through their unique interleaving patterns, has generated a large interest in the research community. The technique, referred to as interleave-division multiple-access (IDMA) [1], has been shown to mitigate multiple access interference while simultaneously achieving a high spectral efficiency. IDMA shares many properties with code division multiple access (CDMA), where user separation is obtained through user-specific spreading codes, and has shown similar performance but with a reduced receiver complexity [1–4].

When the system bandwidth grows in single carrier systems, the equalization process becomes increasingly challenging due to the increase in the number of resolvable paths. Introducing orthogonal frequency division multiplexing (OFDM) simplifies this task by transforming the wideband channel into a set of orthogonal narrow band sub-channels. A simple scalar equalization can then be performed separately for every sub-channel. By combining IDMA and OFDM, an efficient multi-user system is formed which efficiently combats ISI and also reaches a high spectral efficiency [5, 6].

For interference cancellation and equalization in such systems, reliable channel estimates are needed. Channel estimates are usually obtained solely based on pilot symbols, which are known to the receiver. With the breakthrough of turbo-like receivers, however, iterative decision-directed[3] approaches to channel estimation have received increasing attention [7–13]. By using decoded symbols as pilots, more reliable estimates are obtained, at the same time as the pilot overhead is reduced. For a multi-user system that performs iterative MUD, such as OFDM-IDMA, iterative channel estimation can be incorporated in a straightforward way into the receiver structure.

There has only been limited research conducted on the performance of OFDM-IDMA systems employing channel estimation. For example, in [11] an estimator based on the least mean square algorithm is used, and in [12] a least square (LS) estimate is performed in every iteration. Both methods iteratively perform per-user channel estimation using symbol estimates from the channel decoder. As in the above mentioned papers, iterative decision-directed channel estimation algorithms are at focus in this paper, and an evaluation of different algorithms is performed.

Even if only a few channel estimation algorithms have been evaluated for OFDM-IDMA, algorithms for other transmission technologies provide many candidates. For the case of single carrier systems, [8] propose a number of different algorithms for IDMA, both making use of soft interference cancellation

[3] In the following, the term decision-directed will be used to refer to semi-blind schemes making use of both pilot symbols and estimates on the transmitted data symbols.

to estimate the different user channels independently, as well as performing joint MMSE estimation. Unlike in our this paper, where pilot symbols are time-multiplexed, pilot layers are added on top of the data symbols. In [13] an algorithm is derived based on Gaussian message passing for single carrier systems. The expectation maximization (EM) like algorithm is performing MMSE based estimates on soft interference canceled single-user streams. Furthermore, due to shared properties with OFDM-CDMA, and multiple transmit antenna system, algorithms available for these technology may be adopted, as will be discussed below. In [14] a discrete Fourier transform (DFT) based estimator for an OFDM system with transmit diversity is developed. The estimator jointly estimates the channels to all antennas. To reduce complexity, a related estimator based on the EM algorithm is proposed in [15], where the channels are estimated per user through indirect interference cancellation. Related to this work, a similar algorithm is proposed for multi-carrier CDMA systems in [16], and for multiple antenna systems in [17]. In [9] a channel estimator that jointly estimate all user channels is developed for OFDM-CDMA, based on a low rank discrete prolate spheroidal (DPS) sequence approximation of the channel. The algorithm is extended to multiple-input multiple-output (MIMO) OFDM systems in [10] and further developed to utilize time and frequency correlation in [18].

In this paper, the algorithm in [18] is evaluated, alongside two EM based algorithms, for an OFDM-IDMA system. The first EM based algorithms is based on [15], with the DFT base functions replaced by DPS sequences, and with support for using data symbol estimates along with pilot symbols, similar to [17]. The second one can be interpreted as a multi-carrier extension of the algorithm in [13], here derived from an EM perspective. Again, DPS sequences are used to efficiently exploit the frequency correlation. The algorithms all make use of estimates on the transmitted symbols, and the receiver therefore needs to acquire an initial channel estimate. Three pilot based algorithms, based on well known principles, are evaluated for this purpose. The aim is not only to investigate algorithm performance, but also how their implementation complexity relates to performance. Due to limitations in power consumption and chip area, complexity considerations are of high importance when algorithms are implemented in real systems. The main contributions of this paper may be summarized as follows

- Three different decision-directed channel estimation algorithms are evaluated in an OFDM-IDMA system for the first time. One of the algorithms jointly estimates the channels for all users, while the others perform per-user estimates based on the space-alternating EM (SAGE) algorithm. Different algorithms for obtaining an initial pilot based channel estimate

are also evaluated. The algorithms effect on the overall system performance and convergence is studied, along with their complexity.

- A complexity versus performance analysis is performed, where the total number of complex multiplications needed to reach a bit error rate (BER) target is evaluated. For the evaluation, the complete receiver complexity incorporating channel estimation, MUD and data decoding is considered.

The rest of this paper is organized as follows. In Section 2, a description of the considered OFDM-IDMA system is given. The algorithms for obtaining the initial pilot based estimate are presented in Section 3, and the decision-directed algorithms in Section 4. In Section 5 the performance of the different algorithms is investigated, and in Section 6 the complexity of the algorithms is discussed. Finally, the paper is summarized in Section 7.

# 2 System Description

In order to perform a comparison between the channel estimation algorithms, the studied system needs to be defined. First the OFDM-IDMA model is presented, followed by the channel model and its low-rank approximation. The latter needed for deriving the channel estimators.

## 2.1 OFDM-IDMA system model

The system considered in this paper is an uplink OFDM-IDMA system, as shown in Fig.1. It consists of $K$ users transmitting blocks of $S$ OFDM symbols, each with $M$ sub-carriers. The first $S_p$ OFDM symbols are reserved for pilots, known to the receiver, while the following $S - S_p$ OFDM symbols contain data. The total number of signal constellation points per block becomes $L = (S - S_p)M$. Low rate code words are formed by concatenating a forward error correcting code (FEC) with a repetition/spreading code. The code words are interleaved using, randomly generated, user specific interleavers, $\Pi_k$, of length $2L$, before mapped to QPSK symbols. Although QPSK is chosen here, the extension to other constellation sizes is conceptually straightforward.

After OFDM modulation and pilot insertion, the users transmit their signals over a frequency selective block fading channel. Furthermore, to allow for correct OFDM demodulation at the receiver, the users are assumed to be synchronized so that the difference in arrival times is less than the duration of the cyclic prefix minus the channel delay spread.

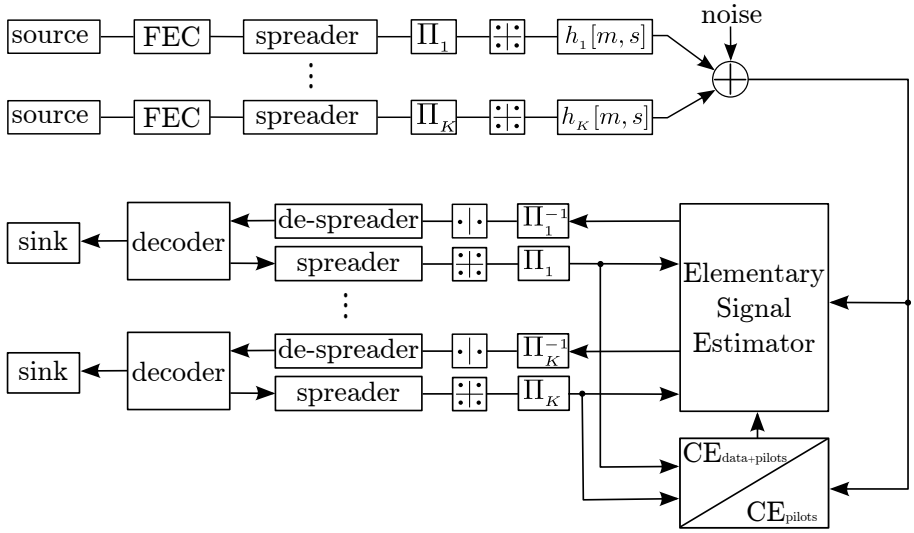


**Figure 1:** A baseband model of an OFDM-IDMA system with K users. The receiver implements an iterative multi-user receiver with channel estimation (CE). The CE is consisting of one pilot based and one decision-directed part.

The received signal, after appropriately demodulated into the complex baseband, is given by

$$r\left[m,s\right]=\sum_{k=0}^{K-1}h_k\left[m,s\right]x_k\left[m,s\right]+w\left[m,s\right]\,, \tag{1}$$

where $h_j[m,s]$, $x_j[m,s]$ and $w[m,s]$ represent the complex valued channel coefficient, transmitted symbol and noise, respectively, at sub-carrier $m$ in OFDM symbol $s$. The complex valued noise is distributed according to $\mathcal{CN}(0,\sigma_w^2)$. Collecting the signal for all subcarriers, an equivalent description of the received signal is

$$\boldsymbol{r}[s]=\sum_k \boldsymbol{X}_k[s]\boldsymbol{h}_k[s]+\boldsymbol{w}[s]\,, \tag{2}$$

where $\boldsymbol{X}_k[s]$ is an $M\times M$ diagonal matrix containing the transmitted symbols, on all subcarriers, from user $k$, $\boldsymbol{h}_k$ the channel frequency response for user $k$, and $\boldsymbol{w}[s]$ a vector containing noise.

Using the received baseband signal, the receiver implements an iterative MUD with channel estimation. Going through the receiver structure, as shown in Fig. 1, an initial pilot based estimate is first obtained. Using this, the receiver implements a per-symbol parallel interference canceling ESE (PIC-ESE) [4]. The ESE, as detailed in Appendix 8, models the interference plus noise as a complex Gaussian process and produces extrinsic log-likelihood ratio (LLR) outputs of the transmitted code bits. After the ESE, the per-user LLR streams are deinterleaved and despread before being fed to the soft-input soft-output (SISO) decoders. The extrinsic information output of the decoders are then respread and reinterleaved before fed back to the ESE and to the second stage of the channel estimation process. The soft symbols are then used to update the channel estimates and LLRs. The channel estimation process is divided into two parts, one pilot based, and one decision-directed. Algorithms for these two parts are presented in Sections 3 and 4.

## 2.2 Channel approximation

The algorithms evaluated in this paper are all based on a low rank approximation of the channel. Therefore, a model for the received signal based on the channel approximation has to be defined before the channel estimation algorithms can be derived. The approximation made is that the channel is limited in the delay domain, and can thus be accurately represented by a limited set of base functions. The optimal base functions in such scenario are presented in [19], and are referred to as DPS sequences. Alternatively, a DFT base could be used but, as seen in e.g. [20], spectral leakage may create an error floor if used for channel estimation.

Using the chosen base, consisting of $I$ base functions, the frequency response for a block fading channel may be expressed as

$$\boldsymbol{h}_k[s] = \boldsymbol{U}\boldsymbol{\psi}_k[s] = \boldsymbol{U}\boldsymbol{\psi}_k \ , \tag{3}$$

where $\boldsymbol{U}$ is an $M \times I$ matrix collecting the base functions, satisfying $\boldsymbol{U}^H\boldsymbol{U} = \boldsymbol{I}_I$, and $\boldsymbol{\psi}_k$ is a vector of length $I$ collecting the channel DPS coefficients. In (3), the second equality holds for a block fading channel. Using this model, the received signal in (2) may be expressed as

$$\boldsymbol{r}[s] = \sum_{k=1}^{K} \boldsymbol{X}_k[s]\boldsymbol{U}\boldsymbol{\psi}_k + \boldsymbol{w}[s] \, . \tag{4}$$

Now, by collecting the received signal for all $S$ OFDM symbols in a vector, and in a similar way collecting the channel coefficients for all users, the received

signal may be expressed using the classical linear model [18, 21]

$$\boldsymbol{r} = \boldsymbol{\Xi}\boldsymbol{\psi} + \boldsymbol{w} \ . \tag{5}$$

In (5) $\boldsymbol{r}$ is a vector of length $SM$ collecting the received signal at all time-frequency positions, $\boldsymbol{\Xi}$ is a $SM \times KI$ observation matrix collecting the transmitted symbols and channel base functions, $\boldsymbol{\psi}$ is a vector of length $KI$ collecting the channel coefficients for all users, and $\boldsymbol{w}$ a vector of length $MS$ collecting noise. More explicitly, the data structures are given by:

$$\begin{aligned}
\boldsymbol{r} &= \left(\boldsymbol{r}^{\mathrm{T}}[1], \ldots, \boldsymbol{r}^{\mathrm{T}}[S]\right)^{\mathrm{T}} \\
\boldsymbol{\Xi} &= \left(\boldsymbol{\Xi}^{\mathrm{T}}[1], \ldots, \boldsymbol{\Xi}^{\mathrm{T}}[S]\right)^{\mathrm{T}} \\
\boldsymbol{\Xi}[s] &= \left(\boldsymbol{\Xi}^{\mathrm{T}}[1, s], \ldots, \boldsymbol{\Xi}^{\mathrm{T}}[M, s]\right)^{\mathrm{T}} \\
\boldsymbol{\Xi}[m, s] &= \left(\boldsymbol{x}[m, s] \otimes \boldsymbol{u}[m]\right)^{\mathrm{T}} \\
\boldsymbol{u}[m] &= \left(u_1[m], \ldots, u_I[m]\right)^{\mathrm{T}} \\
\boldsymbol{U} &= \left(\boldsymbol{u}_1, \ldots, \boldsymbol{u}_I\right) \\
\boldsymbol{x}[m, s] &= \left(x_1[m, s], \ldots, x_K[m, s]\right)^{\mathrm{T}} \\
\boldsymbol{\psi} &= \left(\boldsymbol{\psi}_1^{\mathrm{T}}, \ldots, \boldsymbol{\psi}_K^{\mathrm{T}}\right)^{\mathrm{T}} \\
\boldsymbol{\psi}_k &= \left(\psi_k[1], \ldots, \psi_k[I]\right)^{\mathrm{T}} \\
\boldsymbol{w} &= \left(w[1], \ldots, w[S]\right)^{\mathrm{T}} \\
\boldsymbol{w}[s] &= \left(\boldsymbol{w}^{\mathrm{T}}[1, s], \ldots, \boldsymbol{w}^{\mathrm{T}}[M, s]\right)^{\mathrm{T}} \ ,
\end{aligned}$$

where $\otimes$ denotes the Kronecker product.

The DPS sequences are obtained from solving the eigenvalue equation [9, 19, 20], $\boldsymbol{C}\boldsymbol{u}_i = \lambda_i \boldsymbol{u}_i$, where $\boldsymbol{C}$ is an $M \times M$ correlation matrix. For later use, the eigenvalues $\lambda_i$ are collected in a vector , $\boldsymbol{\lambda} = [\lambda_1, \ldots, \lambda_I]^{\mathrm{T}}$, in descending order.

For any basis expansion, truncating the number of functions will lead to an approximation error. For DPS sequences, the error is proportional to the energy of the eigenvalues corresponding to the discarded sequences. As noted in [19], for $I \geq \lceil \tau_{\max} M \rceil + 1$ the energy of the eigenvalues are small, and rapidly decreasing. Hence, this value can be seen as a bound on the number of DPS sequences needed to adequately represent the channel. Based on the above models, the channel estimation algorithms can now be derived, which is done in Sections 3 and 4.

# 3 Pilot based channel estimators

As was mentioned in Section 2, $S_p$ pilot OFDM symbols are transmitted at the beginning of each data block. The pilot symbols are used to obtain an initial channel estimate, which is used as a starting point for the iterative process in the receiver. It is assumed that the transmission is non-orthogonal in time-frequency and that pseudo-random unit energy pilot symbols are transmitted. Thus, optimal design of the pilot symbols is not considered.

Since the initial estimate can have a large impact on the convergence of an iterative process, an accurate estimate is important. In the following sections, three different algorithms for obtaining the initial estimate are presented. The algorithms range from the simplest per-user LS estimate (ignoring interference), via successive interference cancellation (SIC), to the most complex joint MMSE estimate of all users channels. Note that we in this section only consider transmission of the known pilot symbols, i.e., OFDM symbols $s = 0, \ldots, S_p - 1$.

## 3.1 Per-user LS estimation

The conceptually simplest and most straightforward estimation approach is to perform a per-user LS estimate, based on the received signal and the transmitted pilot symbols, while ignoring the interference from the other users. For this purpose, (4) may be rewritten as

$$\boldsymbol{r}_k[s] = \boldsymbol{X}_k[s]\boldsymbol{U}\boldsymbol{\psi}_k + \tilde{\boldsymbol{w}}_k[s] \tag{6}$$

to represent the received signal for user $k$, where $\tilde{\boldsymbol{w}}_k[s]$ collects the interference plus noise of OFDM symbol $s = 0, \ldots, S_p - 1$. The LS estimates are then given by

$$\hat{\boldsymbol{\psi}}_k[s] = \boldsymbol{U}^H \boldsymbol{X}_k^H[s]\boldsymbol{r}_k[s] \ , \tag{7}$$

and equivalently for the frequency response

$$\hat{\boldsymbol{h}}_k[s] = \boldsymbol{U}\boldsymbol{U}^H \boldsymbol{X}_k^H[s]\boldsymbol{r}_k[s] \ , \tag{8}$$

Note that the operation of $\boldsymbol{U}$ followed by $\boldsymbol{U}^H$ may be seen as a subspace filtering, removing all received energy outside the channel space. If consecutive pilot OFDM symbols are transmitted, time-averaging is used to further improve performance, i.e., $\hat{\boldsymbol{h}}_k = \frac{1}{S_p}\sum_{s=0}^{S_p-1} \hat{\boldsymbol{h}}_k[s] = \frac{1}{S_p}\boldsymbol{U}\boldsymbol{U}^H \sum_{s=0}^{S_p-1} \boldsymbol{X}_k^H[s]\boldsymbol{r}_k[s]$.

A low-complexity version of the algorithm is also considered. By using an identity matrix instead of the DPS sequences in the algorithm, i.e., setting $\boldsymbol{U} = \boldsymbol{I}_M$ in (6)-(8), the frequency filtering and its associated cost is removed. Though this modification lead to a reduced complexity, the loss in performance is also significant, as will be discussed in later sections.

### 3.2 Per-user SIC based LS estimation

In the second pilot based algorithm, SIC is used in an attempt to decrease the effect of inter-user interference. By estimating one user channel at the time, and removing that users signal component, the interference will decrease while going through the users. The procedure may be repeated in additional iterations $i$, using the output of the last step to reinitialize the first, for improved performance. The LS method as presented in Section 3.1 is used to estimate the channels and the algorithm can be summarized as follows:

- Initialization: $\hat{\boldsymbol{r}}[s] = \boldsymbol{r}[s]$.
- For each iteration $i$:
  for $k = 1, \cdots, K$

$$\text{if } i = 0: \quad \hat{\boldsymbol{h}}_k^{(i)}[s] = \boldsymbol{U}\boldsymbol{U}^H \boldsymbol{X}_k^H[s]\hat{\boldsymbol{r}}[s] \tag{9}$$

$$\hat{\boldsymbol{r}}[s] = \hat{\boldsymbol{r}}[s] - \boldsymbol{X}_k[s]\hat{\boldsymbol{h}}_k^{(i)}[s] \tag{10}$$

$$\text{else:} \quad \hat{\boldsymbol{r}}[s] = \hat{\boldsymbol{r}}[s] + \boldsymbol{X}_k[s]\hat{\boldsymbol{h}}_k^{(i-1)}[s] \tag{11}$$

$$\hat{\boldsymbol{h}}_k^{(i)}[s] = \boldsymbol{U}\boldsymbol{U}^H \boldsymbol{X}_k^H[s]\hat{\boldsymbol{r}}[s] \tag{12}$$

$$\hat{\boldsymbol{r}}[s] = \hat{\boldsymbol{r}}[s] - \boldsymbol{X}_k[s]\hat{\boldsymbol{h}}_k^{(i)}[s] \tag{13}$$

Note that the signal component which was subtracted for user $k$ in the previous iteration is first added in (11), before the channel is re-estimated. Furthermore, as for the LS algorithm, when transmitting consecutive pilot symbols, averaging in time is carried out to improve performance.

### 3.3 Joint MMSE estimate

For the two previous algorithms, the channel is estimated per user, either by ignoring interference, or by trying to cancel it. In the last pilot based algorithm, the channels for all users are estimated jointly, taking inter-user correlation into account. Based on the model of the received signal given in (5), the MMSE estimate of $\boldsymbol{\psi}$ is produced as [18, 21]

$$\hat{\boldsymbol{\psi}} = \left(\boldsymbol{\Xi}_p^H \boldsymbol{C}_w^{-1} \boldsymbol{\Xi}_p + \boldsymbol{C}_\psi^{-1}\right)^{-1} \boldsymbol{\Xi}_p^H \boldsymbol{C}_w^{-1} \boldsymbol{r}\,, \tag{14}$$

where $\boldsymbol{C}_w = \sigma_w^2 \boldsymbol{I}_{MS_p}$ is the noise covariance matrix, and $\boldsymbol{C}_\psi = \boldsymbol{I}_K \otimes \mathrm{diag}\,(\boldsymbol{\lambda})$ denotes the covariance matrix of the DPS sequences. The $S_pM \times KI$ observation matrix $\boldsymbol{\Xi}_p$ has the same structure as $\boldsymbol{\Xi}$ in (5), but only containing the $S_p$ pilot symbols.

Since the pilot sequences are known at the receiver, so is the matrix $\mathbf{\Xi}_p$ in (14). If the receiver is designed for a specific noise variance $\sigma_w^2$, and a maximum channel delay spread $\tau_{\max}$, the entire estimator can be precalculated. Therefore, the estimate of the model coefficients can be obtained through a straightforward matrix multiplication. From these estimates, the frequency responses are then created using (3). It can be noted that for a block fading channel with consecutive pilot symbols, the resulting MMSE estimator is performing an operation equivalent to symbol by symbol estimates followed by averaging.

After obtaining our initial channel estimates, the attention is turned to the decision-directed estimation performed in the iterative detector, as described at the end of Section 2.1.

# 4 Decision-directed channel estimation

In this section different algorithms for performing decision-directed channel estimation are presented. The first algorithm, referred to as Full MMSE, performs a joint MMSE estimate of the channel coefficients for all users based on both pilots and soft estimates of the data symbols. The second algorithm iteratively obtains the maximum-likelihood (ML) solution, using SAGE [22], based on pilots and hard decisions of the decoded data symbols, and is referred to as SAGE ML. The third algorithm, SAGE MMSE, borrows ideas from the first two and computes an estimate in a similar way as SAGE ML but using soft estimates of the data symbols.

It can be noted that Full MMSE can be seen as an extension of the pilot based MMSE estimator presented in Section 3. In a similar way, the LS algorithms of Section 3 could be modified and used in a decision-directed mode, but they would not be competitive from a performance and complexity point of view. Similarly, SAGE ML and SAGE MMSE could in theory be used to obtain the initial pilot based estimate, but would require a blind initial guess. A detailed description of the considered algorithms follows.

## 4.1 Joint MMSE estimator using soft decisions (Full MMSE)

When estimating the channel, the optimal and at the same time most costly approach is to estimate the channel for all users jointly. In this section an algorithm that computes a joint MMSE estimate based on (5), using both pilots and soft estimates of the transmitted symbols, is presented. The algorithm has previously been derived for MIMO-OFDM in [18].

Based on (5), the linear MMSE estimate of the DPS channel coefficients is given by [18]

$$\hat{\boldsymbol{\psi}} = \left(\hat{\boldsymbol{\Xi}}^{\mathrm{H}}\boldsymbol{\Delta}^{-1}\hat{\boldsymbol{\Xi}} + \boldsymbol{C}_{\psi}^{-1}\right)^{-1}\hat{\boldsymbol{\Xi}}^{\mathrm{H}}\boldsymbol{\Delta}^{-1}\boldsymbol{r}\,, \tag{15}$$

where $\hat{\boldsymbol{\Xi}}$ has the same structure and size as $\boldsymbol{\Xi}$ in (5), but contains both known pilot symbols and soft estimates of transmitted symbols; $\boldsymbol{\Delta} = \mathrm{diag}(\boldsymbol{\vartheta}) + \sigma_w^2\boldsymbol{I}_{KMS}$, with $\boldsymbol{\vartheta} = \left(\boldsymbol{\vartheta}^{\mathrm{T}}[1],\ldots,\boldsymbol{\vartheta}^{\mathrm{T}}[S]\right)^{\mathrm{T}}$, $\boldsymbol{\vartheta}[s] = \left(\vartheta[1,s],\ldots,\vartheta[M,s]\right)^{\mathrm{T}}$, $\vartheta[m,s] = \left(\sum_{k=1}^{K}\left(1-|\hat{x}_k[m,s]|^2\right)\right)$, and $\{\hat{x}_k[m,s]\}$ are either pilots or soft symbol outputs from the decoder. Note that $\mathrm{diag}(\boldsymbol{\vartheta}) = \mathbb{E}\{\boldsymbol{\Xi}\boldsymbol{\psi}\boldsymbol{\psi}^H\boldsymbol{\Xi}^H\} - \hat{\boldsymbol{\Xi}}\boldsymbol{C}_{\psi}\hat{\boldsymbol{\Xi}}^H$.

## 4.2 SAGE based estimator (SAGE ML)

The algorithm presented in the previous section requires the creation and multiplication of large matrices, and a matrix inversion, leading to a large algorithm complexity. As a low complexity alternative, an algorithm based on SAGE is presented. The SAGE algorithm iteratively computes the ML solution based on an underlying subspace model for the received signal.

Based on (4), by distributing the noise vector over the different subspaces the complete data set $\{\boldsymbol{r}_k[s]\}$ can be written as

$$\boldsymbol{r}_k[s] = \boldsymbol{X}_k[s]\boldsymbol{U}\boldsymbol{\psi}_k + \boldsymbol{w}_k[s],\ \text{for } k = 1,\ldots,K\,, \tag{16}$$

where $\boldsymbol{w}[s] = \sum_k \boldsymbol{w}_k[s]$ is the complete noise vector. As can be seen, $\boldsymbol{r}_k[s]$ is the signal component received from user $k$, and summing over all users gives (4). For the problem at hand, the SAGE algorithm is formulated as [22]

- Initialization: For all $k$ and $s$

$$\hat{\boldsymbol{s}}_k^{(0)}[s] = \boldsymbol{X}_k[s]\boldsymbol{U}\hat{\boldsymbol{\psi}}_k^{(0)}. \tag{17}$$

- For each iteration $i$:
  for $k = 1 + [i \text{ modulo } K]$, and for all $s$, compute

  *E-step:*

$$\hat{\boldsymbol{r}}_k^{(i)}[s] = \hat{\boldsymbol{s}}_k^{(i)}[s] + \left(\boldsymbol{r}[s] - \sum_{j=1}^{K}\hat{\boldsymbol{s}}_j^{(i)}[s]\right) \tag{18}$$

*M-step:*

$$\begin{aligned}
&\hat{\boldsymbol{\psi}}_k^{(i+1)}[s] \\
&= \arg\min_{\boldsymbol{\psi}_k[s]} \left( \left\| \hat{\boldsymbol{r}}_k^{(i)}[s] - \boldsymbol{X}_k[s]\boldsymbol{U}\boldsymbol{\psi}_k[s] \right\|^2 \right) \\
&= \boldsymbol{U}^H \boldsymbol{X}_k^H[s] \hat{\boldsymbol{r}}_k^{(i)}[s], \qquad (19) \\
&\hat{\boldsymbol{\psi}}_k^{(i+1)} = \frac{1}{S} \sum_{s=0}^{S-1} \hat{\boldsymbol{\psi}}_k^{(i+1)}[s] \\
&= \frac{1}{S} \boldsymbol{U}^H \sum_{s=0}^{S-1} \boldsymbol{X}_k^H[s] \hat{\boldsymbol{r}}_k^{(i)}[s], \qquad (20) \\
&\hat{\boldsymbol{s}}_k^{(i+1)}[s] = \boldsymbol{X}_k[s]\boldsymbol{U}\hat{\boldsymbol{\psi}}_k^{(i+1)}. \qquad (21)
\end{aligned}$$

for all $j$, $j \neq k$,

$$\hat{\boldsymbol{s}}_j^{(i+1)}[s] = \hat{\boldsymbol{s}}_j^{(i)}[s]. \qquad (22)$$

Since $\boldsymbol{X}_k[s]$ are initially unknown at the receiver, estimates must be used. The estimates are then updated by the decoders in every iteration, using the most recent channel estimate. Here, hard decisions $\hat{\boldsymbol{X}}_k[s] = \text{sign}(\tilde{\boldsymbol{X}}_k[s])$ of the decoded symbols are used. The initial $\hat{\boldsymbol{\psi}}_k^{(0)}[s]$ is obtained from pilot symbols as described in Section 3. Furthermore, all $K$ user channels are updated, instead of just one, before the data symbols are re-estimated.

As for the pilot based LS algorithm in Section 3.1, a low-complexity version is considered where the frequency filtering is removed, i.e., setting $\boldsymbol{U} = \boldsymbol{I}_M$ in (17)-(22). The modification leads to a reduced complexity, as well as a loss in performance, as discussed in later sections.

## 4.3 Modified SAGE estimator (SAGE MMSE)

The drawback of SAGE ML is that it does not support direct use of soft symbol estimates. In this section, an algorithm is proposed where SAGE ML is altered to support the use of soft symbols by deriving the MMSE solution instead of the ML solution in (19). The resulting algorithm share some properties with the single-carrier algorithm presented in [13].

By appropriately collecting the received signal components from different time instances $s$, the model for the received signal from user $k$ may be written in the same form as in (5), i.e.,

$$\boldsymbol{r}_k = \boldsymbol{\Xi}_k \boldsymbol{\psi}_k + \tilde{\boldsymbol{w}}_k \ , \qquad (23)$$

where the definitions of $\boldsymbol{\Xi}_k$ and $\boldsymbol{\psi}_k$ are found in Section 4.1 using $K = 1$. Note that $\tilde{\boldsymbol{w}}_k \sim \mathcal{CN}(0, \sigma^2_{\tilde{\boldsymbol{w}}})$ contains both noise and interference. An estimate of the variance $\sigma^2_{\tilde{w}}$ can be provided by the ESE. For the above model, the MMSE estimate is given, similar to (15), by

$$\begin{aligned}\hat{\boldsymbol{\psi}}_k &= \left(\hat{\boldsymbol{\Xi}}_k^{\mathrm{H}} \boldsymbol{\Delta}_k^{-1} \hat{\boldsymbol{\Xi}}_k + \boldsymbol{C}_{\psi_k}^{-1}\right)^{-1} \hat{\boldsymbol{\Xi}}_k^{\mathrm{H}} \boldsymbol{\Delta}_k^{-1} \boldsymbol{r}_k \\ &= \boldsymbol{A}_k \boldsymbol{r}_k \ , \end{aligned} \tag{24}$$

where the sub-index $k$ indicates that the data structures are user specific.

The proposed SAGE MMSE algorithm can now be summarized as follows:

- Initialization: For all $k$ and all $s$

$$\hat{\boldsymbol{s}}_k^{(0)}[s] = \boldsymbol{X}_k[s]\, \boldsymbol{U}\, \hat{\boldsymbol{\psi}}_k^{(0)}, \tag{25}$$

$$\hat{\boldsymbol{s}}_k^{(0)} = [\hat{\boldsymbol{s}}_k^{(0)T}[0], \ldots, \hat{\boldsymbol{s}}_k^{(0)T}[S-1]]^T. \tag{26}$$

- For each iteration $i$:

  for $k = 1 + [i \text{ modulo } K]$ compute

$$\text{E-step:} \qquad \hat{\boldsymbol{r}}_k^{(i)} = \hat{\boldsymbol{s}}_k^{(i)} + \left(\boldsymbol{r} - \sum_{j=1}^{K} \hat{\boldsymbol{s}}_j^{(i)}\right) \tag{27}$$

$$\text{M-step:} \qquad \hat{\boldsymbol{\psi}}_k^{(i+1)} = \boldsymbol{A}_k^{(i)} \hat{\boldsymbol{r}}_k^{(i)}, \tag{28}$$

$$\hat{\boldsymbol{s}}_k^{(i+1)}[s] = \boldsymbol{X}_k[s]\, \boldsymbol{U}\, \hat{\boldsymbol{\psi}}_k^{(i+1)}. \tag{29}$$

  for all $j$, $j \neq k$,

$$\hat{\boldsymbol{s}}_j^{(i+1)}[s] = \hat{\boldsymbol{s}}_j^{(i)}[s] \ . \tag{30}$$

# 5 Simulation results

The evaluation of the proposed algorithms are performed using system simulations. In the simulations, each user transmits code words covering $S - S_p = 19$ OFDM symbols, with $M = 256$ subcarriers. One OFDM symbol is dedicated for training information, i.e., $S_p = 1$, which is generated randomly for each user. A rate 1/2 convolutional code with generator polynomial $(7, 5)_8$ is used, followed by a rate 1/8 repetition code (spreading). Since QPSK is used as modulation, each code word consists of 608 information bits. With the chosen coding and spreading rates, the maximum number of users is observed to be

$K = 17$, given perfect channel state information (PCSI) at the receiver. Similar numbers are observed in [6] and [5].

For the simulations, a fading multi-path channel model, mimicking a rich scattering environment, is used. The channel impulse response for user $k$ is given by [23]

$$g_k(\tau) = \sum_{p=0}^{P-1} \alpha_{p,k}\delta(\tau - \tau_{p,k}),$$

where $\alpha_{p,k}$ are zero-mean complex Gaussian random variables with an exponential power delay profile, $\theta(\tau_{p,k}) = Ce^{-\tau_{p,k}/\tau_{\text{rms}}}$, where $C$ is a constant, and the delays $\tau_{p,k}$ are uniformly distributed within the cyclic prefix (CP). In this paper, the length of the channel, normalized to the symbol duration, is $\tau_{\max} = 0.1$, the root mean square delay spread set to $\tau_{\text{rms}} = 0.03$, and the number of multi-path components $P = 100$. The channel delay is assumed to be no longer than the cyclic prefix, and the block fading channel is generated independently for each user. The number of DPS sequences used in the channel estimation process is given by $I = \lceil \tau_{\max} M \rceil + 1 = 27$, which is a sufficient number as discussed in Section 2.2. It is interesting to note that for the given choice of parameters, the channel is initially under-sampled if $K > 9$. But as will be seen, with the assistance of estimated data symbols, accurate channel estimates can be obtained.

To begin with, the impact of the initial pilot based estimate is investigated by looking at the system performance. Then, the performance of the decision-directed channel estimation algorithms is evaluated. The results show both the BER, as well as mean square estimation error (MSE), after each receiver iteration, averaged over all users in the system. Different number of users $K$ and SNR per bit, $E_b/N_0$, are used to investigate the performance of the algorithms. Here, $E_b$ is the average received energy per bit.

## 5.1 Influence of the initial channel estimate

In Section 3 three different pilot based algorithms were presented. Here, the effect of the initial estimates on the overall system performance is investigated, and Fig. 2 shows the BER when different pilot based estimators are used. For the comparison we are only presenting the performance obtained when using SAGE ML in the decision-directed mode. Similar results are observed for the other two algorithms.

To illustrate the impact of user load, results are shown for $K = 6$, 10 and 14 users, at an $E_b/N_0 = 6$ dB. The SIC based estimator is set to perform 3 internal

iterations, giving a tradeoff between reasonable interference cancellation at high SNR and poor convergence at low SNR.

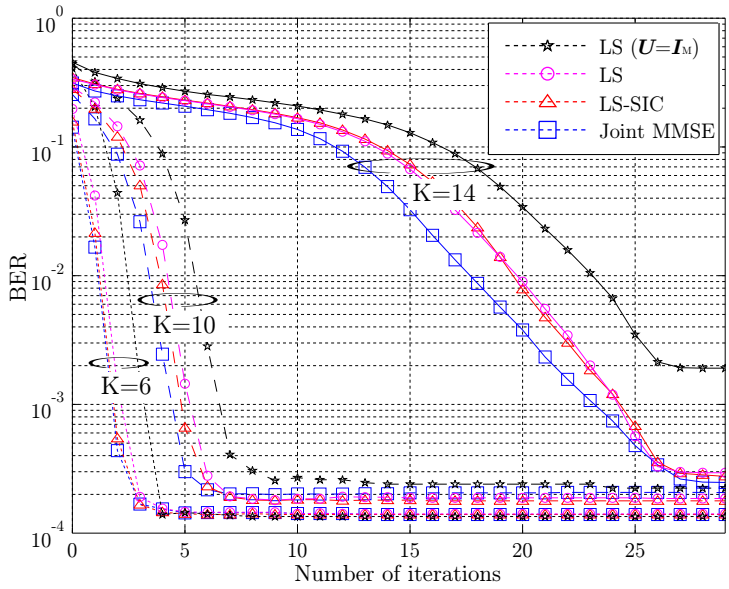


**Figure 2:** The BER is shown for the decision-directed SAGE-ML estimator for 6, 10 and 14 users. Different algorithms are used to obtain the initial pilot based estimate, and the results are shown for $S = 20$ OFDM symbols, $S_p = 1$ OFDM pilot symbol, $M = 256$ subcarriers and at an $E_b/N_0 = 6$ dB.

As can be observed in Fig. 2, the difference between the algorithms is relatively small for $K = 6$ users, with a possible save of $1 - 2$ iterations. When increasing the user load, the LS estimator not making use of the frequency correlation, i.e., $\boldsymbol{U} = \boldsymbol{I}_M$, is observed to degrade. Due to the poor initial estimate, the convergence speed is decreased and the error floor is elevated by more frequent convergence failures. This is especially evident at $K = 14$ users. Overall, the joint MMSE algorithm shows the best performance, especially at high user loads, followed by the LS-SIC. At a user load of $K = 14$, the interference cancellation process has an insignificant gain due to unreliable cancellation. Thus, the LS and LS-SIC algorithms show a similar performance.

## 5.2 Performance of the decision-directed algorithms

Having covered the pilot based estimators, the performance of the decision-directed algorithms is investigated next. In this investigation, the initial estimate is obtained using the joint MMSE approach. Again, $S = 20$ and $S_p = 1$ OFDM symbols, $M = 256$ subcarriers.

In Fig. 3, the BER is shown for $K = 14$ users, at $E_b/N_0 = 6$ dB. For comparison, single user performance with PCSI at the receiver is also shown. As seen, with the chosen pilot density, using decoded data in the estimation process greatly improves performance. The exception being for SAGE ML with $\boldsymbol{U} = \boldsymbol{I}_M$, where convergence is not observed. The other algorithms reach close to single user performance after $20 - 30$ iterations. Amongst these, the Full MMSE has the fastest convergence. The SAGE MMSE, using soft decisions, shows the best performance among the SAGE based estimators.

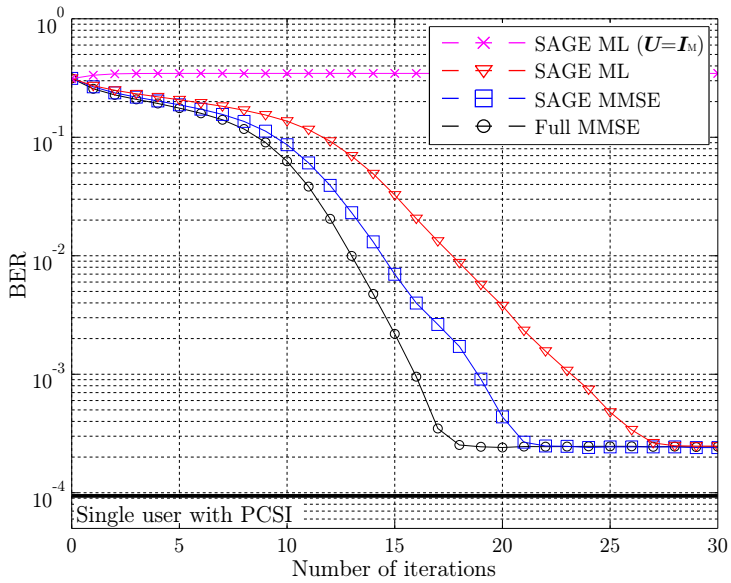


**Figure 3:** Convergence, when using the different decision-directed algorithms, in terms of BER, when $S = 20$ OFDM symbols, $S_p = 1$ OFDM pilot symbol, $M = 256$ subcarriers, $K = 14$ users and at an $E_b/N_0 = 6$ dB. The initial estimate is obtained using the joint MMSE estimator, and the case of PCSI and when pilots only are used in the CE, are shown for comparison.

Now, looking at the MSE presented in Fig. 4, with the same system settings

as above, the same general conclusions as for the BER can be drawn. The Full MMSE estimator has the fastest convergence, followed by the SAGE based estimators making use of the frequency correlation. If the channel correlation is not exploited, the MSE is increasing due to divergence caused by unreliable decisions on the transmitted symbols. For comparison, the analytical minimum MSE [21] in the case of a single user is shown. The observed loss as compared to this value is mainly due to the truncation of the number of DPS sequences used. Furthermore, the two MMSE based estimators converge to a smaller MSE since the noise variance is accounted for when producing the estimates. This also shows that SAGE MMSE iteratively reach Full MMSE performance. Further, the algorithms all reach comparable MSE values since they exploit the strong correlation properties of the channel in similar ways.

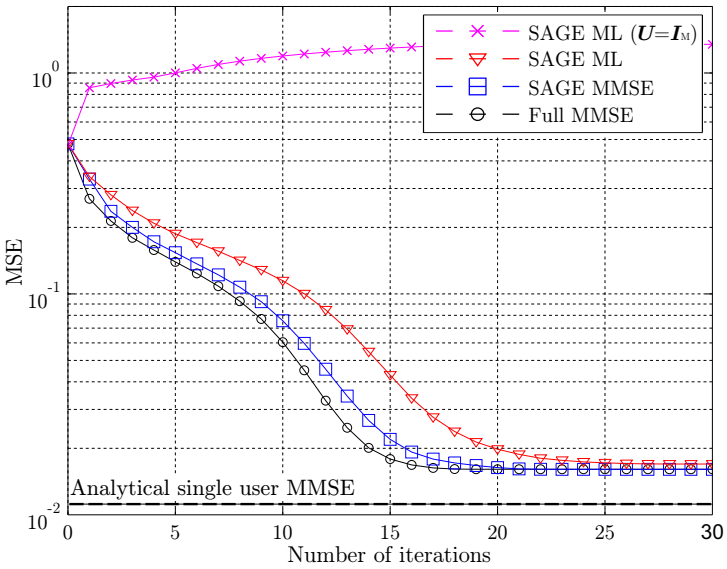


**Figure 4:** Convergence, when using the different decision-directed algorithms, in terms of MSE, when $S = 20$ OFDM symbols, $S_p = 1$ OFDM pilot symbols, $M = 256$ subcarriers, $K = 14$ users and at an $E_b/N_0 = 6$ dB. The initial estimate is obtained using the joint MMSE estimator, and the case when pilots only are used in the CE, are shown for comparison.

Next, the receiver performance at different $E_b/N_0$ is considered. In Fig. 5 the BER is shown for the case of $K = 14$ users, at $E_b/N_0 = 6$ and 8 dB. Again, single user performance is shown for comparison. At this high system load,

SAGE ML with $\boldsymbol{U} = \boldsymbol{I}_M$ does not converge. Amongst the other algorithms, Full MMSE shows the best convergence performance, with larger gain at low SNR. The gain as compared to SAGE MMSE is $1-4$ iterations, and $2-9$ iterations as compared with SAGE ML. Comparing the two SAGE based estimators, there is a clear difference in convergence speed. By using soft decisions in the estimation process, i.e., using SAGE MMSE, the convergence speed is significantly improved. Furthermore, as seen in Fig. 5, when the noise level decreases, so does the gain of using soft decisions. This occurs since the soft and hard symbols are nearly the same at high SNRs. Again, close to single user performance is observed.

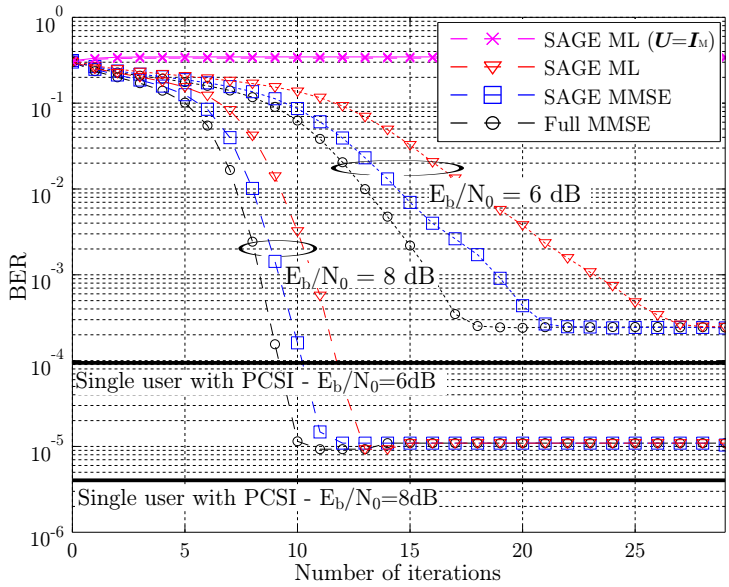


**Figure 5:** Convergence, when using the different decision-directed algorithms, in terms of BER, when $S = 20$ OFDM symbols, $S_p = 1$ OFDM pilot symbol, $M = 256$ subcarriers, $K = 14$ users and at different noise levels, i.e., $E_b/N_0 = 6$ and 8 dB. The initial estimate is obtained using the joint MMSE estimator.

Next, the impact of system load on performance is considered. In Fig. 6 the BER is shown for $K = 6, 10$ and 14 users, at an $E_b/N_0 = 6$ dB. Single user performance is presented for comparison. For the two lower user numbers, looking at the algorithms making use of the frequency correlation, convergence is relatively fast, with convergence after $5-10$ iterations. The relative order of

the algorithms is the same as previously observed, and as the number of users decrease, so does the difference in convergence speed. When $K = 6$ users, the difference is insignificant. As the number of users grows, the gain of using soft decisions, i.e., the MMSE based estimators, increases. This is especially evident for $K = 14$, as discussed earlier. The results indicate that the use of soft decisions only provide a significant gain at high user loads.

Looking at SAGE ML with $\boldsymbol{U} = \boldsymbol{I}_M$, no convergence is reached at high user load. Reducing the number of users to $K = 6$, the algorithm is just starting to converge. The BER performance is improved if the number of users is further reduced, or if the SNR is increased. Though the BER performance is poor, for systems operating at high SNR or with few users, the algorithm may still be interesting due to its simplicity, as will be seen below.

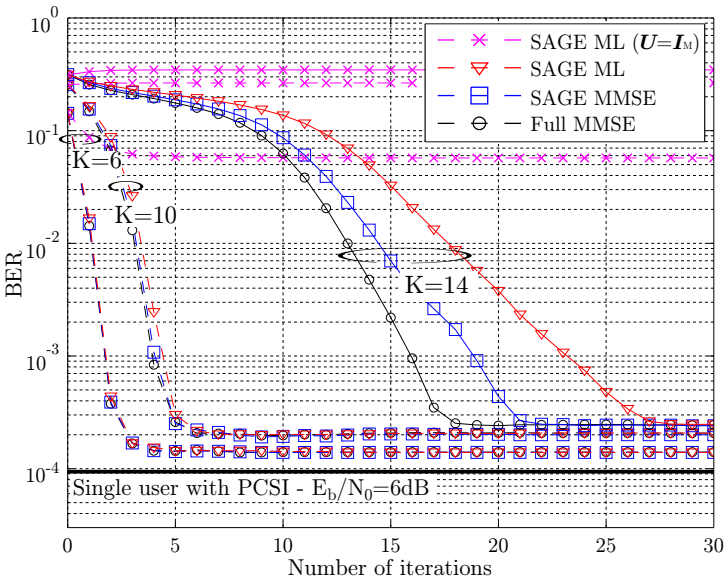


**Figure 6:** Convergence, when using the different decision-directed algorithms, in terms of BER, when $S = 20$ OFDM symbols, $S_p = 1$ OFDM pilot symbol, $M = 256$ subcarriers, $E_b/N_0 = 6$ dB and at different number of users, i.e., $K = 6, 10$ and 14. The initial estimate is obtained using the joint MMSE estimator.

# 6 Complexity analysis

When it comes to practical implementations of iterative multi-user systems, complexity considerations are of importance. In this section the proposed algorithms are compared based on their complexity in terms of the required number of complex multiplications. This measure is chosen since it provides a reasonable balance between accuracy and analytical tractability.

Below, the complexity of both the initial pilot based, as well as the decision-directed algorithms, is presented. The expressions for the complexity per user are given in Table 1. Note that the DPS sequences are assumed to be precalculated and read from memory. In Table 2, the expressions for the complexity are evaluated for the same system settings as in Section 5, i.e., $S = 20$ and $S_p = 1$ OFDM symbols, $M = 256$ subcarriers and $I = 27$ DPS sequences. For later use, the complexity of the ESE operation and data decoding is also shown. For the system under consideration, their complexity is approximated to $C_{ESE+DEC} \approx 50MS$ complex multiplications. As seen from the two tables, depending on the choice of estimator, the ESE and decoder will either dominate the receiver complexity of constitute a small part.

**Table 1:** Complexity per user for obtaining the channel estimates

| Pilot based estimators | |
|---|---|
| *Algorithm* | *Multiplications* |
| LS* | $MS_p$ |
| LS+ | $2IM + MS_p$ |
| LS-SIC | $N_{sic}(2IM + MS_p + 2M) - M$ |
| Joint MMSE** | $IMS_p + IM$ |
| Joint MMSE | $3MS_p + MKS_p + IMK + 2IM + (M+1)KI^2 + K^2I^3$ |
| Decision-directed estimators (complexity per iteration) | |
| SAGE ML* | $3MS$ |
| SAGE ML | $2IM + 3MS$ |
| SAGE MMSE | $5MS + 3IM + (M+1)I^2 + I^3$ |
| Full MMSE | $3MS + MSK + IMK + 2IM + (M+1)KI^2 + K^2I^3$ |
| ESE + decoder | $\approx 50MS$ |

* Without using frequency correlation, i.e., $\boldsymbol{U} = \boldsymbol{I}_M$.
+ Can be reduced to $IM + MS_p$ when $S_p = 1$.
** Assuming precalculated MMSE estimation matrix.

**Table 2:** Number of complex multiplications per user for obtaining the channel estimates. The numbers are given for $S_p = 1$ and $S = 20$ OFDM symbols, $M = 256$ subcarriers and $I = 27$ DPS sequences. Also, the approximate cost of performing the ESE operation and data decoding is shown.

| Initial pilot based estimators | |
|---|---|
| *Algorithm* | *Multiplications per user* |
| LS* | 256 |
| LS | 13824 |
| LS-SIC (3 iterations) | 43520 |
| Joint MMSE** | 13824 |
| Joint MMSE $K = 6$ | 1890306 |
| Joint MMSE $K = 14$ | 6595754 |
| Decision-directed estimators | |
| SAGE ML* | 15360 |
| SAGE ML | 29184 |
| SAGE MMSE | 253372 |
| Full MMSE $K = 6$ | 1934082 |
| Full MMSE $K = 14$ | 6678442 |
| ESE + decoder | $\approx 256000$ |

* Without using frequency correlation, i.e., $\boldsymbol{U} = \boldsymbol{I}_M$.

** Assuming precalculated MMSE estimation matrix.

## 6.1 Pilot based estimators

In the following, the complexity of the different pilot-based channel estimation algorithms presented in Section 3 is discussed. To begin with, the per-user LS algorithm is considered, being the one with the lowest complexity. The complexity is dominated by the frequency domain filtering, given that the number of pilot symbols is smaller than the filter dimension, i.e., $S_p < I$. Removing the frequency filtering, the complexity is significantly reduced. For the example in Table 2, the complexity is reduced by a factor of 54. As seen in Section 5, this come at a significant loss in performance, especially at high user loads.

Introducing interference cancellation, through the LS-PIC algorithm, will only slightly increase the complexity, given that only one internal iteration is performed. With internal SIC iterations, the complexity grows linearly with

iterations. This is seen in the example in Table 2, where 3 iterations are used, leading to a threefold increase in complexity as compared to the LS estimator.

The last algorithm considered is the joint MMSE estimator, performing joint estimation of all user channels. For a fixed set of users the estimator can be predesigned, assuming a certain $E_b/N_0$. The choice of $E_b/N_0$ may cause a mismatch error, but as was seen in [20], the error is relatively small. If the number of users and/or the pilot sequences changes, the estimator needs to be updated. For a system with a flexible design, a large number of estimator matrices has to be stored, increasing the memory requirements. Alternatively, the estimator can be redesigned whenever needed. This causes a large increase in the required number of multiplications, as seen in Table 2. The complexity is related to creating the matrix $\boldsymbol{\Xi}_p^H \boldsymbol{C}_w^{-1} \boldsymbol{\Xi}_p$, and performing the matrix inversion, in (14). The latter dominating when many users $K$ in the system. Due to the structure of $\boldsymbol{\Xi}_p$ under the block fading assumption, becoming a product between a block diagonal matrix and a block matrix with diagonal sub-matrices, increasing $S_p$ turn out to have a small impact on complexity. Further, the complexity can be lowered by reducing the number of DPS sequences $I$, which at the same time would decrease performance. If the estimator is predesigned, the complexity is comparable to that of the per-user LS estimator.

## 6.2 Decision-directed estimators

In this section the complexity of the different decision-directed channel estimation algorithms from Section 4 is presented. As can be seen in Table 1 and Table 2, there is a significant difference in complexity between the different algorithms.

The one with the smallest complexity is SAGE ML, using hard symbol decisions. The filtering in the frequency domain constitute a large part the algorithm complexity. Therefore, by omitting this operation the complexity is reduced, as seen in Table 2, where a reduction by a factor of 2 is observed. As seen in Section 5, this complexity reduction comes at a significant loss in performance, especially at high user loads. With an adaptive receiver design, the frequency filtering could be turned on or off, depending on the current user load. By doing so, the benefits of the two approaches could be combined. At the same time, it should be noted that the cost of SAGE ML is small as compared to the total receiver complexity, taking the ESE and decoder into account, making the possible savings relatively small.

Considering the SAGE MMSE estimator using soft symbol decisions, performance was improved as seen in Section 5.2. At the same time, complexity increases significantly. For the example in Table 2, the complexity increases by factor of 9 as compared to SAGE ML. This increase comes from creating

the per-user MMSE estimator in (24), where the operation $\hat{\boldsymbol{\Xi}}_k^{\mathrm{H}} \boldsymbol{\Delta}_k^{-1} \hat{\boldsymbol{\Xi}}_k$ is dominating. Similar to the pilot based joint MMSE estimator, under the block fading assumption, the impact of the block size $S$ on this operation is small due to the structure of $\hat{\boldsymbol{\Xi}}_k^{\mathrm{H}}$. The complexity can therefore primarily be lowered by reducing the number of DPS sequences $I$, also leading to a reduced performance.

If the Full MMSE estimator is considered, the complexity increases even further. As for the previously discussed MMSE estimators, the complexity lies in creating the estimation matrix. The dominating operations relate to creating $\boldsymbol{\Xi}^H \boldsymbol{\Delta}^{-1} \boldsymbol{\Xi}$, and performing the matrix inversion, in (15). For low user numbers, the former operation dominate and complexity grows linearly in $K$. As $K$ grows, the cost of performing the inverse start to dominate, and the per user complexity grows quadratic in $K$. As for SAGE MMSE, increasing the block size $S$ has a small impact on the complexity growth, assuming a block fading channel. In Table 2, the per-user complexity is shown for the cases of $K = 6$ and 14 users. Compared to the SAGE MMSE algorithm, the increase in complexity is by a factor of 8 and 26, respectively.

## 6.3 Complexity versus performance tradeoff

From a receiver design point of view, the complexity-performance tradeoff is important. In an attempt to shed some light on this aspect, the total receiver complexity, in terms of the number of complex multiplications, needed to reach a specific target BER is investigated. The complexity depends both on the choice of pilot based algorithm and decision-directed algorithm, the cost of the ESE and decoder, as well as on the number of iterations needed to reach the target. For the evaluation, the chosen target is a BER of $10^{-3}$. The system settings are the same as before, i.e., $S_p = 1$ and $S = 20$ OFDM symbols, $M = 256$ subcarriers and $I = 27$ DPS sequences.

To start with, the case of $K = 14$ users, signaling at an $E_b/N_0 = 6$ dB, is considered. In Fig. 7, the BER is plotted versus the number of complex multiplications per user, after every iteration, for all combinations of the pilot based and decision-directed algorithms. As previously seen in Fig. 3, SAGE ML with $\boldsymbol{U} = \boldsymbol{I}_M$ does not converge in this case. Amongst the other algorithms, SAGE ML gives the lowest complexity, requiring $\sim 6 \times 10^6$ multiplications per user to reach the BER target.Note that the target is not reached if using the LS algorithm with $\boldsymbol{U} = \boldsymbol{I}_M$. Due to the simplicity of SAGE ML, the complexity is in this case completely dominated by the ESE and decoder. Looking at SAGE MMSE, the required multiplications increase with 50% to $\sim 9 \times 10^6$, eventhough the per iteration complexity has doubled. This due to the faster convergence of the algorithm. If Full MMSE is considered, the complexity

increases by an order of magnitude to $\sim 10^8$. Its faster convergence can not compensate for its large complexity. Finally, looking at the impact of the initial pilot based algorithms, the difference between the algorithms are small, but the joint MMSE estimator provide the best complexity performance tradeoff.

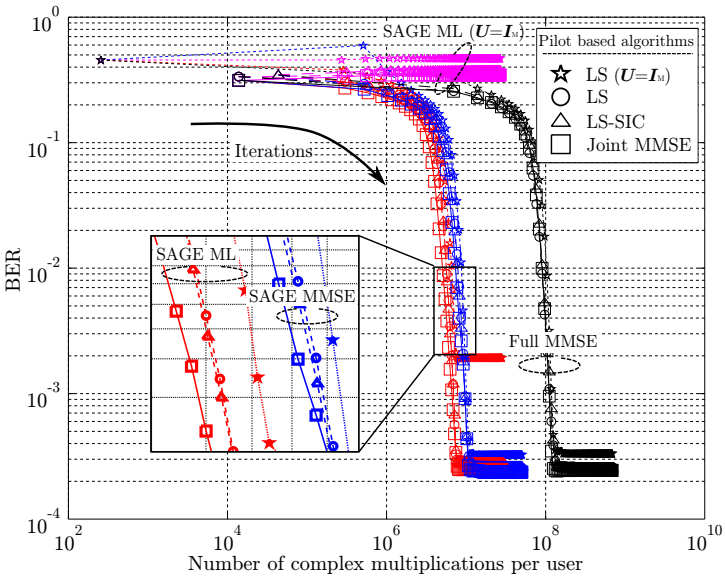


**Figure 7:** The BER versus the number of complex multiplications per users for the different algorithms at an $E_b/N_0 = 6$ dB and $K = 14$ users. The BER is plotted after every iteration performed. The system settings are $S_p = 1$ and $S = 20$ OFDM symbols, $M = 256$ subcarriers and $I = 27$ DPS sequences. The marker shape indicates which pilot based algorithm is used.

Finally, an overview of which algorithm combinations to choose in different scenarios is given, based on the previously stated system settings. In Fig. 8, the algorithm combinations with the lowest complexity at different user loads and $E_b/N_0$ are shown for a target BER of $10^{-3}$. The color indicates which decision-directed algorithm, and shape which pilot based algorithm, is used. For the decision-directed algorithms, there are certain regions where different algorithms are suitable, as highlighted by colored areas. At few users and high SNR, the algorithm with the lowest complexity, i.e., SAGE ML with $\boldsymbol{U} = \boldsymbol{I}_M$, is sufficient. But for higher system loads, making use of the correlation is needed for convergence. Increasing the number of users towards the maximum system load, SAGE MMSE is needed to reach the target. Hence, from a complexity

point of view, using soft decisions in the estimation process is only needed in extreme cases. Furthermore, Full MMSE is never considered due to its high complexity. Amongst the initial pilot based algorithm, Fig. 8 shows that joint MMSE is the best choice in most cases, though the gain as compared to the LS algorithms is generally small.

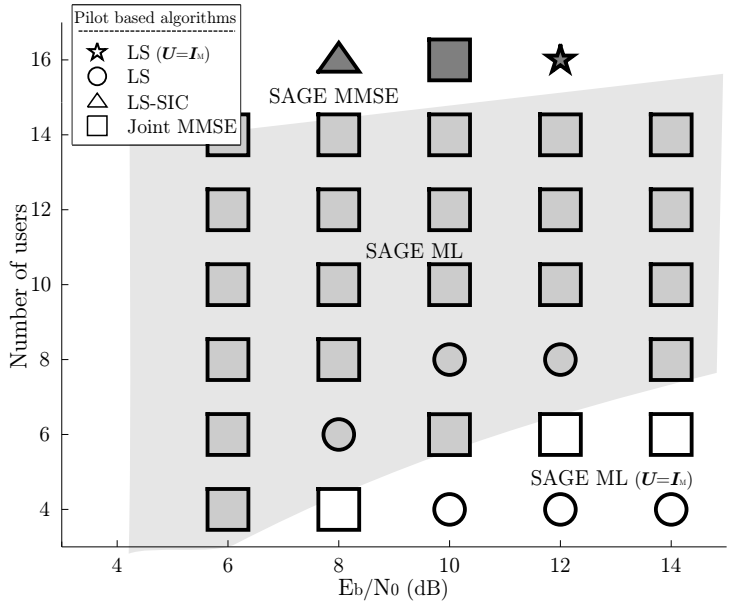


**Figure 8:** The algorithm combinations with the lowest total complexity, reaching a BER=$10^{-3}$, at different user numbers and $E_b/N_0$. Shape indicates which pilot based algorithms were used, and color indicates which decision-directed algorithms that were used. The system settings are $S_p = 1$ and $S = 20$ OFDM symbols, $M = 256$ subcarriers and $I = 27$ DPS sequences.

# 7 Conclusion

In this paper a number of channel estimation algorithms for OFDM-IDMA have been evaluated in terms of algorithm complexity and system performance. The channel estimation procedure is divided into two parts, one initial part where the estimate is obtained using pilot symbols, and one decision-directed part where both pilots and estimates of the transmitted symbols are used. For the

initial pilot based algorithms, the best performance is obtained by the joint MMSE estimator, which jointly estimates the channel for all users. Overall, the algorithm also gives the best tradeoff between complexity and performance, given that the estimator matrices are precalculated and stored in memory. For the decision-directed algorithms, the best performance, in terms of convergence speed, is obtained using the Full MMSE estimator. Taking complexity into account, SAGE ML is the best choice in most situations. If operating on the limit of the maximal system load, the SAGE MMSE estimator provides the best tradeoff. Overall, SAGE ML is most attractive due to its low complexity, and by allowing the frequency filtering to be switched on/off, the complexity can be further reduced at low user loads.

# 8 Appendix: The ESE in a complex scalar channel

The ESE, being the core of the IDMA receiver, assumes that the interference plus noise has a complex Gaussian distribution, and produces symbol-by-symbol extrinsic log-likelihood outputs based on estimates of the mean and variance of this process. The estimates are obtained using extrinsic information on the transmitted symbols acquired from the SISO decoders. In this paper an appropriately designed OFDM system is considered, which results in a per tone complex scalar channel. The ESE procedure for such channel is briefly summarized below. For a more detailed description of the ESE, the reader is referred to [4].

Suppose that the signal transmitted from user $j$ is to be handled. Rearranging (1) by collecting the contribution from user $j$ outside the summation, the received signal may be expressed as

$$r[m,s] \quad = \quad h_j[m,s]x_j[m,s] + \xi_j[m,s], \tag{31}$$

where $\xi_j[m,s]$ is the collected interference plus noise term influencing user $j$. With the above model, the extrinsic LLR output of the ESE is given by [4]

$$\begin{aligned} &e_{ESE}\left[\mathrm{Re}\left(x_j[m,s]\right)\right] = 2\left|h_k[m,s]\right|^2 \cdot \\ &\frac{\mathrm{Re}\left(h_j^*[m,s]r[m,s]\right) - \mathbb{E}\left\{\mathrm{Re}\left(h_j^*[m,s]\xi_j[m,s]\right)\right\}}{\mathrm{Var}\left\{\mathrm{Re}\left(h_j[m,s]^*\xi_j[m,s]\right)\right\}} \end{aligned} \tag{32}$$

where closed form expressions of $\mathbb{E}\left\{\mathrm{Re}\left(h_j[m,s]^*\xi_j[m,s]\right)\right\}$ and $\mathrm{Var}\left\{\mathrm{Re}\left(h_j[m,s]^*\xi_j[m,s]\right)\right\}$ are given in [4]. A similar expression can be derived for $e_{ESE}\left(\mathrm{Im}\left(x_j[m,s]\right)\right)$.

## References

[1] L. Ping, L. Liu, and W. Leung, "A simple approach to near-optimal multiuser detection: Interleave-division multiple-access," in *Proc. IEEE Wireless Communications and Networking Conference*, vol. 1, pp. 391–396, 2003.

[2] K. Kusume and G. Bauch, "CDMA and IDMA: Iterative multiuser detections for near-far asynchronous communications," in *Proc. IEEE International Symposium on Personal, Indoor and Mobile Radio Communications*, vol. 1, pp. 426–431, 2005.

[3] H. Schoeneich and P. A. Hoeher, "Adaptive interleave-division multiple access - a potential air interference for 4G bearer services and wireless LANs," in *Proc. IEEE International Conference on Wireless and Optical Communications Networks*, pp. 179–182, June 2004.

[4] L. Ping, L. Liu, K. Wu, and W. Leung, "Interleave-division multiple-access," *IEEE Transactions on Wireless Communications*, vol. 5, no. 4, pp. 938–947, 2006.

[5] L. Ping, Q. Guo, and J. Tong, "The OFDM-IDMA approach to wireless communication systems," *IEEE Wireless Communications Magazine*, vol. 14, no. 3, pp. 18–24, 2007.

[6] R. Zhang and L. Hanzo, "Three design aspects of multicarrier interleave division multiple access," *IEEE Transactions on Vehicular Technology*, vol. 57, no. 6, pp. 3607–3617, 2008.

[7] M. Valenti and B. Woerner, "Iterative channel estimation and decoding of pilot symbol assisted turbo codes over flat-fading channels," *IEEE Journal on Selected Areas in Communications*, vol. 19, no. 9, pp. 1697–1705, 2001.

[8] H. Schoeneich and P. A. Hoeher, "Iterative pilot-layer aided channel estimation with emphasis on interleave-division multiple access systems," *EURASIP Journal on Applied Signal Processing*, vol. 2006, pp. 1–15, 2006.

[9] T. Zemen, C. Mecklenbrauker, J. Wehinger, and R. Muller, "Iterative joint time-variant channel estimation and multi-user detection for MC-CDMA," *IEEE Transactions on Wireless Communications*, vol. 5, pp. 1469–1478, Jun. 2006.

[10] P. Salvo Rossi and R. Müller, "Joint iterative time-variant channel estimation and multi-user detection for MIMO-OFDM systems," in *Proc. IEEE Global Communications Conference*, pp. 4263–4268, Nov. 2007.

[11] S. Suyama, L. Zhang, H. Suzuki, and K. Fukawa, "Performance of iterative multiuser detection with channel estimation for MC-IDMA and comparison with chip-interleaved MC-CDMA," in *Proc. IEEE Global Communications Conference*, pp. 1–5, 2008.

[12] A. Mukherjee and H. Kwon, "Multicarrier interleave-division multiple-access systems with adaptive pilot-based user interleavers," in *Proc. IEEE Vehicular Technology Conference*, pp. 1–5, 2009.

[13] Q. Guo, L. Ping, and D. Huang, "A low-complexity iterative channel estimation and detection technique for doubly selective channels," *IEEE Transactions on Wireless Communications*, vol. 8, pp. 4340 –4349, Aug. 2009.

[14] Y. Li, N. Seshadri, and S. Ariyavisitakul, "Channel estimation for OFDM systems with transmitter diversity in mobile wireless channels," *IEEE Journal on Selected Areas in Communications*, vol. 17, pp. 461–471, Mar. 1999.

[15] Y. Xie and C. Georghiades, "Two EM-type channel estimation algorithms for OFDM with transmitter diversity.," *IEEE Transactions on Communications*, vol. 51, no. 1, pp. 106–116, 2003.

[16] H. Dogan, E. Panayirci, and H. Curpan, "Iterative channel estimation techniques for uplink MC-CDMA systems," in *Proc. IEEE International Symposium on Signal Processing and Information Technology*, pp. 302–306, 2007.

[17] M. Münster and L. Hanzo, "Parallel-interference-cancellation-assisted decision-directed channel estimation for OFDM systems using multiple transmit antennas," *IEEE Transactions on Wireless Communications*, vol. 4, no. 5, pp. 2148–2162, 2005.

[18] P. Salvo Rossi and R. Müller, "Slepian-based two-dimensional estimation of time-frequency variant MIMO-OFDM channels," *IEEE Signal Processing Letters*, vol. 15, pp. 21–24, 2008.

[19] D. Slepian, "Prolate spheroidal wave functions, Fourier analysis, and uncertainty - V: The discrete case," *Bell System Technical Journal*, vol. 57, pp. 1371–1430, May/Jun. 1978.

[20] O. Edfors, S. Wilson, and P. Börjesson, "OFDM channel estimation by singular value decomposition," *IEEE Transactions on Communications*, vol. 46, no. 7, pp. 931–939, 1998.

[21] S. M. Kay, *Fundamentals of Statistical Signal Processing, Volume I: Estimation Theory*. Prentice Hall, 1993.

[22] J. Fessler and A. Hero, "Space-alternating generalized expectation-maximization algorithm," *IEEE Transactions on Signal Processing*, vol. 42, pp. 2664 –2677, Oct. 1994.

[23] P. Hoeher, "A statistical discrete-time model for the WSSUS multipath channel," *IEEE Transactions on Vehicular Technology*, vol. 41, pp. 461–468, Nov. 1992.